ELECTRON SELF EXCHANGE REACTIONS OF ELECTROACTIVE IONIC LIQUID AND NANOPARTICLE MATERIALS

Joshua E. F. Weaver

A dissertation submitted to the faculty of the University of North Carolina at Chapel Hill in partial fulfillment of the requirements for the degree of Doctor of Philosophy in the Department of Chemistry.

Chapel Hill

2010

Approved by:

Royce W. Murray

Maurice Brookhart

Michel Gagné

R. Mark Wightman

Wei You

ABSTRACT

Joshua E. F. Weaver

Electron Self Exchange Reactions of Electroactive Ionic Liquid and

Nanopariticle Materials

(Under the Direction of Royce W. Murray)

Chapter One is a basic introduction to the background and basic chemistry of both ionic liquid and gold nanoparticle materials. This chapter sets in place many concepts that are expanded upon in greater detail in later chapters.

Chapter Two contains the synthesis and electrochemical analysis of a series of redox functionalized phosphonium ionic liquid materials. These materials were synthesized and characterized using NMR (^{1}H, ^{13}C, and ^{31}P) and mass spectroscopy by Paul Ragogna's laboratory at the University of Western Ontario. Solution and neat melt electrochemistry (including cyclic voltammetry, chronoamperometry, and AC Impedance) was carried out to characterize the electrochemical behavior of these compounds and compare them to previous studies of other similar molecules.

Chapter Three contains the successful synthesis of redox functionalized dendritic ionic liquids base on tris(2-aminoethyl)amine, poly(propylene imine) (PPI), and

polyamidoamine (PAMAM) dendrimers. These redox functionalized dendritic ionic liquid materials were analyzed using NMR, mass spectroscopy, and solution and solid state electrochemistry. Despite the high melting points of these materials, electrochemical data was obtained for some neat materials at elevated temperatures and some were obtained using a special CO_2 plasticization method.

Chapter Four contains the use of the updated $Au_{25}(SCH_2CH_2Ph)_{18}$ synthesis, ligand exchange of $Au_{25}(L)_{18}$ nanoparticles, and the ligand effects on electron self exchange kinetics in solid state mixed valency films. The updated synthetic method has proven to be of great consequence by significantly increasing nanoparticle yield, purity, and ease of synthesis. MALDI data is presented to show purity of the materials and also to accurately show the extent of ligand exchange achieved. Linear sweep voltammetry was used to measure conductivity in solid state films of nanoparticles over the temperature range -10˚C to 30˚C with various para-substituted (electron withdrawing, donating, or neutral) mercaptobenzene ligands. The results of the solid state linear sweep measurements are also compared to a short study of the same ligand effect measured using AC impedance data. The results of this study indicate that nanoparticle film conductivity may be tuned by careful ligand selection.

ACKNOWLEDGEMENTS

I would like to begin by acknowledging my research advisor, Professor Royce Murray, for all of his guidance and support through the last five years. Especially when things were difficult, Professor Murray helped me stay focused on learning and trying new things, and was never afraid to let me make my own mistakes while always guiding me back to more firm footing.

I would like to thank several lab members who over the years have helped me by either contributing to my research or my thin grasp of sanity. I would like to thank Ramjee Balasubramanian for helping to get me off the ground in the Murray group by teaching me how to be both a synthetic and analytical chemist. I would like to thank Joe Parker, Chris Beasly, and Christina Fields-Zinna for several successful collaborations as well as great friendships that helped me to endure the rigors of graduate school. I would also like to thank present and previous Murray group members for boundless help and support as well as many other great friendships.

I would like to acknowledge my parents, Bonnie Frye and Michael Weaver, who always provided me with the means and the encouragement to be creative and hardworking. I have no doubt that without their inspiration and guidance, I would never have accomplished so much. I would also like to acknowledge my brother, Asher, who has always been a great friend and a constant reminder that doing great things and being a great person are not mutually exclusive. I would like to acknowledge my Grandmother and other family

members, who have never let me lose sight of the fact that all of the work that I have done in all of my years of school is no small feat. I would further like to acknowledge my parents as well as my mother, father, and brother-in-law for continuous financial, moral, and emotional support through my entire graduate career.

I would like to thank all of my undergraduate professors at Wabash College for making me fully prepared to tackle the challenges of graduate school. In particular, I would like to thank both of my undergraduate advisors, Scott Feller and Lon Porter, who encouraged me through my undergraduate education and encouraged me to go to graduate school.

Most of all, I would like to thank my wife, Lindsay, who encouraged me to come to UNC, and who packed up everything to come with me. She has provided boundless encouragement and support over the years that have kept me both sane and happy. I would very much like to thank her for her patience and understanding while I have completed this degree. I would also like to acknowledge my dogs, Bentley and Lola, who have always given me distractions when I needed them, and have been more or less patient with me when I did not.

TABLE OF CONTENTS

LIST OF TABLES

LIST OF FIGURES

LIST OF ABBREVIATIONS AND SYMBOLS

A	the pre-exponential factor of the Arrhenius equation
AC	alternating current
C	concentration
CV	cylclic voltammetry
δ	average center to center distance between two redox sites
D_{app}	apparent diffusion coefficient
D_{cion}	physical diffusion coefficient of counter ions
D_e	electron diffusion coefficient
D_{phys}	physical diffusion coefficient of redox species
DFT	density functional theory
DPV	differential pulse voltammetry
E_A	activation energy
F	Farraday's constant
E	potential
E_R	rest potential
E^0	formal potential

Fc	ferrocene
HOMO	highest occupied molecular orbital
i	current
IDA	interdigitated array
k_{ex}	rate constant for electron self-exchange reaction
k_{het}	heterogeneous rate constant
k_{homo}	homogeneous rate constant
LUMO	lowest unoccupied molecular orbital
m/z	mass to charge ratio
N_A	Avagadro's number
Ω	ohm
PSI	pounds per square inch
r	radius
R	molar gas constant
R_{CT}	charge transfer resistance
σ	conductivity
t	time

T	temperature
z	ionic charge
Z	impedance

CHAPTER 1

INTRODUCTION TO IONIC LIQUIDS AND GOLD NANOPARTICLES

1.1 Introduction

It is no secret that today's energy economy is changing drastically in the face of concerns over the lifetime and cost of fossil fuels as well as anthropogenic carbon dioxide emissions. The result of this is a large movement in recent years to produce more cost efficient and less fossil fuel dependent sources of renewable energy. Some of the primary focuses have included converting large energy sources such as hydrogen and solar fuels into electrical energy as well as the requisite need for energy storage systems such as capacitors and batteries. While hydrogen and solar fuels seem to have very large potential in terms of energy production, harvesting energy from these systems has been fraught with problems on many fronts. Hydrogen fuels for example are highly flammable and may not be ideal for vehicles, and they also can also have a large energy cost to produce. Solar energy on the other hand is relatively harmless and requires no energy on earth to produce, but there has been great difficulty in terms of converting this energy into practical electrical power and there is the problem with its lack of availability during some portion of the day. Both hydrogen and solar fuels would benefit greatly from having both a low energy loss conversion as well as reliable and efficient storage systems in place. Fundamental studies of electron exchange and electron exchange materials are a very promising route to helping in the understanding of these problems and many more.

This research has focused on two types of materials, electroactive ionic liquids and nanoparticles, and the ability of these materials to transport electrons. The ionic liquids described in this paper are interesting because a single molecule is acting as a redox species, electrolyte, and solvent all in one single system. This innate behavior allows for the electrochemical study of electron transfer in a very controlled way where there are no other molecules involved. The gold nanoparticles are interesting because, despite being composed of many transition metal atoms that are conductive as a bulk material, the particles behave as semiconductors because of their specific size and atom content.

1.2 Ionic Liquids

1.2.1 General Properties and Characteristics

Room temperature molten salts, or now referred to more commonly as ionic liquids, are complexes that consist generally of an organic cation and an inorganic anion and are also liquid at or around room temperature. Some examples of organic cations include ammonium, sulphonium, phosphonium, imidazolium, pyridinium, piperidinium and pyrrolydinium (Figure 1.1-A). Some of the more common anions are tetrachloroaluminate, hexafluorophosphate, tetrafluoroborate, and bis(trifluoromethylsulfonyl)imide (Figure 1.1-B). These substances have been known since at least 1914 when alkyl ammonium nitrate was first published in literature.[1,2] During the past 30 years, ionic liquids have gained a significant amount of attention and become a large growth area for research in many fields, and have developed for a variety of commercial applications in electrochemical devices and processes such as batteries and capacitors as well as metal deposition.[3,4] The emergence in 1992 of ionic liquids stable at ambient conditions, arguably did more than anything else to

Figure 1.1 Some common ionic liquid cations (A) and anions (B).

(A) $[NR_xH_{4-x}]+$ $[SR_xH_{3-x}]+$ $[PR_xH_{4-x}]+$

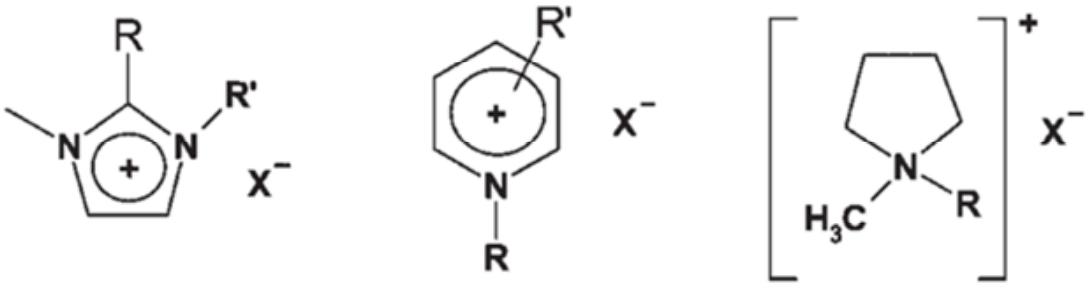

(B) $AlCl_4^-$, $AlCl_7^-$

PF_6^-, BF_4^-, SbF_6^-

$[(CF_3SO_2)_2N]^-$, $CF_3SO_2\text{-}N^-\text{-}COCF_3$

$ROSO_3^-$, RSO_3^-

boost interest in ionic liquids for their exceptional properties and potential uses.[5,6] The last 20 years have generously expanded the potential for practical applications of ionic liquids into the areas of organic synthesis[7] and catalytic solvents,[8,9,10] and have also given a tremendous rise in electrochemical applications.[11,12] This interest inspired the production of more than 10,000 papers[13] in the last decade.

A survey of reviews about ILs will quickly show that Ils have recently been implicated for use in many practical applications including using Ils that have imidazolium cations functionalized with groups reactive to CO_2 in order to capture the greenhouse gas.[14] Another review documents the use of Ils with multiple cations in a single contiguous structure as stationary phases for gas chromatography.[15] Interestingly, similar structures with dications separated by long alkyl or ethylene oxide chains have been shown to be very good chemical lubricants as compared to more traditional silicone and olefin oils among others.[16] Room temperature Ils, and their higher melting point cousins commonly referred to as molten salts, have found wide applicability in the industrial realm of electrodeposition.[17] Ionic liquids are ubiquitously praised for their properties of high thermal and chemical stability, negligible vapor pressure, low toxicity, innate ionic conductivity, and their large electrochemical window.[18-24]

When it comes to Ils and electrochemistry, it would be very difficult to express the vast number of applications and publications available in a reasonable space. The 2009 edition of *Modern Aspects of Electrochemistry* contains an entire chapter detailing many of the uses and advances of Ils in terms of electroanalytical chemistry.[14] Some of the more ubiquitous applications of Ils to electrochemistry include their use as electrolytes for double-layer electrochemical capacitors, lithium batteries, and fuel cells. In order to achieve the

most useful electrolytes for safe and efficient batteries and other electrochemical storage devices, ionic liquids must be designed with greatly improved conductivity while maintaining a wide electrochemical potential window. Very recently, ionic liquids have seen a tremendous amount of interest and support for use as battery electrolytes, and with the current state of energy use and needs around the world, it will likely be only a matter of time before ionic liquids are seen to be widely used for battery technologies.

This research in particular has focused on studying electron transfer events in neat (solvent free) ionic liquid systems. The easiest way to conduct this study involves incorporating both the ionic liquid functionality as well as the redox functionality into the same molecule making liquid ionic redox materials. This special molecule allows for fluidity while not adding the complications of a solvent/solvate system and greatly simplifies the calculations involved with determining diffusion coefficients and electron transfer rate constants. These values tell much about the way molecules and electrons move in these interesting liquid phases, and understanding this is a large step toward designing and applying these materials to commercial and industrial energy applications.

1.2.2 Electron Transport Basics

A scheme of the experimental setup that is essential to the ionic liquid electrochemistry that has been studied can be seen in Figure 1.2. The homemade setup consists of 4 electrodes contained within a stainless steel tube and sealed within an epoxy resin. The details of the setup's construction can be found in Lee et al.[25] The 4 electrodes contained in the setup are a 25um diameter platinum micro-disk working electrode, a .5mm Ag quasi-reference electrode, and two .4mm diameter platinum disk counter electrodes. For

Figure 1.2 A schematic depicting the temperature controlled glass vacuum chamber that was used to conduct neat melt electrochemistry. The red box inset shows the detail of the electrode setup from the side and a top down view.

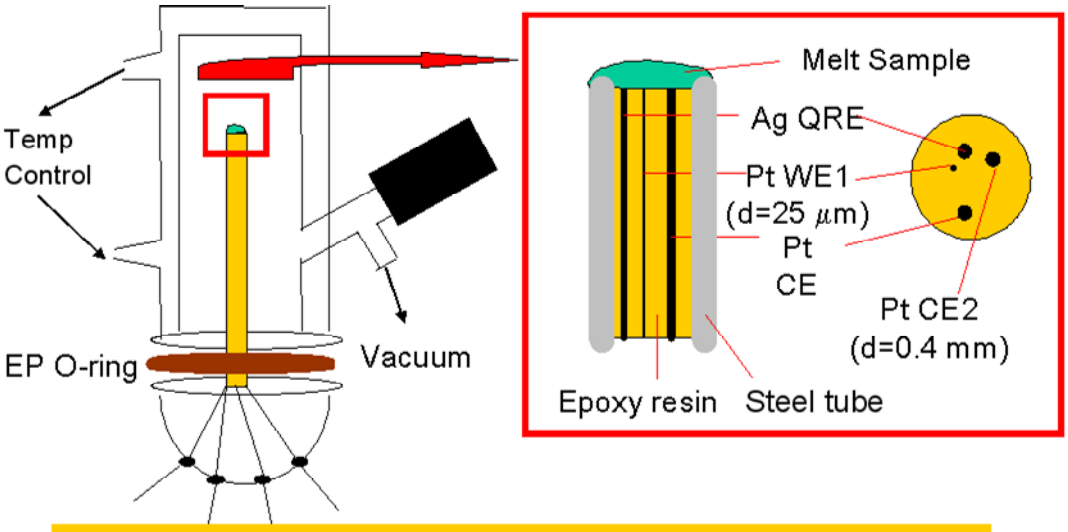

Four-electrode Assembly for Voltammetry and AC Impedance in Vacuum w/ Temp Control

voltammetry and amperometric measurements, a 3 electrode system is employed that consists of the working, quasi-reference, and one counter electrode. In the case of AC Impedance measurements, a 2 electrode system is employed that consists only of the two platinum counter electrodes. To perform the neat melt state electrochemistry, a temperature controlled vacuum chamber is employed. The ionic liquid is dropcast from dichloromethane on to the electrode surface, which is then placed in the temperature controlled chamber (at elevated temperatures) and high vacuum is used to assure removal of casting solvent.

Redox functionalized ionic liquids are remarkably useful for this study due to their inherent properties of being liquid, ionic and conductive, as well as having redox sites when functionalized in this way. This system provides a single molecule that provides every aspect necessary to carry out electrochemical measurements. The systems employed also have inherent features that make them ideal for studying electron transfer (hopping) phenomena. The concentration of redox sites is usually in the range of approximately 2M, and at the same time the bulky redox piece of the ionic liquid often has very little if any mobility in the neat melt state. This means that, as shown in Figure 1.3, electron diffusion (D_e, electron hopping) is much much faster than physical diffusion (D_{phys}) of the redox species and is described by the Dahms-Ruff equation:[26-28]

$$D_{app} = D_{phys} + D_e = D_{phys} + \frac{k_{ex}\delta^2 C}{6} \qquad \text{(eqn. 1)}$$

Where D_{app} is the apparent (measured) diffusion coefficient, δ is the equilibrium center to center distance between the electron donor and acceptor, C is the concentration of all redox sites, k_{ex} is the electron exchange rate constant, and 6 is the number of directions an electron can exchange to (assuming a cubic lattice model[28]).

Figure 1.3 This diagram gives a simple illustration of the electron hopping mechanism that is observed in the neat melt electrochemistry and is responsible for the observed $D_{app} = D_e$.

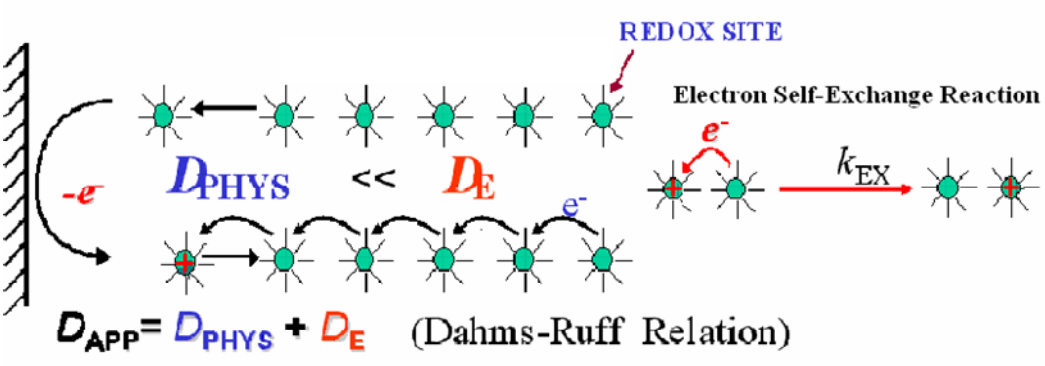

$D_{APP} = D_{PHYS} + D_E$ (Dahms-Ruff Relation)

$$D_E = \frac{k_{EX}\delta^2 C}{6}$$

In fluid solutions: $D_{PHYS} >> D_E$; In melts: $D_{PHYS} << D_E$

A previous group study showed that in a Co metal complex molten salt (ionic liquid) that had two electron transfer events, one with very slow electron self exchange kinetics, Co(III/II), and one with very fast electron exchange kinetics, Co(II/I), there are two very different quantities of current in a cyclic voltammogram.[29,30] In solution, the redox waves for each redox couple would be nearly the same, but in a melt where the physical diffusion is very slow, a redox couple that has very slow self exchange kinetics will have very low current. However, a redox couple with fast electron self exchange kinetics will have much higher current despite the low physical diffusion contribution and will be dominated by electron hopping.

1.3 Gold Nanoparticles

Similarly to ionic liquids, gold nanoparticles have garnered significant interest in the last 20 years. Gold nanoparticles have become popular due in part to their electron transfer and optical properties[34,35]as well as their general potential for biological applications.[36,37] Gold nanoparticles are most often capped with thiolate ligands, which add a great deal of functionalization potential for these small molecules. These nanoparticles can also be engineered in a variety of sizes with very high levels of mondispersity for some size regimes.

The story of $Au_{25}L_{18}$ NPs is certainly an interesting one. It has been misidentified over the years as both $Au_{28}(SG)_{16}$ (SG=Glutathione)[38,39] and as $Au_{38}(SCH2CH2Ph)_{24}$[40] only to later be confirmed as Au25L18 by both mass spectrometry[41,42] and x-ray crystallography of both the reduced[43] and later the oxidized[44] form of the structure that agreed with a theoretical DFT prediction[45] released at the same time as the reduced particle crystal

structure. At this point, the structure has been characterized extremely well making these particles exceptional candidates for studying electron self exchange kinetics.

The $Au_{25}L_{18}$ particles that have been the focus of this research are very small, on the order of 1.1nm in diameter. They are composed of 25 gold atoms and 18 thiolate ligands, where the core of the particle is a slightly distorted geometrical icosohedron consisting of 12 gold atoms with an additional gold atom at the very center of the core. Attached to the core and surrounding the periphery are 6 -SR-Au-SR-Au-SR- semi-ring "staple" structures. The reduced form of this material has a native -1 charge and has a tetraoctylammonium counter cation. The cation is most likely tetrabutylammonium in any case where tetrabutylammonium perchlorate has been used as an electrolyte. The oxidized for of the material has a native neutral charge and is without a stabilizing counterion of any kind. As expected, the reduced structure has the semi-rings slightly puckered to accommodate the association of the cation when in the dry (solvent free) form, where the oxidized form has no semi-ring puckering when dry as there is no counterion to accommodate. The ligand that is generally used to synthesize these materials is 2-phenylethanethiolate, but it is easily replace with many other thiolate ligands through a simple ligand exchange to be described later.

The electronic and optical properties can be easily tuned by changing the size of the particles. Large particles have bulk metal like behavior and show featureless voltammetry and optical spectra with the exception of the surface Plasmon that occurs around 520nm.[46] Smaller particles such as Au_{144} (1.6nm) show evenly spaced oxidation and reduction peaks that represent single electron transfer called quantized double layer charging.[47] Even smaller particles, such as the Au_{25} (1.1nm) particle that is the focus of this research, show distinct molecule like electron transfer events with a larger band gap between the first and second

oxidation states in voltammetry (Figure 1.4) and a step like absorbance spectrum (Figure 1.5).

As can also be seen in Figures 1.4 and 1.5, changes to the electronic nature of the ligand can have a very large impact on both the electrochemistry and the optical spectra of the nanoparticle and have been previously documented by both Guo et al.[48] and Parker et al.[49-50] These studies found that substituting a SCH_2CH_2Ph ligand with a para-substituted thiophenol (SPh-X, where X = NO_2, Br, H, CH_3, or OCH_3) ligand results in changes to the formal potential (E^0) of all redox waves with no noticeable effect on the HOMO-LUMO energy gap (the difference between the $Au_{25}L_{18}^{-1/0}$ couple and the $Au_{25}L_{18}^{0/+1}$ couple). In the case of electron withdrawing ligands ($SPhNO_2$ or SPhBr), the formal potentials are shifted to more positive potentials. It has also been shown that rates for ligand exchange follow the same order with more electron withdrawing ligands exchanging faster than less electron withdrawing ligands.[51] Furthermore, experimental and theoretical (DFT calculations) work has also shown that the $Au_{25}L_{18}^{-1/0}$ formal potential shifts linearly with each ligand addition (42mV/ligand in the case of $SPhNO_2$ and 60mV/ligand in the, theoretical only, case of SCH_2Cl).[50]

One of the end results of these previous findings is that we now have a redox active, highly characterized, semiconductor nanoparticle, with a HOMO-LUMO energy gap that can be tuned (increased or decreased in energy) by simply changing the surface ligands. There are still many questions left to be answered about these highly intriguing particles, but the one this research has sought to answer is whether changing the surface ligands in such a way that the HOMO-LUMO energy gap changes noticeably also affects the ability of the nanoparticle to undergo electron self exchange reactions? More specifically, does changing

Figure 1.4 UV-visible spectroscopy data collected for A) $Au_{25}(SC2Ph)_{18}$ and B) $Au_{25}(SCH_2CH_2Ph)_7(SPhBr)_{11}$, which demonstrate the subtle differences that come from exchanging on electron withdrawing ligands.

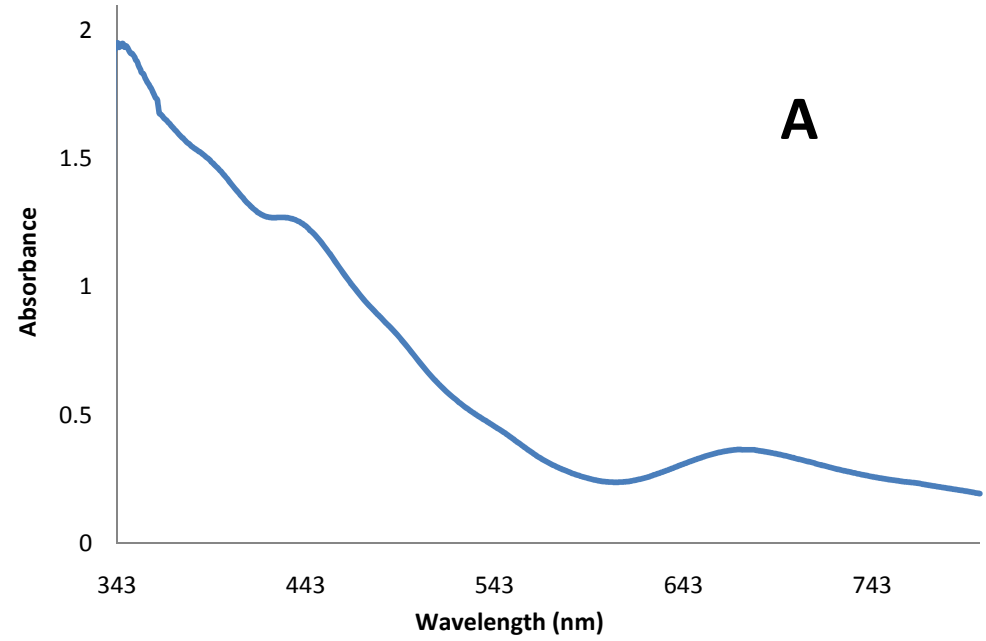
A
Absorbance
2
1.5
1
0.5
0
343
443
543
643
743
Wavelength (nm)

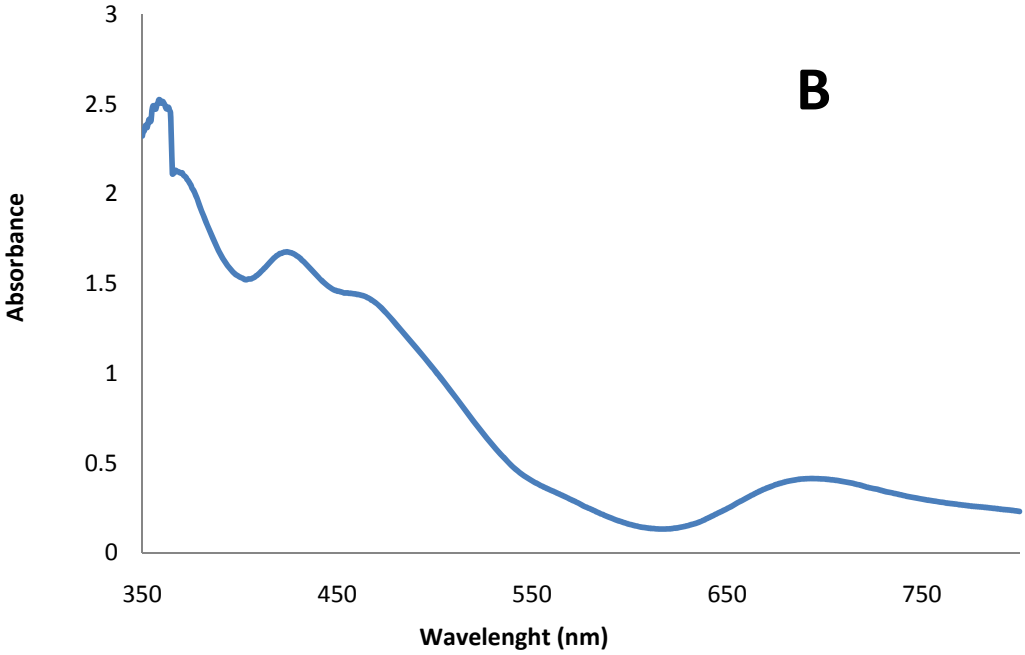
B
Absorbance
3
2.5
2
1.5
1
0.5
0
350
450
550
650
750
Wavelenght (nm)

Figure 1.5 Sample cyclic voltammograms of A) $Au_{25}(SC2Ph)_{18}$ and B) $Au_{25}(SCH_2CH_2Ph)_7(SPhBr)_{11}$ that clearly demonstrate the large shift to positive potentials of the E^0 of both the -1/0 and 0/+1 redox couples when electron withdrawing ligands are exchanged for less electron withdrawing ligands.

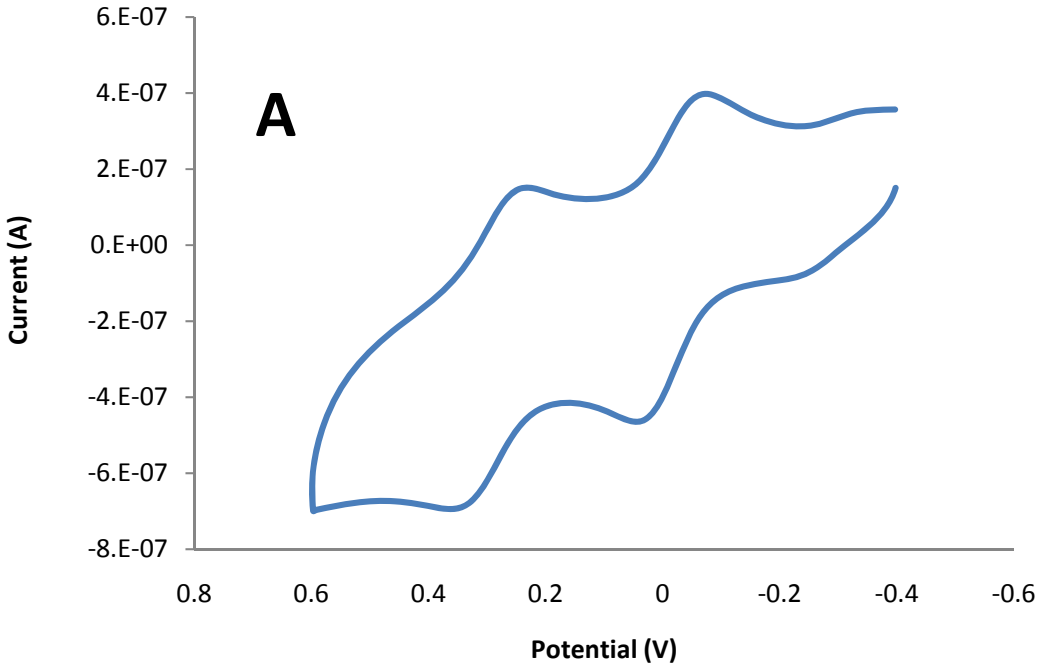
A
6.E-07
4.E-07
2.E-07
0.E+00
-2.E-07
-4.E-07
-6.E-07
-8.E-07
Current (A)
0.8
0.6
0.4
0.2
0
-0.2
-0.4
-0.6
Potential (V)

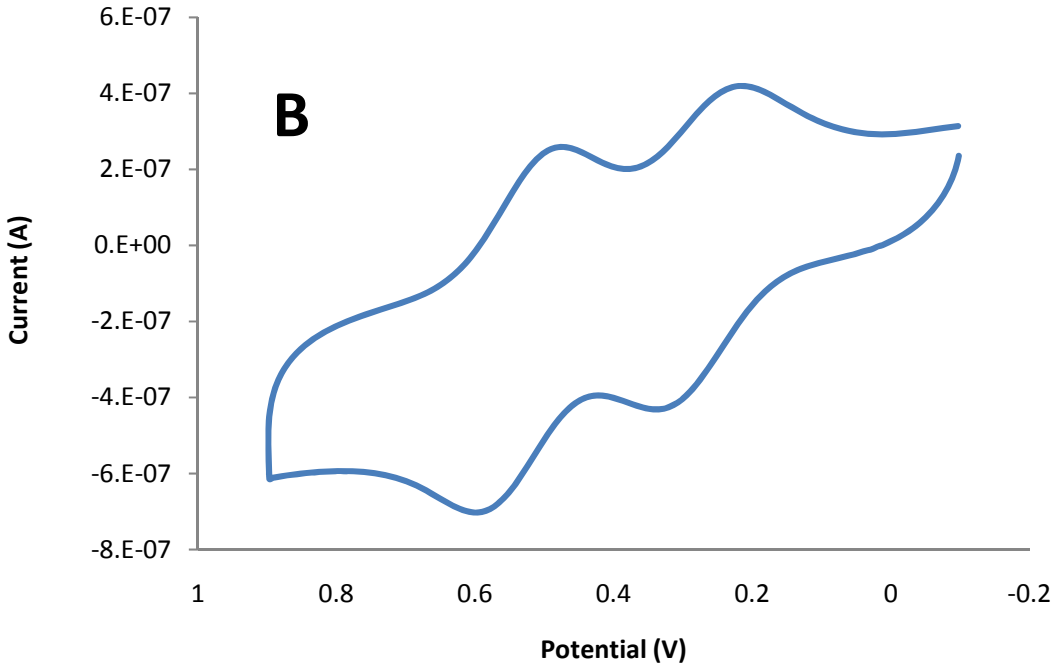
B
6.E-07
4.E-07
2.E-07
0.E+00
-2.E-07
-4.E-07
-6.E-07
-8.E-07
Current (A)
1
0.8
0.6
0.4
0.2
0
-0.2
Potential (V)

the surface ligands to electron donating or withdrawing have any impact on the rate of electron self exchange (kex), and if so, how great is the impact?

References:

(1) Walden, P. *Isv. Imp. Akad. Nauk* **1914**, 1800.

(2) Sudgen, S.; Wilkins, H. *J. Chem. Soc.* **1929**, 1291.

(3) Hussey, C.L. in *Chemistry of Nonaqueous Solvents*, Popov, A. and Mamantov, G., Eds, Ch. 4, VCH Publishers, New York **1994**.

(5) Hussey, C.L. in *Advances of Molten Salt Chemistry*, Vol. 5, Mamantov, G., Ed., p.185, Elsevier Science Publishers, New York **1983**.

(6) Wilkes, J.S.; Azworotko, M.J. *Chem. Soc. Chem. Commun.* **1992**, 965.

(7) Fuller, J.; Carlin, R.T.; De Long, H.C.; Haworth, D.J. *Chem. Soc. Chem. Commun.* **1994**, 299.

(8) *Ionic Liquids in Syntheses*, Wassercheid, P.; Welton, T., Eds., Wiley-VCH, Weinhein, **2002**.

(9) Dupont, J.; de Souza, R.F.; Suarez, P.A.Z. *Chem. Soc. Rev.* **2002**, 102, 3667.

(10) Sheldon, R. *Chem. Commun*. **2001**, 2399.

(11) Welton, T. *Chem. Rev.* **1999**, 99, 2071.

(12) Buzzeo, M.C.; Evans, R.G.; Compton, R.G. *Chem. Phys. Chem.* **2004**, 5, 1106.

(13) Zhang, J.; Bond, A.M. *Analyst* **2005**, 130, 1132.

(14) Estimated from SciFinder® Search Results

(15) Bara, J.E., Camper, D.E., Gin, D.L., and Noble, *R.D.* Room-Temperature Ionic Liquids and Composite Materials: Platform Technologies for CO_2 Capture. *Acc. Chem. Res.* **2010**, 43, 152-159.

(16) Armstrong, D.W., Payagala, T., Sidisky, L.M. The Advent and Potential Impact of Ionic Liquid Stationary Phases in GC and GCXGC. *LC-GC Europe* **2009**, 22, 459-467.

(17) Armand, M. and Tarascon, J.-M. Building Better Batteries. *Nature* **2008**, 451, 652-657.

(18) Armand, M., Endres, F., MacFarlane, D.R., Ohno, H., and Scrosati, B. Ionic-Liquid Materials for the Electrochemical Challenges of the Future. *Nature Mater*. **2009**, 8, 621-629.

(19) Handy, S.T., *Chem. Eur. J.* **2003**, 9, 2938.

(20) Dupont, J.; de Souza, R.F.; Suarez, P.A.Z., *Chem. Rev.* **2002**, 102,3667.

(21) Endres, F., *ChemPhysChem*, **2002**, 3, 144

(22) Wilkes, J.S., *Green Chem.* **2002**, 4, 73.

(23) Sheldon, R., *Chem. Commun.* **2001**, 2399.

(24) Wasserscheid, P. and Keim, W., *Angew. Chem. Int. Ed.* **2000**, 39, 3772.

(25) Welton, T., *Chem. Rev.* **1999**, 99, 2071.

(26) Lee, D.; Huthchison, J.C.; Leone, A.M.; DeSimone, J.M.; Murray, R.W. *J. Am. Chem. Soc.* **2002**, 124, 9310.

(27) Dahms, H. *J. Phys. Chem.* **1968**, 72, 362.

(28) Ruff, I.; Friedrich, V.J. *J. Phys. Chem.* **1971**, 75, 3297.

(29) Majda, M. In *Molecular Design of Electrode Surfaces*; Murray, R.W., Ed.; John Wiley & Sons: New York, **1992**.

(30) Williams, M.E.; Lyons, L.J.; Long, J.W.; Murray, R.W. *J. Phys. Chem.* **1997**, 101, 7584.

(31) Williams, M.E.; Masui, H.; Long, J.W.; Malik, J.; Murray, R.W. *J. Am. Chem. Soc.* **1997**, 199, 1997.

(32) Zhou, F., Liang, Y., and Liu, W. Ionic Liquid Lubricants: Designed Chemistry for Engineering Applications. *Chem. Soc. Rev.* **2009**, 38, 2590-2599.

(33) Simka, W., Puszczyk, D., and Nawrat, G. Electrodeposition of Metals from Non-Aqueous Solutions. *Electrochim. Acta* **2009**, 54, 5307-5319.

(34) Tsuda, T. and Hussey, C.L. Electrochemistry of Room-Temperature Ionic Liquids and Melts. In *Modern Aspects of Electrochemistry*; White, R.E., Ed.; Springer Science, **2009**, 45, 63-174.

(35) Templeton, A.C.; Wuelfing, W.P.; Murray, R.W. Monolayer-Protected Cluster Molecules *Accts. Chem. Res.* **2000**, 33, 27-36.

(36) Wang, G.; Huang, T.; Murray, R.W.; Menard, L.; Nuzzo, R.G. Near-IR Luminescence of Monolayer-Protected Metal Clusters *J. Am. Chem. Soc.* **2005**, 127, 812-813.

(37) Rose, N.L.; Mirkin, C.A. Nanostructures and Biodiagnostics. *Chem. Rev.* **2005**, 105, 1547-1562.

(38) Andreas, R.P.; Bein, T.; Dorogi, M.; Feng, S.; Henderson, J.I.; Kubiak, C.P.; Mahoney, W.; Osifchin, R.G.; Reifenberger, R. "Coulomb Staircase" at Room Temperature in a Self-Assembled Molecular Nanostructure *Science* **1996**, 272, 1323-1325.

(39) Schaaf, T.D.; Knight, G.; Shafigullin, M.N; Borkman, R.F.; Whetten, R.L. Isolation and Selected Properties of a 10.4 kDa Gold:Glutathione Cluster Compound. *J. Phys. Chem. B* **1998**, 102, 10643-10646.

(40) Negishi, Y.; Takasugi, Y.; Sato, S.; Yao, H.; Kimura, K.; Tsukuda, T. Magic-Numbered Au_n Clusters Protedted by Glutathione Monolayers (n=18, 21, 25, 28,32, 39): Isolation and Spedtroscopic Characterization. *J. Am. Chem. Soc.* **2004**, 126, 6518-6519.

(41) Donkers, R.L; Lee, D.; Murray, R.W. Synthesis and Isolation of the Molecule-like Cluster Au38(SCH2CH2Ph)24. *Langmuir* **2004**, 20, 1945-1952.

(42) Tracy, J.B.; Crowe, M.C.; Parker, J.F.; Hampe, O.; Fields-Zinna, C.A.; Dass, A.; Murray, R.W. *J. Am. Chem. Soc.* **2007**, 129, 6706-6707.

(43) Tracy, J.B.; Crowe, M.C.; Parker, J.F.; Hampe, O.; Fields-Zinna, C.A.; Dass, A.; Murray, R.W. *J. Am. Chem. Soc.* **2007**, 129, 16209-16215.

(44) Heaven, M.W.; Dass, A.; White, P.S.; Holt, K.M.; Murray, R.W. *J. Am. Chem. Soc.* **2008**, 130, 3754-3755.

(45) Zhu, M.; Eckenhoff, W.R.; Pintauer, T.; Jin, R. *J. Phys. Chem. C* **2008**, 112, 14221-14224.

(46) Akola, J.; Walter, M.; Whetten, R.L.; Hakkinen, H.; Gronbeck, H. *J. Am. Chem. Soc.* **2008**, 130, 3756-3757.

(47) Hostetler, M.J.; Wingate, J.E.; Zhong, C.-Z.; Harris, J. E.; Vachet, R.W.; Clark, M.R.; Londono, J.D.; Green, S.J.; Stokes, J.J.; Wignall, G.D.; Glish, G.L.; Porter, M.D.; Evans, N.D.; Murray, R.W. *Langmuir* **1998**, 14, 17.

(48) Ingram, R.S.; Hostetler, M.J.; Murray, R.W.; Schaaf, R.G.; Khoury, J.T.; Whetten, R.L.; Bigioni, T.P.; Guthrie, D.K.; First, P.N. *J. Am. Chem. Soc.* **1997**, 119, 9279.

(49) Guo, R.; Murray, R.W. *J. Am. Chem. Soc.* **2005**, 127, 12140-12143.

(50) Parker, J.F; Choi, J-P; Wang, W.; Murray, R.W. *J. Phys. Chem. C* **2008**, 112, 13976-13981.

(51) Parker, J.F.; Kacprzak, K.A.; Lopez-Acebedo, O.; Häkkinen, H.; Murray, R.W. *J. Phys. Chem. C* **2010**, 114 (18), 8276.

(52) Guo, R.; Song, Y.; Wang, G.; Murray, R.W. *J. Am. Chem. Soc.* **2005**, 127, 2752-2757.

CHAPTER 2

ELECTROCHEMICAL CHARACTERIZATION OF REDOX FUNCTIONALIZED PHOSPHONIUM IONIC LIQUIDS

2.1 Introduction

In recent years ionic liquids have begun to move from the realm of novel chemical materials to materials with many practical applications. These uses are centered on the unique property of being both innately conducting and liquid, and are often associated with electrochemical applications.[1] Practical applications now include use as electrolyte-solvents in batteries, fuel cells, and capacitors. Some recent studies have examined the behavior of various solutes in ionic liquids,[2] molecular force fields of ionic liquids,[3] hydrogen oxidation in ionic liquids at a platinum electrode surface,[4] density estimation of ionic liquids,[5] the applicability of Marcus theory to ionic liquid redox processes,[6] and the evaluation of new materials such as tetraalkylphosphonium polyoxometalate ionic liquids.[7]

Previous research in this group has investigated the electrochemical phenomena of various classes of ionic liquid materials that have included redox active polyether hybrids, DNA complexes, and imidazolium systems.[8-16] Redox functionalized ionic liquids inherently offer unique opportunities for investigations of electron transfer and mass transport in melt phases, when used in their undiluted forms. These materials often have melting points below 100°C, are are sufficiently ionically conductive as to permit quantitative voltammetry in the undiluted state. They can be designed to incorporate a variety of redox species.[17]

Out studies have focused on investigating and understanding the rates of mass and electron transport in semi-solid media, choosing as model media, redox functionalized ionic liquids. With very high redox site concentrations, such as ferrocene in the 1 – 2 M range, the neat melt materials are concurrently both electron and ionically conductive. An important property of the neat redox ionic liquids is that the spacing between redox sites is small, allowing facile electron self-exchange (hopping). The viscosities of the neat materials are substantial, so that physical diffusion of redox sites is greatly retarded, and becomes less significant[8] than the transport of electrochemical charge by electron hopping. The electron hopping process is initiated by electrochemical voltammetry that generates a mixed valent layer at the electrode interface, which supports the hopping process.

The general expression for the combined electron hopping and physical diffusion processes, i.e., the apparent diffusion (D_{app}), is the summation of the Dahms-Ruff equation:[18-20]

$$D_{app} = D_{phys} + D_e = D_{phys} + \frac{k_{ex}\delta^2 C}{6} \qquad \text{(eqn. 1)}$$

where D_{phys} is the actual physical diffusion coefficient of the redox sites, D_e is the electron diffusion coefficient that describes the rates of electron transport. D_e has often been translated into k_{ex} , an electron self-exchange rate constant based on a hexagonal packing model in which δ is the equilibrium center-to-center distance between redox sites, C is the bulk concentration of redox sites, and 6 represents the theoretical number of directional electron hopping possibilities. The values of D_{PHYS} have in previous undiluted redox ionic liquid been shown to be much smaller than those of D_E; the general range of parameters in the phosphonium ionic liquids is similar and we presume here then that $D_{PHYS} << D_E$ in them.

The current study makes use of an ion association model in Marcus theory[21,22] and the related ion atmosphere relaxation model,[23] which has shown to be applicable to a wide range of redox ionic liquid systems.[12,15] The ion atmosphere relaxation model proposes that when an electron hops between oxidized and reduced species, as part of a diffusive charge transport process, the rate determining step for charge transport is the rearrangement of the counter anion to relax the coulombic dis-equilibrium caused by the electron motion. The ion atmosphere relaxation model has been demonstrated to account for electron transport rates in redox ionic liquids through comparisons of observed redox species' diffusion rates (D_{app}) to measurements of counter anion diffusivity (D_{cion}), and of their activation energy barriers.

These phosphonium materials serve to add to an already developing understanding of electron transfer and mass transport in semi-solid phases. Phosphonium ionic liquids present new and interesting challenges for electrochemistry in the solid state because of their reported ability to pack and even form liquid crystalline phases.[24] Although this report will not deal in matters of these materials liquid crystalline nature, it does show that these materials have some characteristic differences in the diffusion of these materials in the melt phase based on electrochemical studies. This study includes investigation of electron transport by examination of apparent diffusion and counter anion relaxation as well as investigation of any potential contribution from physical diffusion for a series of phosphonium ionic liquid materials (Figure 2.1).

2.2 Experimental

2.2.1 Chemicals and Reagents

Figure 2.1 The four samples used for the neat electrochemical study included two molecules with an alkyl chain linker between ferrocene and the phosphonium group, one with a hexafluorophosphate counter anion (A) and the other with a tosylate counter anion (B); and two molecules with an acyl linkage between the two, hexafluorophosphate counter anion (C) and tosylate (D).

A 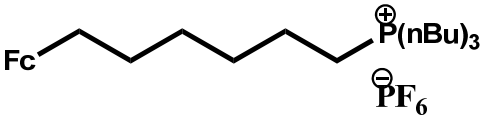
Fc
P(nBu)3
PF6

B 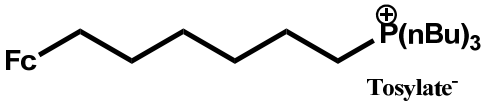
Fc
P(nBu)3
Tosylate-

C 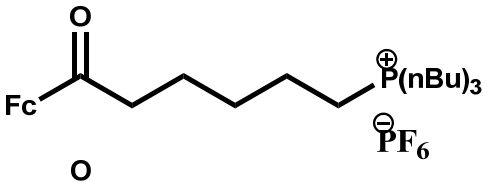
O
Fc
P(nBu)3
PF6

D 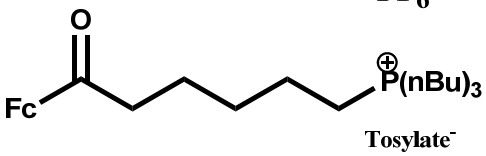
O
Fc
P(nBu)3
Tosylate-

All phosphonium ionic liquid samples were synthesized and furnished by Paul Ragogna's laboratory at the University of Western Ontario. All solvents and reagents were used with no further purification unless otherwise noted.

2.2.2 Synthesis

All synthetic manipulations were performed in an MBraun Labmaster 130 N_2 filled drybox and/or using standard Schlenk line techniques, unless otherwise indicated. Flash column chromatography was performed using (70-230 mesh ASTM) silica gel 60 and the thin layer chromatography (TLC) was carried out on silica gel 60 F_{254} TLC plates. All TLC and flash column chromatography was carried out using varying ratio of hexanes and acetone as indicated in the specific procedure. Solution NMR data were collected on a Varian Mercury 400 MHz using $CDCl_3$ as a solvent. The ^{31}P NMR spectra used 85% phosphoric acid referenced to 0 ppm. Electro-spray ionization mass spectrometry (ESI-MS) data was collected on a Micromass LCT Mass Spectrometer. Thermal Gravimetric Analysis (TGA) were determined on a Mettler Toledo TGA 851^e instrument. A 5-10 mg sample was heated at a rate of 10°C/min over a temperature range of 25 – 600°C. Ferrocene was purchased from Aldrich Chemical Co, twice sublimed and stored in the dry box. Oxalyl chloride, 3-bromopropanoic acid, 6-bromohexanoic acid, mercury chloride, zinc granules, aluminum trichloride and all other chemicals were purchased from Aldrich Chemical Co. and used as received, unless otherwise indicated. Common orgnic solvents were obtained from Caledon Laboratories and dried using the Innovative Technology Inc. Controlled Atmospheres Solvent Purification System, which utilizes dual-alumina columns. All dry solvents were stored in Strauss flasks over N_2 or stored in the drybox over 4Å molecular sieves. *n*-Butyl

phosphine and *n*-octyl phosphine were donated by Cytec Technology Corp. and used as received.

2.2.3 Synthesis of Fc-CO$(CH_2)_5$Br

At room temperature, a double-necked round bottom flask was charged with 6-bromohexanoic acid (21.0 mmol) in toluene (30 mL) and stirred under nitrogen, to which 1.2 equivalents of oxalyl chloride (3.17 g, 25.2 mmol) was added dropwise, followed by addtion of dimethylformamide (0.3 mL). Stirring was continued for 30 min and then for a further 90 min at 55 °C. The reaction mixture was cooled to r.t. and the toluene was removed *in vacuo*. A separate 250 mL round bottom was loaded with ferrocene (3.91 g, 21.0 mmol) in dry CH_2Cl_2 (40 mL) in the drybox. 1.2 equivalents of Aluminum trichloride (3.22 g, 24.2 mmol) was dissolved in dry CH_2Cl_2 (80 mL) in the drybox, transferred to the Schlenk line and was added to the 6-bromohexyl chloride under N_2. The resulting solution was added dropwise to a stirred (0 °C) ferrocene solution. The reaction mixture was allowed to warm to r.t. over 3 hours, and was washed with water (2 × 10 mL). The organic layer was separated, dried with $MgSO_4$, and the solvent was evaporated. The product was purified using a silica gel column with a 2.5% acetone in hexanes solution (4.36 g, 57%). ^{1}H NMR ($CDCl_3$, δ/ppm): 1.51 (m, 2H), 1.71 (q, 2H), 1.90 (q, 2H), 2.70 (t, 2H), 3.42 (t, 2H), 4.17 (s, 5H), 4.47 (t, 2H), 4.75 (t, 2H); ^{13}C NMR ($CDCl_3$, δ/ppm): 23.8, 28.3, 32.9, 24.0, 39.6, 69.5, 70.0, 72.4, 79.3; EI-MS $[M^+]$ = 362, $[M^+$-HBr] = 282, $[M^+$-$C_5H_{10}Br]$ = 213, $[M^+$-$(CO)C_5H_{10}Br]$ = 185.

2.2.4 Synthesis of Fc-$(CH_2)_6$Br

The reduction of **Fc-CO$(CH_2)_5$Br** followed the procedure used by Vogel et al. in the reducton of acylated ferrocene.[27] A 250 mL double-necked round bottom flask was charged with acylated ferrocene (**Fc-CO$(CH_2)_5$Br**) (0.908 g, 2.51 mmol) in toluene (10 mL). Fresh

Zn/Hg amalgum was prepared by stirring 2.5 g of Zn granules and 0.169 g of $HgCl_2$ in water (3.0 mL) and concentrated HCl (0.2 mL) and left to stir for 5 min. The aqueous supernatent was discarded. A mixture consisting of water (6 mL) and concentrated HCl (8 mL) was added to the amalgum, the acylated ferrocene mixture was promptly added dropwise, over five min. The reaction mixture was set to reflux for 18 h. Two aliquots (2 × 2 mL) of concentrated HCl were added to the mixture after 1 and 3 hours, respectively. The resulting mixture was allowed to cool to r.t., followed by addition of toluene (10 mL), and the organic layer was separated. The volatiles were removed *in vacuo* and the resulting liquid purified using a silica gel column with a 1.25% acetone in hexanes solution (0.637 g, 73%). ^{1}H NMR ($CDCl_3$, δ/ppm): 1.35 (m, 2H), 1.46 (m, 2H), 1.52 (m, 2H), 1.86 (q, 2H), 2.33 (t, 2H), 3.41 (t, 2H), 4.05 (s, 4H), 4.10 (t, 5H); ^{13}C NMR ($CDCl_3$, δ/ppm): 27.9, 28.6, 29.4, 30.9, 33.9, 66.8, 67.1, 67.8, 68.1, 68.2, 68.5, 89.1; EI-MS $[M^+]$ = 348, $[M^+$-HBr] = 268, $[M^+$-$C_5H_{10}Br]$ = 199.

2.2.5 General procedure for the preparation of ferrocene containing ILs with bromide anions

A 100 mL round bottom multi-necked flask was charged with a solution of the alkylated or acylated ferrocene (0.70 mmol) in dimethylformamide (5 mL). A solution containing 1.2 equivalents of the phosphine in DMF (10 mL) was added dropwise to the stirred ferrocene mixture. A reflux condenser was attached, and the reaction mixture heated to 70 °C under N_2. The reaction was monitored by ^{31}P NMR until no further change in the spectra was observed. The volatiles were removed *in vacuo* at 100 °C.

2.2.6 Synthesis of $[(n\text{-}Bu)_3P(CH_2)_5COFc]Br$

The reaction of acylated ferrocene (**$Fc\text{-}CO(CH_2)_5Br$**) (0.255 g, 0.702 mmol) and tributyl phosphine (0.164 g, 0.810 mmol) according to the general procedure afforded the

desired product with an isolated yield of (0.327 g, 83%). ^{1}H NMR ($CDCl_3$, δ/ppm): 0.95 (s, 9H), 1.51 (s, 18H), 1.74 (br s, 2H), 1.97 (br s, 2H), 2.36 (br s, 4H), 2.71 (br s, 2H), 4.15 (s, 5H), 4.47 (s, 2H), 4.75 (s, 2H); ^{13}C NMR ($CDCl_3$, δ/ppm): 13.4, 18.9, 19.4, 21.2, 23.5, 23.8, 24.1, 30.9, 39.1, 69.3, 69.8, 72.3; ^{31}P NMR ($CDCl_3$, δ/ppm): 35.100; ESI-MS [M^+] = 485, [M_2Br^+] = 1049; TGA: decomposition onset = 144.6 °C.

2.2.7 Synthesis of [(n-Bu)$_3$P(CH$_2$)$_6$Fc]Br

The reaction of alkylated ferrocene (**Fc-(CH$_2$)$_6$Br**) (0.284 g, 0.813 mmol) and trioctyl phosphine (0.181 g, 0.894 mmol) according to the general procedure afforded the desired product with an isolated yield of (0.219 g, 57%). ^{1}H NMR ($CDCl_3$, δ/ppm): 0.96 (m, 9H), 1.51 (m, 20H), 1.85 (br, 8H), 2.31 (t, 2H), 4.02 (s, 4H), 4.07 (s, 5H); ^{13}C NMR ($CDCl_3$, δ/ppm): 13.4, 18.9 (d), 19.2 (d), 21.7 (d), 23.7, 23.9, 28.6, 29.3, 30.5 (d), 30.7, 66.9, 67.9, 68.3; ^{31}P NMR ($CDCl_3$, δ/ppm): 34.819; ESI-MS [M^+] = 471; TGA: decomposition onset = 253.4 °C.

2.2.8 Synthesis of [(n-Bu)$_3$P(CH$_2$)$_6$Fc]PF$_6$ (A)

The reaction of [(*n*-Bu)$_3$P(CH$_2$)$_6$Fc]Br (1.60 g, 2.91 mmol) and 1.5 equiv. of $NaPF_6$ (0.734 g, 4.37 mmol) according to the general procedure afforded the desired product with an isolated yield of (1.238 g, 69%). ^{1}H NMR ($CDCl_3$, δ/ppm): 0.93 (m, 9H), 1.27 (m, 2H), 1.48 (m, 18H), 2.08 (m, 8H), 2.31 (t, 2H), 4.01 (s, 4H), 4.07 (s, 5H); ^{13}C NMR ($CDCl_3$, δ/ppm): 13.3, 18.1 (d), 18.4 (d), 21.5, 23.5, 23.7 (d), 28.6, 29.4, 30.4 (d), 30.8, 67.1, 68.1, 68.5, 76.7, 77.0, 77.2, 77.3; ^{31}P NMR ($CDCl_3$, δ/ppm): 33.887; ^{19}F NMR ($CDCl_3$, δ/ppm): -71.529, -73.426; ESI-MS [M^+] = 471, [$(M_2PF_6)^+$] = 1087; TGA: decomposition onset = 191.8 °C.

2.2.9 Synthesis of [(n-Bu)$_3$P(CH$_2$)$_5$COFc]PF$_6$ (B)

The reaction of compound [(n-Bu)$_3$P(CH$_2$)$_5$COFc]Br (0.79 g, 1.40 mmol) and 1.5 equiv. of $NaPF_6$ (0.353 g, 2.10 mmol) according to the general procedure afforded the desired product with an isolated yield of (0.530 g, 60%). ^{1}H NMR ($CDCl_3$, δ/ppm): 0.952 (m, 9H), 1.489 (m, 18H), 1.722 (m, 2H), 2.104 (m, 6H), 2.744 (t, 2H), 4.178 (s, 5H), 4.489 (s, 2H), 4.773 (s, 2H); ^{13}C NMR ($CDCl_3$, δ/ppm): 13.3, 18.2, 18.4, 18.7, 18.9, 21.4, 23.3, 23.5, 23.8, 23.9, 30.2, 30.3, 38.9; ^{31}P NMR ($CDCl_3$, δ/ppm): 33.961; ^{19}F NMR ($CDCl_3$, δ/ppm): -71.554, -73.449; ESI-MS [M^+] = 485; TGA: decomposition onset = 165.3 °C.

2.2.10 Synthesis of [(n-Bu)$_3$P(CH$_2$)$_6$Fc]OTs (C)

The reaction of compound [(n-Bu)$_3$P(CH$_2$)$_6$Fc]Br (0.69 g, 1.08 mmol) and ~2 equiv. of toluene sulphonic acid (0.328 g, 1.92 mmol) according to the general procedure afforded the desired product with an isolated yield of (0.492 g, 77%). ^{1}H NMR ($CDCl_3$, δ/ppm): 0.89 (t, 9H), 1.42 (d, 18H), 2.24 (m, 12 H), 2.278 (s, 2H), 4.01 (s, 4H), 4.05 (d, 5H), 7.07 (d, 2H), 7.73 (d, 2H); ^{13}C NMR ($CDCl_3$, δ/ppm): 13.3, 18.5 (d), 18.8 (d), 21.1, 21.6 (d), 23.6, 23.7 (t), 28.7, 29.3, 30.5 (d), 30.7, 67.3, 68.4, 68.8, 125.9, 128.2, 138.5, 144.3; ^{31}P NMR ($CDCl_3$, δ/ppm): 33.83; ESI-MS [M^+] = 471, [($M_2OTs)^+$] = 1113; TGA: decomposition onset = 308.5 °C.

2.2.11 Synthesis of [(n-Bu)$_3$P(CH$_2$)$_5$COFc]OTs (D)

The reaction of compound [(n-Bu)$_3$P(CH$_2$)$_5$COFc]Br (0.588 g, 1.04 mmol) and ~2 equiv. of toluene sulphonic acid (0.356 g, 2.08 mmol) according to the general procedure afforded the desired product with an isolated yield of (0.367 g, 56%). ^{1}H NMR ($CDCl_3$, δ/ppm): 0.915 (m, 9H), 1.452 (m, 18H), 1.539 (s, 2H), 1.686 (s, 2H), 2.287 (m, 7H), 2.700 (s, 2H), 4.154 (s, 5H), 4.470 (s, 2H), 4.748 (s, 2H), 7.094 (br s, 2H), 7.759 (br s, 2H); ^{13}C NMR ($CDCl_3$, δ/ppm): 13.302, 18.462, 18.935 (t), 21.244, 21.785 (d), 23.432, 23.775 (t), 24.003,

30.368 (d), 38.981, 35.402, 69.271, 69.767, 72.282, 78.852, 126.048, 128.381, 138.716, 204.358; ^{31}P NMR ($CDCl_3$, δ/ppm): 33.874; ESI-MS [M^+] = 485, [$(M_2OTs)^+$] = 1141; TGA: decomposition onset = 277.4 °C.

2.2.12 Dilute Solution Voltammetry

Cyclic voltammetry to inspect for general electrochemical behavior was performed on ca. 1.0 mM solutions of the phosphonium ionic liquids in dichloromethane or acetonitrile with 0.1 M tetrabutylamonium perchlorate as supporting electrolyte. The 20 mL glass vial cells contained 1.6 mm diameter Pt disk working, Pt mesh counter, and aqueous Ag/AgCl/0.1M NaCl reference electrodes, which were controlled using a CHI Instruments Electrochemical Workstation. Scan rates of 50, 100, and 200 mV/s were commonly employed for these voltammetry measurements.

2.2.13 Undiluted Ionic Liquid Electrochemistry

The electrochemistry of non-dilute ionic liquids is carried out using a setup that has been described previously for redox polyether hybrids.[25] Approximately 15-20 mg of an ionic liquid is drop-cast using dichloromethane as the solvent onto the surface of a homemade four electrode assembly consisting of a 25µm diameter Pt micro-disk working electrode, Ag quasi-reference, and two 0.4 mm diameter Pt disk electrodes. The two 0.4mm Pt disk electrodes are used together for 2-electrode AC impedance spectroscopy measurements, and one is used as a counter electrode for 3-electrode voltammetry. All four electrodes are placed in a 0.25 inch stainless steel tube and sealed with an epoxy resin. After drop-casting, samples are placed in the temperature controlled chamber described[25] in the reference above and held under vacuum at approximately 75 ºC for at least 12 hours to assure complete dryness. Both voltammetry and AC impedance measurements were performed in a

Faraday cage using a CH Instruments Electrochemical Workstation. Samples were kept under vacuum for the duration of the experiments and measurements were taken at various temperatures with time given between temperature changes to assure equilibration.

AC impedance spectroscopy measurements were taken over a range of frequencies from 1 Hz to 100 KHz, with a 0 V DC bias, 2 second quiet time, and a 5 mV to 400 mV amplitude. Ionic conductivity was calculated from the real x-axis intercept found in a Nyquist plot. Cyclic voltammetry was performed with a 30 second quiet time, 10 mV/s scan rate, with a varied potential range depending on the redox potentials of the specific material and the amount of Ohmic drop observed. The cyclic voltammogram of each material at each temperature was used to determine the potential step used (approximately 300-400mV overstep beyond E^0) in chronoamperometry. Chronoamperometry was performed with a 400 second pulse width and a 450 to 600 second quiet time.

2.3 Results and Discussion

2.3.1 Dilute Solution and Undiluted Voltammetry

Both dilute solution and undiluted (neat) voltammetry was conducted to inspect the samples for electrochemical purity and to evaluate the E^o for each sample for use in chronoamperometric measurements. The E^o for **A** was found to be 445mV (vs. Ag/AgCl) and **B** was found to be 732mV (vs. Ag/AgCl), which is a significant shift to more positive potentials do to the strongly electron withdrawing nature of the carbonyl group directly attached to the cyclopentadienyl ring of ferrocene (2.2 A). The solution voltammetry was also compared to solution voltammetry of analogous non-ionic liquid ferrocene samples ethylferrocene (476mV) and acetylferrocene (782mV), and it was clearly observed that, as

Figure 2.2 A) Example solution voltammetry of Samples [Fc-C_6-P$(Bu)_3$][PF_6] and [Fc-COC_5-P$(Bu)_3$][PF_6] showing the large diifference in E^o (444mV for [Fc-C_6-P$(Bu)_3$][PF_6] and 732mV for [Fc-COC_5-P$(Bu)_3$][PF_6]) between the two types of linker (alkyl and acyl). B) Comparison of [Fc-C_6-P$(Bu)_3$][PF_6] to its non-IL counterpart ethylferrocene and [Fc-COC_5-P$(Bu)_3$][PF_6] to its counterpart acetylferrocene. The E^0 values of the related linker species vary by very little.

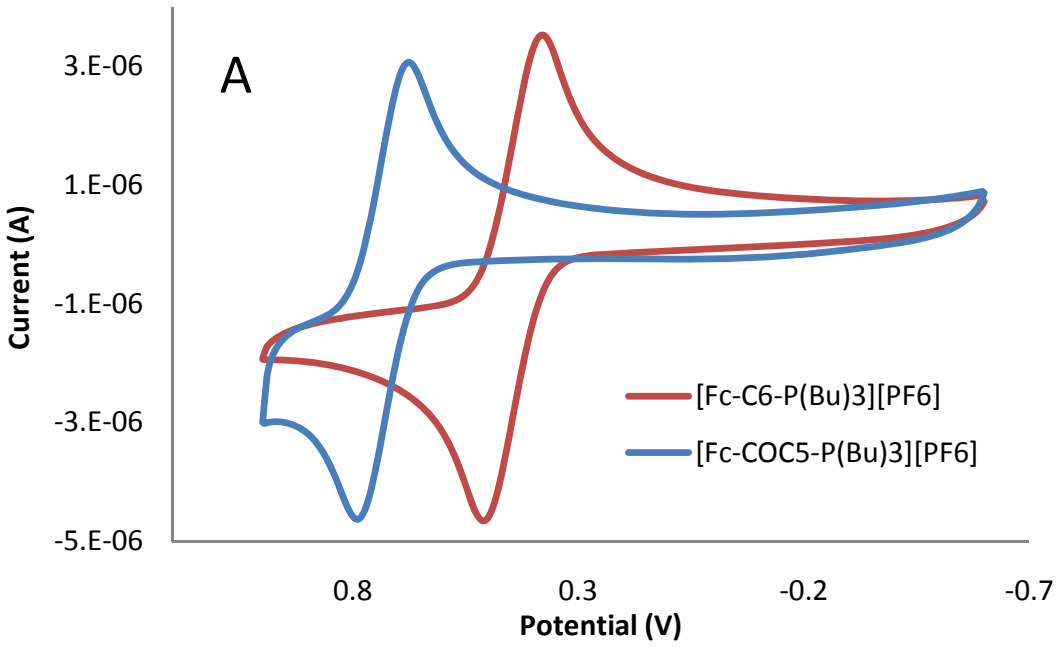
A
3.E-06
1.E-06
-1.E-06
-3.E-06
-5.E-06
Current (A)
0.8
0.3
-0.2
-0.7
Potential (V)
[Fc-C6-P(Bu)3][PF6]
[Fc-COC5-P(Bu)3][PF6]

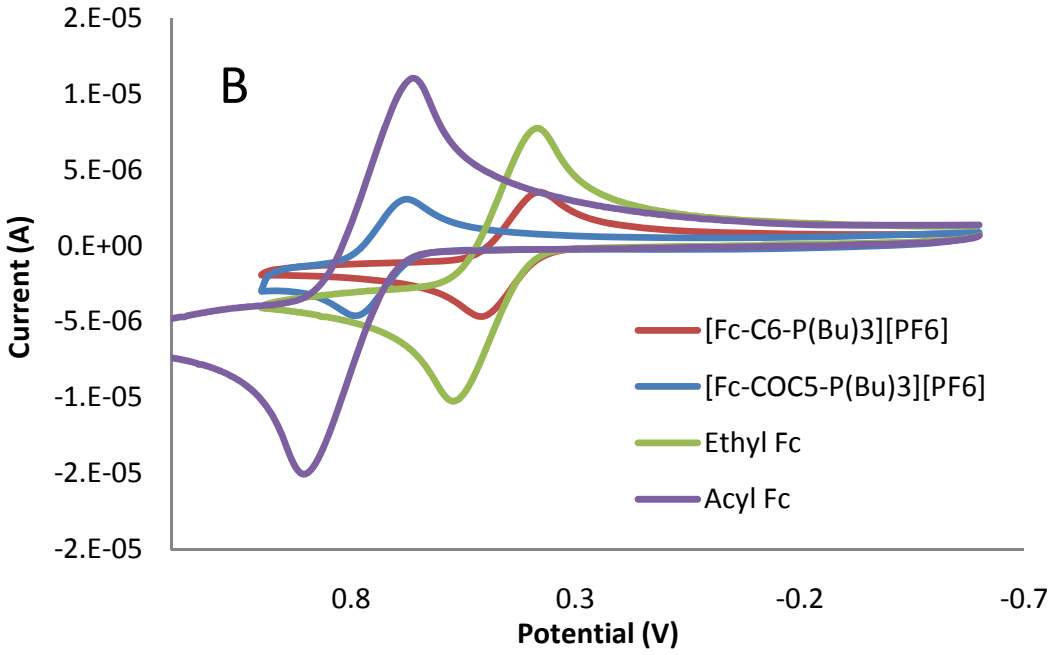
B
2.E-05
1.E-05
5.E-06
0.E+00
-5.E-06
-1.E-05
-2.E-05
-2.E-05
Current (A)
0.8
0.3
-0.2
-0.7
Potential (V)
[Fc-C6-P(Bu)3][PF6]
[Fc-COC5-P(Bu)3][PF6]
Ethyl Fc
Acyl Fc

expected, there are no distinct differences in the solution electrochemistry of these modified phosphonium ionic liquid molecules and their non-ionic liquid counterparts (2.2 B).

Melt voltammetry was also analyzed to assure that the materials were not degraded in any way by the drop-casting procedure, and also serves as an illustrative depiction of how the differences in electrochemical behavior are unchanged in the neat system; aside from the large decrease in sample mobility (Fig 2.3-A) and the temperature dependence of this mobility loss (Fig 2.3-B). Due to the necessary use of a silver quasi-reference in the melt electrochemistry setup, the E^o values cannot be assumed to be accurate and are not mentioned nor compared with those of solution measurements.

2.3.2 Electron Transport

Cyclic voltammograms (CV) of undiluted samples of three of the four phosphonium ionic liquids are shown in Figure 2.2. (The fourth sample (Figure 2.1D) was overtly highly viscous and transport data could not be obtained even at elevated temperatures). As noted above, the oxidation and reduction waves seen, and the difference in formal potential between the alkyl and acyl linkage units, are consistent with the well-known $Fc^{+/0}$ couple including that seen in previously studied melt phases.[8] All of the CVs exhibit substantial peak potential separations (ΔE_{PEAK}) indicative of very modest levels of ionic conductivity (even given the use of a 25μm dia. Pt microelectrode). The ΔE_{PEAK} values vary substantially with variation in temperature (Figure 2.2B); the melts are of course much more fluid at elevated temperatures. While the levels of uncompensated resistance are large, they are not unprecedented for undiluted ionic liquids. Besides an increase in ΔE_{PEAK} values, there is also a decrease in current with decreasing temperature (Figure 2.2B); this is qualitatively expected

Figure 2.3 Cyclic voltammetry highlights the differences in E_0 between having an alkyl or acyl linkage to ferrocene, and also the effect of counter anion on resistance when the melts are neat (A), which was previously described by Harper et al.[10] as an ion-pairing effect that may in part be responsible for the reduced conductivity; the effect of temperature change on the melt resistance is also quite clear (B).

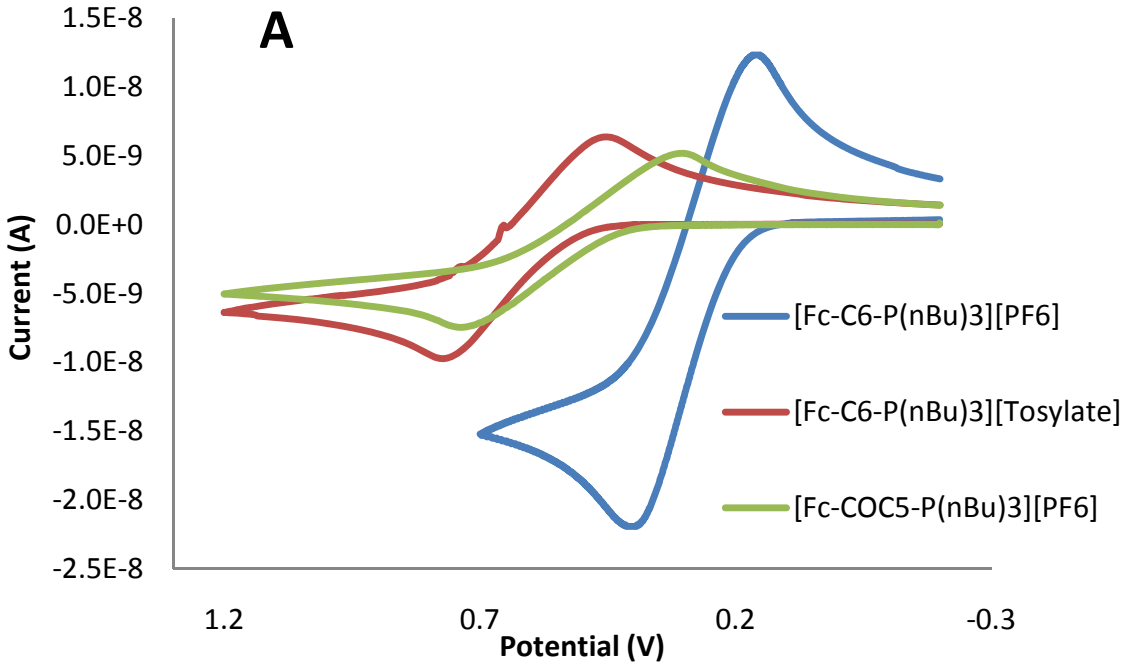
A
1.5E-8
1.0E-8
5.0E-9
0.0E+0
-5.0E-9
-1.0E-8
-1.5E-8
-2.0E-8
-2.5E-8
Current (A)
1.2
0.7
0.2
-0.3
Potential (V)
[Fc-C6-P(nBu)3][PF6]
[Fc-C6-P(nBu)3][Tosylate]
[Fc-COC5-P(nBu)3][PF6]

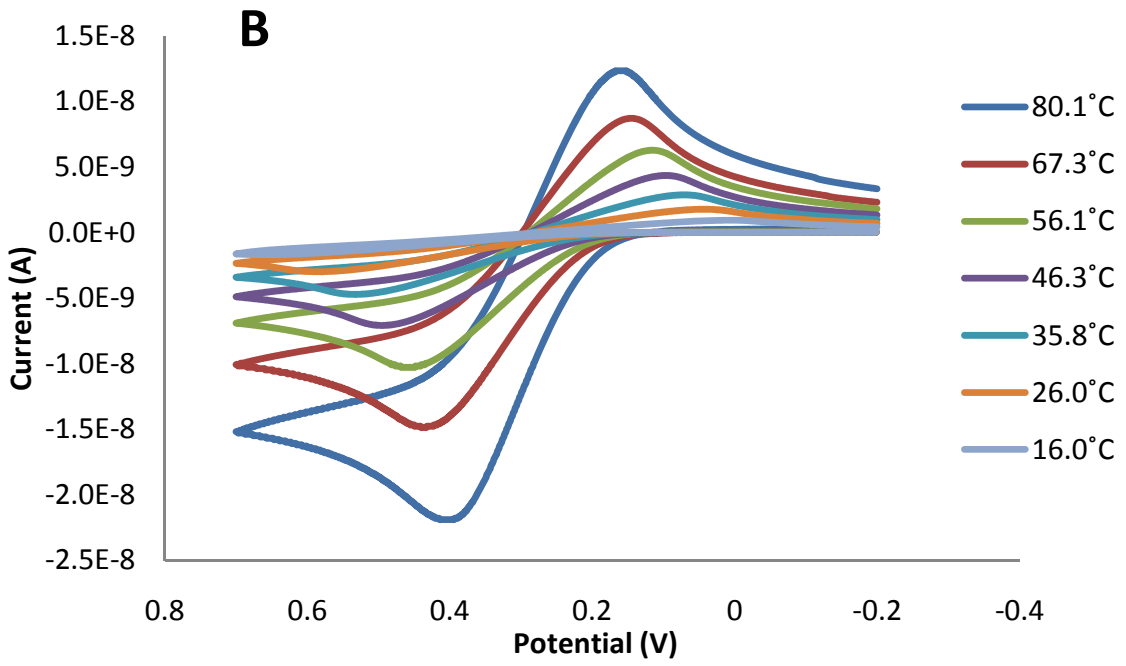
B
1.5E-8
1.0E-8
5.0E-9
0.0E+0
-5.0E-9
-1.0E-8
-1.5E-8
-2.0E-8
-2.5E-8
Current (A)
0.8
0.6
0.4
0.2
0
-0.2
-0.4
Potential (V)
80.1˚C
67.3˚C
56.1˚C
46.3˚C
35.8˚C
26.0˚C
16.0˚C

since lowered temperature causes a decrease in fluidity and a consequent decrease in charge transport coefficients and ionic mobilities.

Chronoamperometric potential steps (to values calculated to overwhelm ΔE_{PEAK} effects) were employed to measure the apparent diffusion coefficient (D_{app}) in the ionic liquid melts. Values of D_{APP} (Table 2.1) are obtained from current vs. $t^{-1/2}$ plots[26] of the current-time responses. As noted above, by analogy to previous experience,[9-16] we assume that physical diffusion (D_{phys}) is very slow given both the steric bulk of the phosphonium cation and the melt viscosity, so that electron hopping (D_E) is the primary source of charge diffusion. This assumption has been amply justified by experimental measurements of D_{phys} for other similar redox ionic liquid species.[8]

By assuming a cubic lattice model for the system it is possible to derive a value for the apparent rates of electron self-exchange (k_{EX}) from the calculated D_e value through the extension of the Dahms-Ruff equation shown above. These, given in Table 2.1, can be plotted as $\ln(k_{ex})$ against reciprocal temperature (Arrhenius plot) to derive the heat of activation for the electron transport parameter ($E_{a,et}$) from the slope of the derived Arrhenius equation (Table 2.1, Figure 2.4)

$$\ln(k_{EX}) = \frac{-E_{a,et}}{R}\frac{1}{T} + \ln(A) \qquad \text{(eqn. 2)}$$

where R is the ideal gas constant and A is the pre-exponential factor of the Arrhenius equation. Because the electron self-exchange is symmetrical, the entropy of activation is zero and the activation barrier energies are also free energies of activation.

The k_{EX} and $E_{A,ET}$ values have been corrected for coupling between the counterion and electron motions. This is an electronic migration effect[27] and its details have been amply

Table 2.1 The comprehensive data for all three samples described in this paper are given, and it is easily seen that there are strong similarities between them and the previously described [Fc-C_6-Im-Bu][PF_6] system.[7] E_A is calculated from the slope of an Arrhenius plot (ln$k$ vs. 1/T) using k_{EX} and $k_{EX,corr}$ respectively for EA and EA,corr.

Sample	Temp (K)	D_{APP} (cm^2/s) ($x10^{-9}$)	k_{EX} (M^{-1} s^{-1}) ($x10^5$)	$k_{EX,corr}$ (M^{-1} s^{-1}) ($x10^5$)	$E_{A,ET}$ (KJ/mol)	$E_{A,ET,corr}$ (KJ/mol)	D_{CION} (cm^2/s) ($x10^{-10}$)	$E_{A,ION}$ (KJ/mol)
[Fc-C6-P(nBu)$_3$][PF_6]	353	15.3	52.3	41.7	**48**	**47**	21.5	**47**
	340	8.3	28.4	21.9			11.4	
	329	5.1	17.4	13.5			6.7	
	319	2.8	9.5	7.6			3.9	
	309	1.5	5.1	4.0			2.1	
[Fc-C6-P(nBu)$_3$][Tosylate]	350	3.5	21.7	13.4	**65**	**52**	8.3	**40**
	339	2.4	13.5	7.7			5.3	
	329	1.2	4.0	3.5			3.4	
	319	0.7	2.5	2.2			2.2	
	309	0.4	1.2	1.1			1.4	
[Fc-COC5-P(nBu)$_3$][PF_6]	350	6.4	25.9	16.0	**55**	**53**	4.1	**65**
	339	4.0	16.1	9.3			2.1	
	329	2.7	11.0	5.9			1.0	
	319	1.3	5.2	2.8			0.5	
	309	0.5	2.0	1.2			0.2	
*[Fc-C_6-Im-Bu][PF_6]	298	10.0	32.0	32.0	**56**	**56**	1.7	**55**

Figure 2.4 The nearly identical slopes that are found in the dual k_{ex} (slope = -5.71)and D_{cion} (slope = -5.67)Arrhenius plots for sample A are indicative of an ion-atmosphere relaxation dominated electron exchange system as described above.

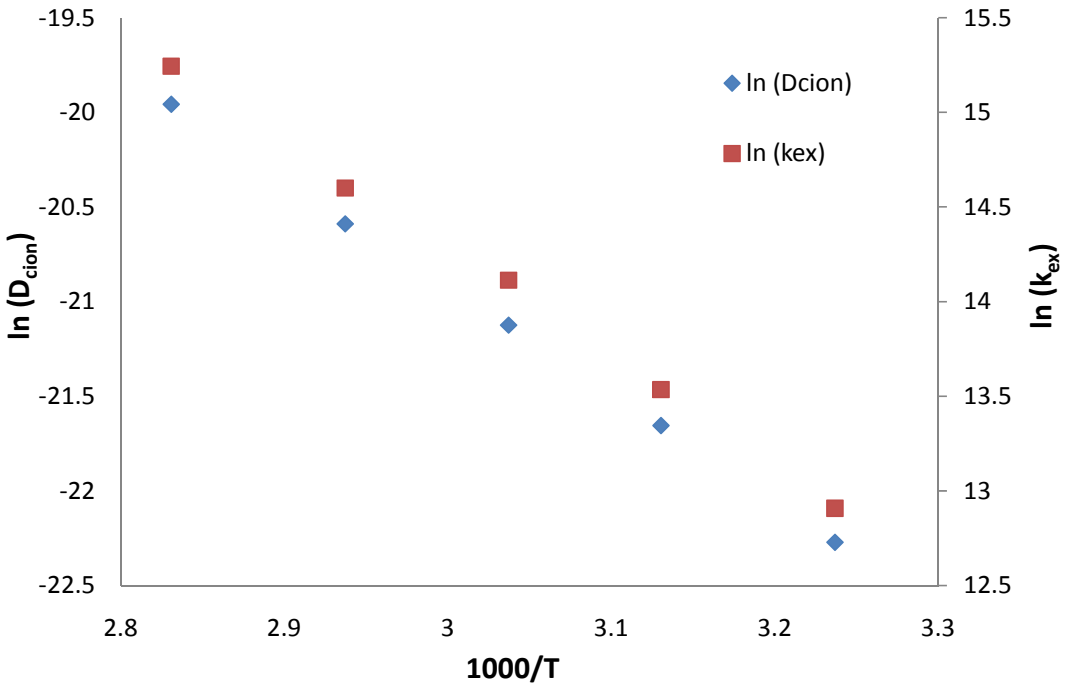
-19.5
-20
-20.5
-21
-21.5
-22
-22.5
15.5
15
14.5
14
13.5
13
12.5
2.8
2.9
3
3.1
3.2
3.3
1000/T
ln (Dcion)
ln (kex)
ln (Dcion)
ln (kex)

discussed.[10] The value corrections described here are meant to compensate for electronic migration effects, which are the result of D_e (D_{app}) values that are much larger than the counterion diffusion coefficient D_{cion}. This can result in an electric field gradient that can cause accelerated electron hopping and a larger than anticipated D_e value. Saveant et al. published a relatively straight forward method to correct D_e values for the electronic migration effects.[27] Table 2.2 shows the initial D_{app} and D_{cion} values, some of the factors ($\log(i/i^0)$) required to perform corrections for electronic migration effects,[27] and finally the first $D_{app,corr}$ values. A plot of uncorrected values and corrected values (Figure 2.5) shows that there is a substantial difference in some samples and not as large a difference in others. However, for each sample there is an obvious decrease in the value of D_e when corrected, as expected due to the large differentiation in D_e and D_{cion} observed from measured data. This effect is not unprecedented, and has previously been seen in every electroactive IL sample studied to date where corrections have been previously used very effectively.[8-16] This may be the result of different counterions having very different mobilities and consequentially more or much less problem with migration affects in the uncorrected D_{app} values. As seen in Table 2.1, the electronic migration correction is generally a modest factor in terms of energy of activation (E_A).

2.3.3 Counterion Transport Rates

Testing the ion atmosphere relaxation model that has been successfully applied to other ionic liquid systems[10,13,16] requires measurement of the physical diffusivity of the melts' counterions. The counterion diffusion coefficient (D_{cion}) can be calculated using the Nernst-Einstein equation where z, D, and C are charge, diffusion coefficient, and concentration of

Table 2.2 The initial D_{app} and D_{cion} values are given along with the other required electron migration correction factors and calculations.[27] The factors are fully outlined and explained by Saveant et al., and are used in conjunction with plots of these factors in relationship to measured currents (i and $i°$) and D_{cion}/D_{app} values.[27]

Sample	Temp	D_{app}	D_{cion}	D_{cion}/D_{app}	$\log(D_{cion}/D_{app})$	log(i/i°)	$D_{app(1st\ Corr)}$	$D_{cion}/D_{app(1corr)}$
[Fc-C6-P(nBu)3][PF6]	353	1.5E-08	2.2E-09	0.14	-0.84	0.10	**1.2E-08**	0.18
	340	8.3E-09	1.1E-09	0.13	-0.88	0.11	**6.4E-09**	0.17
	329	5.1E-09	6.7E-10	0.13	-0.88	0.11	**3.9E-09**	0.17
	319	2.8E-09	3.9E-10	0.14	-0.85	0.10	**2.2E-09**	0.18
	309	1.5E-09	2.1E-10	0.14	-0.85	0.10	**1.2E-09**	0.18
[Fc-C6-P(nBu)3][Tos]	350	3.5E-09	8.3E-10	0.24	-0.63	0.08	**3.0E-09**	0.28
	339	2.4E-09	5.3E-10	0.22	-0.66	0.08	**2.0E-09**	0.26
	329	1.2E-09	3.4E-10	0.29	-0.54	0.07	**1.0E-09**	0.33
	319	7.4E-10	2.2E-10	0.30	-0.53	0.06	**6.4E-10**	0.34
	309	3.7E-10	1.4E-10	0.38	-0.42	0.05	**3.3E-10**	0.43
[Fc-COC5-P(nBu)3][PF6]	350	6.4E-09	4.1E-10	0.06	-1.19	0.21	**3.9E-09**	0.10
	339	4.0E-09	2.1E-10	0.05	-1.28	0.24	**2.3E-09**	0.09
	329	2.7E-09	9.5E-11	0.04	-1.45	0.27	**1.4E-09**	0.07
	319	1.3E-09	4.7E-11	0.04	-1.44	0.27	**6.9E-10**	0.07
	309	5.0E-10	2.1E-11	0.04	-1.38	0.25	**2.8E-10**	0.07

Figure 2.5 Comparison of corrected and uncorrected values reveals an obvious electronic migration effect present in the sample. Each sample shows higher D_e (D_{app}) values prior to correction.

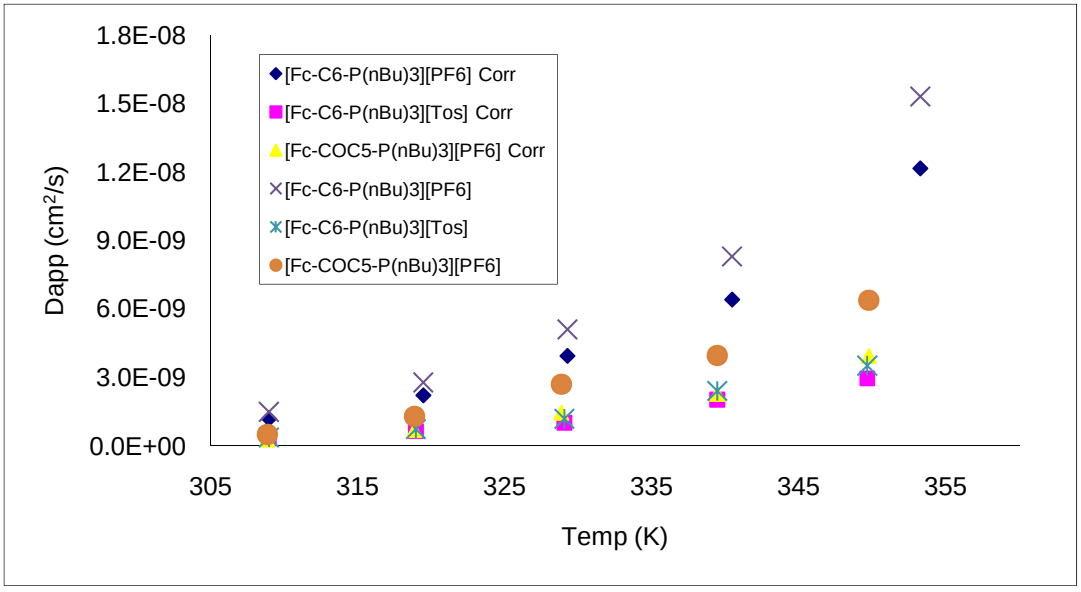
1.8E-08
1.5E-08
1.2E-08
9.0E-09
6.0E-09
3.0E-09
0.0E+00
Dapp (cm²/s)
305
315
325
335
345
355
Temp (K)
[Fc-C6-P(nBu)3][PF6] Corr
[Fc-C6-P(nBu)3][Tos] Corr
[Fc-COC5-P(nBu)3][PF6] Corr
[Fc-C6-P(nBu)3][PF6]
[Fc-C6-P(nBu)3][Tos]
[Fc-COC5-P(nBu)3][PF6]

the noted species respectively, F is Faraday's constant and σ_{ion} is the measured ionic conductivity for the undiluted ionic liquid.[28]

$$\sigma_{ion} = \frac{F^2}{RT}[z_{Fc}^2 D_{Fc} C_{Fc} + z_{counterion}^2 D_{counterion} C_{counterion}] \qquad \text{(eqn. 3)}$$

We assume that the diffusivity of the bulky phosphonium cation (D_{Fc}) is negligible in comparison to that of the two smaller nimble anions. Thus, measurement of σ_{ion} provides a path to calculation of the counterion D_{cion}. The ionic conductivities (σ_{ion}) were measured using AC impedance (Figure 2.6) using an electrode specific cell constant, and are given in Table 2.1. The collective D_{cion} values can then be applied to an Arrhenius type plot similar to that for k_{EX}, and the activation energy of anion atmosphere rearrangement ($E_{a,ion}$) then be calculated.

The collected electron transport and counterion diffusivity data in Table are fully consistent with the ionic atmosphere relaxation model developed previously.[12,15,23] Key points are that a) the values of D_{APP} (= D_E) and D_{CION} are numerically similar, b) the values of activation barrier energies—while more scattered—are also reasonably similar, and c) a log-log comparison (Figure 2.7A) of numerical values of $k_{EX,CORR}$ (proportional to corrected values of D_{app}) gives correlations with near unity slopes and that agree with a collective plot (solid line average in Figure 2.7A and detailed in Figure 2.7B) of previous data on other redox ionic liquid systems. Figure 2.7B contains data from widely disparate redox couples, including ferrocene, cobalticenium, cobalt poly-pyridine complexes, Ru poly-pyridine complexes, and examples plasticized under high pressure CO_2. This disparate group of redox couples is "leveled" to common values of apparent k_{EX} because the apparent, net electron transfer is a *transport* rate controlled by the redistribution of charge-compensating counterions subsequent to electron transfer.

Figure 2.6 Sample AC impedance plot for sample A ([Fc-C_6-P(nBu)$_3$][PF_6]). Measurement was taken as a neat (solvent free sample) under vacuum with temperature controlled at 76°C.

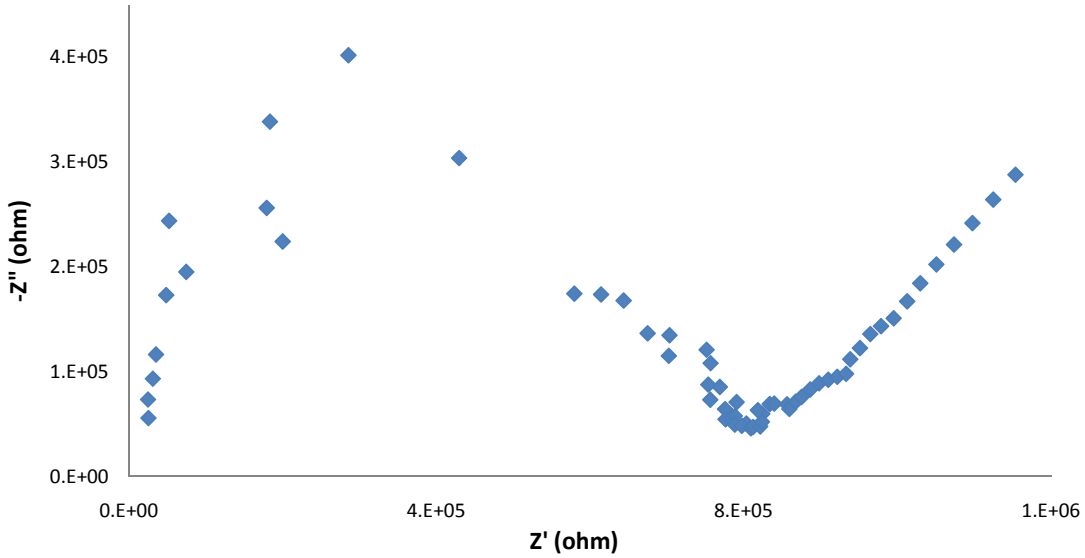
4.E+05
3.E+05
2.E+05
1.E+05
0.E+00
-Z'' (ohm)
0.E+00
4.E+05
8.E+05
1.E+06
Z' (ohm)

Figure 2.7 The plot of log($k_{ex,corr}$) vs. log(D_{cion}) further illustrates the relationship between these two measured electron transfer parameters. A) The "Slope of all Samples" is the average slope of many different types of redox-functionalized ionic liquids studied over the course of many years[7-15,18,20] (seen in B) and the slope of each new sample can be found in (A) legend. B) Taken specifically from Harper et al.[10] The gray box highlights the region that (A) is taken from and enlarged to show detail.

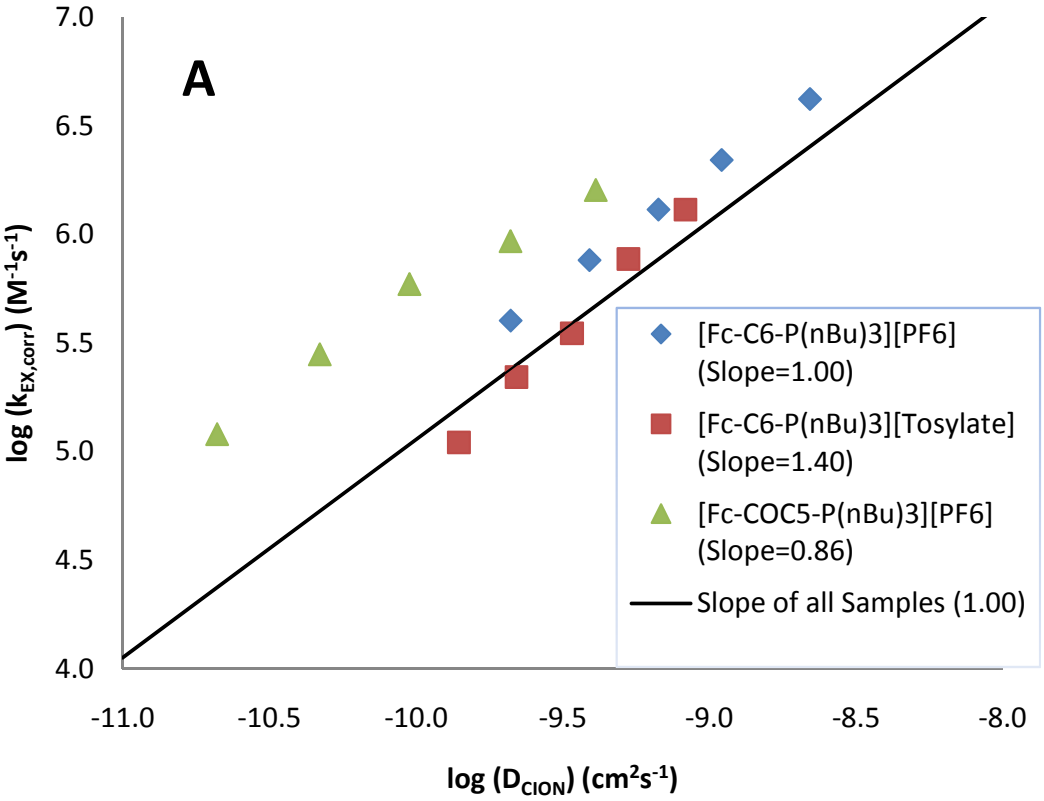
A
7.0
6.5
6.0
5.5
5.0
4.5
4.0
-11.0
-10.5
-10.0
-9.5
-9.0
-8.5
-8.0
log (k_EX,corr) (M^-1 s^-1)
log (D_CION) (cm^2 s^-1)
[Fc-C6-P(nBu)3][PF6] (Slope=1.00)
[Fc-C6-P(nBu)3][Tosylate] (Slope=1.40)
[Fc-COC5-P(nBu)3][PF6] (Slope=0.86)
Slope of all Samples (1.00)

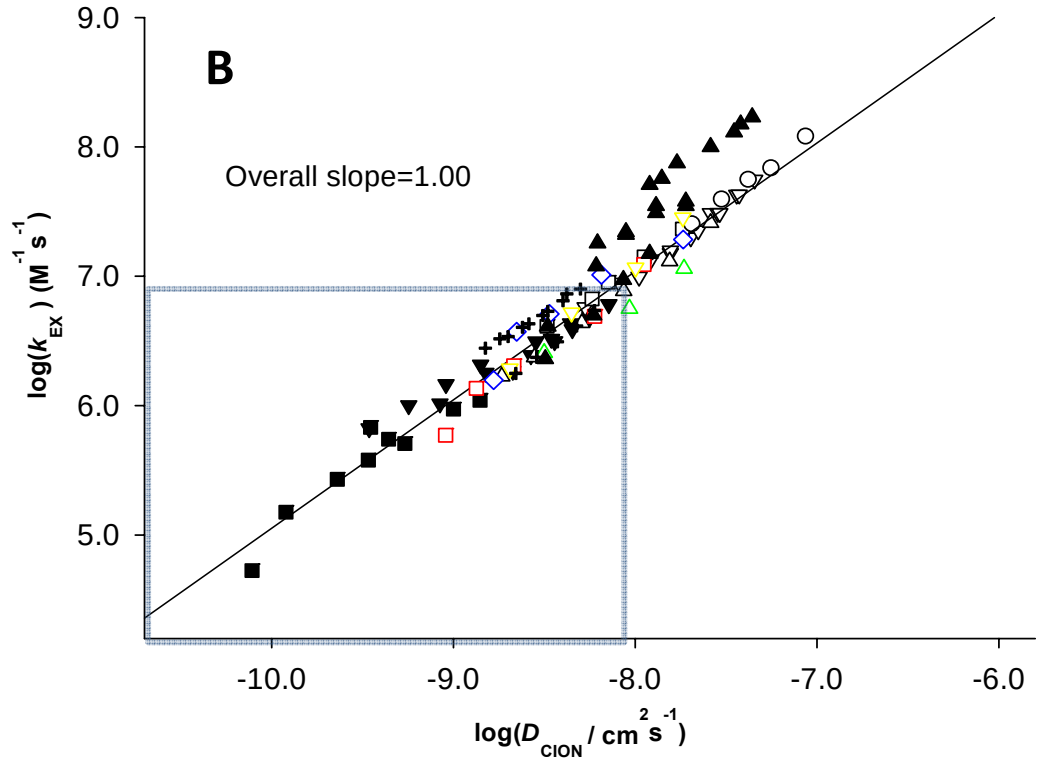
B
Overall slope=1.00
9.0
8.0
7.0
6.0
5.0
-10.0
-9.0
-8.0
-7.0
-6.0
log(k_EX) (M^-1 s^-1)
log(D_CION / cm^2 s^-1)

2.4 Conclusion

These phosphonium ionic liquids exhibit thermodynamic and kinetic behavior that agree with other previously studied redox functionalized ionic liquids in a neat environment. These materials do display a correlation between their apparent charge transport diffusion as measured by chronoamperometry and their counterion diffusion as measured by AC impedance. This correlation has been shown to be indicative of the ion atmosphere relaxation model, and these species do appear to have their electron exchange limited by counterion relaxation.

References

(1) Tsuda, T.; Hussey, C.L. *Interface* **2007**, Spring, 42-49.

(2) Lopes, J. N. C.; Gomes, M. F. C.; Padua, A. A. H. *J. Phys. Chem. B* **2006**, *110*, 16816-16818.

(3) Canongia Lopes, J. N.; Padua, A. A. H. *J. Phys. Chem. B* **2006**, *110*, 19586-19592.

(4) Silvester, D. S.; Aldous, L.; Hardacre, C.; Compton, R. G. *J. Phys. Chem. B* **2007**, *111*, 5000-5007.

(5) Ye, C.; Shreeve, J. n. M. *J. Phys. Chem. A* **2007**, *111*, 1456-1461.

(6) Lynden-Bell, R. M. *J. Phys. Chem. B* **2007**, *111*, 10800-10806.

(7) Rickert, P. G.; Antonio, M. R.; Firestone, M. A.; Kubatko, K.-A.; Szreder, T.; Wishart, J. F.; Dietz, M. L. *J. Phys. Chem. B* **2007**, *111*, 4685-4692.

(8) Balasubramanian, R.; Wang, W.; Murray, R. W. *Journal of the American Chemical Society* **2006**, *128*, 9994-9995.

(9) Harper, A. S.; Lee, D.; Crooker, J. C.; Wang, W.; Williams, M. E.; Murray, R. W. *J. Phys. Chem. B* **2004**, *108*, 1866-1873.

(10) Harper, A. S.; Leone, A. M.; Lee, D.; Wang, W.; Ranganathan, S.; Williams, M. E.; Murray, R. W. *J. Phys. Chem. B* **2005**, *109*, 18852-18859.

(11) Leone, A. M.; Brennaman, M. K.; Tibodeau, J. D.; Papanikolas, J. M.; Murray, R. W.; Thorp, H. H. *J. Phys. Chem. B* **2003**, *107*, 6469-6473.

(12) Leone, A. M.; Hull, D. O.; Wang, W.; Thorp, H. H.; Murray, R. W. *J. Phys. Chem. A* **2004**, *108*, 9787-9793.

(13) Leone, A. M.; Tibodeau, J. D.; Bull, S. H.; Feldberg, S. W.; Thorp, H. H.; Murray, R. W. *Journal of the American Chemical Society* **2003**, *125*, 6784-6790.

(14) Leone, A. M.; Weatherly, S. C.; Williams, M. E.; Thorp, H. H.; Murray, R. W. *Journal of the American Chemical Society* **2001**, *123*, 218-222.

(15) Ranganathan, S.; Murray, R. W. *J. Phys. Chem. B* **2004**, *108*, 19982-19989.

(16) Wang, W.; Lee, D.; Leone, A. M.; Murray, R. W. *Chem. Phys.* **2005**, *319*, 126-135.

(17) Forsyth, S. A.; Pringle, J. M.; MacFarlane, D. R. *Australian Journal of Chemistry* **2004**, *57*, 113-119.

(18) Dahms, H. *J. Phys. Chem.* **1968**, 72, 362.

(19) Ruff, I.; Friedrich, V.J. *J. Phys. Chem.* **1971**, 75, 3297.

(20) Majda, M. In *Molecular Design of Electrode Surfaces*; Murray, R.W., Ed.; John Wiley & Sons: New York, **1992**.

(21) Marcus, R.A.; *Discuss. Faraday Soc.* **1960**, 29, 21-31.

(22) Marcus, R.A. *J. Phys. Chem. B* **1998**, 102, 10071-10077.

(23) Carbonell, E.; Andres, J.L.; Lledos, A.; Duran, M.; Bertran, J. *J. Am. Chem. Soc.* **1988**, 110, 996-1001.

(24) Chen, H.; Kwait, D. C.; Goenen, Z. S.; Weslowski, B. T.; Abdallah, D. J.; Weiss, R. G. *Chemistry of Materials* **2002**, *14*, 4063-4072.

(25) Lee, D.; Hutchison, J. C.; Leone, A. M.; DeSimone, J. M.; Murray, R. W. *Journal of the American Chemical Society* **2002**, *124*, 9310-9317.

(26) Bard, A.J.; Faulkner, L.R. *Electrochemical Methods: Fundamentals and Applications*, 2nd ed.; Wiley and Sons: New York, 2001.

(27) Andrieux, C. P.; Saveant, J. M. *Journal of Physical Chemistry* **1988**, *92*, 6761-6767.

(28) Lee, D.; Harper, A. S.; DeSimone, J. M.; Murray, R. W. *Journal of the American Chemical Society* **2003**, *125*, 1096-1103.

CHAPTER 3

SYNTHESIS OF REDOX FUNCTIONALIZED DENDRIMER BASED IONIC LIQUIDS

3.1 Introduction

Dendrimers, like ionic liquids, are a relatively new class of chemicals that were first synthesized in 1978 by Vogtle et al.[1] whose procedure is now referred to as a divergent synthesis, which consists of a series of repetitive iterations of the same synthetic procedure where each step produces a new level or generation of the molecule. Denkewalter et al. went on to patent a synthesis of L-lysine based dendritic structures a few years later in the early 80's.[2] It is, however, fair to say that dendrimers were popularized more recently by Tomalia's synthesis of polyamidoamine (PAMAM),[3,4] which was relatively easy to make as well as easy to functionalize. Other early examples of divergently synthesized molecules that had an impact on the field include Newkome's "arborol" synthesis and the poly(propylene imine) molecules produced by both Mülhaupt[5] and de Brabander.[6] The convergent type of synthesis was first introduced by Fréchet[7,8] in 1990 with his work on aromatic polyether dendrimers and later the same convergent synthesis was used by Moore[9-12] to produce phenylacetylene dendrimers.

While Dendrimers have proven to be very interesting materials to work with and study, they have been somewhat plagued by difficulties with purity and in characterization. Bosman et al.[13] points out many important problems with dendrimers that have proven to be

sticking points over the years such as not knowing dendrimer shapes in solution and on dry surfaces, and most importantly the fact that statistical defects in dendrimers are an insurmountable reality. The example given in Bosman et al. is that a reaction with an average selectivity of 99.5% will result in a dendrimer product that is only 29% defect free fifth generation dendrimer (64 end groups: 248 reactions at .995 gives $.995^{248} = .288$). Bosman also points out that the difficulty in characterizing these materials is that techniques such as NMR (nuclear magnetic resonance) only show averages for bulk materials, and it is very easy to not notice a few defects out of many in large (e.g. fifth generation) structures. ESI (electrospray ionization) and MALDI (matrix assisted laser desorption ionization) mass spectrometry have proven very effective for dendrimer characterization, but has limitations for what dendrimers are able to be sprayed well for analysis. Poly(propylene imine)[14] (PPI) and poly amido amine[15] (PAMAM) have both shown to be easily characterizable by ESI-MS due to their polar and basic natures.

There has already been a fair amount of work done in examining the behavior of redox active species attached to dendrimer cores. Notably, Barron et al. looked at $Ru(bpy)_3^{2+}$ species as pendant species on PAMAM dendrimer backbones and looked at the effect of having multiple electrochemiluminescent (ECL) species on a single molecule.[16] Despite a negative result, ECL decreases with increasing groups on the same molecule, this finding was important in showing the limitations that dendrimers have in terms of stacking chemical reactions (e.g. it is also well known that dendrimers with multiple catalytic groups also show a decrease in catalytic activity). Another study of interest is that of Takada et al. that examined a series of diaminobutane based dendrimers that had been funtionalized with peripheral electroactive ferrocene groups.[17] This study mostly examined the molecules as

films because it was found that they formed films very easily at a potential of 0V, and even more so at oxidizing potentials due to the lack of ferrocenium solubility in the methylene chloride solvent.

The findings also included the observation that the dendrimer structure tended to flatten out on the electrode surface and that, although in appearance the ferrocene groups all oxidize and reduce at the same potential, the ferrocene groups actually have very tiny differences in redox potential. An extension of this study by Casado et al. (an author of the previous paper) took similar dimaminobutane poly(propyleneamine) dendrimers and ferrocene functionalized them as before, but also added an azo-crown ether functionalization to the periphery.[18] The idea is an interesting one regarding using dendrimers for ion sensing where the crown ether binds an ion and subsequently changes the redox potential of the ferrocene group.

In recent years ionic liquids have become more important for their potential in practical applications and have moved away from their previous status as no more than interesting. The interesting properties are, however, the reason that interest in their potential use has surged. This interest is centered on ionic liquid's unique property of being both innately conducting and liquid, and is often associated with electrochemical applications.[19] Practical applications are now seen to include use as electrolyte-solvents in batteries, fuel cells, and capacitors and in many cases show great promise in these areas. Recent studies have examined the behavior of various solutes in ionic liquids,[20] molecular force fields of ionic liquids,[21] hydrogen oxidation in ionic liquids at a platinum electrode surface,[22] density estimation of ionic liquids,[23] the applicability of Marcus theory to ionic liquid redox

processes,[24] and the evaluation of new materials such as tetraalkylphosphonium polyoxometalate ionic liquids.[25]

Previous research in this group has investigated the electrochemical phenomena of various classes of ionic liquid materials that have included redox active polyether hybrids, DNA complexes, and imidazolium systems.[26-34] Redox functionalized ionic liquids inherently offer unique opportunities for investigations of electron transfer and mass transport in melt phases, when used in their undiluted forms. These materials often have melting points below 100°C and are sufficiently ionically conductive as to permit quantitative voltammetry in the undiluted state. They can also be designed to incorporate a variety of redox species and other functionality.[35]

The Armstrong group at the University of Texas at Arlington has been responsible for a number of publications in the area of multiply ionic molecules (dendrimers), and notably many of these publications have suggested a number of practical applications for these materials, which makes this one of the hottest areas of dendrimer research as of late. One example of this is the use of dicationic liquid species for organic reaction solvents for high temperature reactions such as a Claisen rearrangement or a Diels-Alder reaction, where most interestingly the overall yields are affected by the specific cation used and thus are somewhat tunable[36] and a second paper details a large number of possible dication combinations that could greatly increase the tunability of these molecules.[37] Other work has been done using various tricationic liquid materials[38] that have been shown to be useful as gas phase ion pairing agents in ESI-MS for detecting divalent anions in positive mode[39,40] as well as showing promise as stationary phase materials for gas chromatography.[41]

Our studies have focused on investigating and understanding the rates of mass and electron transport in semi-solid media, choosing as model media, redox functionalized ionic liquids. With very high redox site concentrations, such as ferrocene in the 1 – 2 M range, the neat melt materials are concurrently both electron and ionically conductive. An important property of the neat redox ionic liquids is that the spacing between redox sites is small, allowing facile electron self-exchange (hopping). The viscosities of the neat materials are substantial, so that physical diffusion of redox sites is greatly retarded, and becomes less significant[26] than the transport of electrochemical charge by electron hopping. The electron hopping process is initiated by electrochemical voltammetry that generates a mixed valent layer at the electrode interface, which supports the hopping process. Dendritic materials add a new aspect to the investigation, namely the effect of multiple redox sites within a single molecule, and the effect of each redox site on another in a closely packed melt state.

3.2 Experimental

3.2.1 Chemicals and Reagents

Tris(2-aminoethyl)amine (96%), Polyamidoamine (PAMAM) (20 wt. % in methanol), propylamine (≥ 99%), Generation 0), and DAB-Am-4 (diaminobutane based) Polypropylenimine tetraamine (PPI) dendrimer (Generation 1.0, pH 12, 25 wt. % in water) were all purchased from Sigma-Aldrich (St. Louis, MO) and 1,4-diaminobutane (≥ 99%) was purchased from Fluka. The PPI material was repeatedly azeotroped (as many as 10x100mL) with dry acetone to remove as much water content as possible, but the other materials were used with no further purification. Toluene and methylene chloride were dried using molecular sieves when necessary and tetrahydrofuran was used from a normal still

process. All other chemicals and reagents were used with no further purification, unless otherwise described.

3.2.2 Dilute Solution Voltammetry

Cyclic voltammetry to inspect for general electrochemical behavior was performed on ca. 1.0 mM solutions in dichloromethane or acetonitrile with 0.1 M tetrabutylamonium perchlorate as supporting electrolyte. The 20 mL glass vial cells contained 1.6 mm diameter Pt disk working, Pt mesh counter, and aqueous Ag/AgCl/0.1M NaCl reference electrodes, which were controlled using a CH Instruments Electrochemical Workstation. Scan rates of 50, 100, and 200 mV/s were commonly employed for these voltammetry measurements.

3.2.3 Undilute (Neat) Melt Electrochemistry

The electrochemistry of non-dilute ionic liquids was carried out using a setup that has been described previously for redox polyether hybrids.[32] Approximately 15-20 mg of an ionic liquid is drop-cast using dichloromethane as the solvent onto the surface of a homemade four electrode assembly consisting of a 25µm diameter Pt micro-disk working electrode, Ag quasi-reference, and two 0.4 mm diameter Pt disk electrodes. The two 0.4mm Pt disk electrodes are used together for 2-electrode AC impedance spectroscopy measurements, and one is used as a counter electrode for 3-electrode voltammetry. All four electrodes are contained in a 0.25 inch stainless steel tube that is sealed with an epoxy resin. After drop-casting, samples are placed in the temperature controlled chamber described[25] in the reference above and held under vacuum at approximately 75 ºC for at least 12 hours to assure complete solvent removal. Both voltammetry and AC impedance measurements were performed in a Faraday cage using a CH Instruments Electrochemical Workstation. Samples

were kept under vacuum for the duration of the experiments and measurements were taken at various temperatures with time given between temperature changes to assure equilibration.

AC impedance spectroscopy measurements were taken over a range of frequencies from 1 Hz to 100 KHz, with a 0 V DC bias, 2 second quiet time, and a 5 mV to 400 mV amplitude. Ionic conductivity was calculated from the real x-axis intercept found in a Nyquist plot. Cyclic voltammetry was performed with a 30 second quiet time, 10 mV/s scan rate, with a varied potential range depending on the redox potentials of the specific material and the amount of ohmic drop observed. The cyclic voltammogram of each material at each temperature was used to determine the potential step used in chronoamperometry. Chronoamperometry was performed with a 400 second pulse width and a 450 to 600 second quiet time.

3.2.4 6-Bromohexanoylcyclopentadienyl iron (2)

This precursory molecule was produced and then used to react with several different dendiritic compounds as described below (Figure 3.1). 6-bromohexanoic acid (1 equivalent) is reacted with oxalyl chloride (1.6 equivalents) in a small amount of sieve-dry toluene under argon atmosphere. The reaction is initiated through the use of a heat gun (until violent bubbling begins), and the reaction is then stirred for an additional 30 minutes. The resulting 6-bromohexanoylchloride (**1**) was reacted with 1 equivalent of ferrocene and 1.4 equivalents of aluminum chloride in methylene chloride. The ferrocene and aluminum chloride were combined and dissolved in methylene chloride and allowed to stir for 15 minutes under argon atmosphere. Then 6-bromohexanoylchloride, dissolved in methylene chloride, was added drop wise over the course of approximately 10 minutes and the reaction allowed to stir for an

Figure 3.1 A) Synthesis of the 6-bromohexanoyl chloride **1** reagent from the 6-bromohexanoic acid starting material, which is used to make 6-Bromohexanoylcyclopentadienyl iron **2** and also used in the synthesis of the dendrimer reagents later. B) The reduction of the carbonyl group on **2** to form 6-Bromohexylcyclopentadienyl iron **3**. C) Finally the addition of imidazole to **3** as the final step to creating the precursor reagent 6-Imidazolehexylcyclopentadienyl iron **4**.

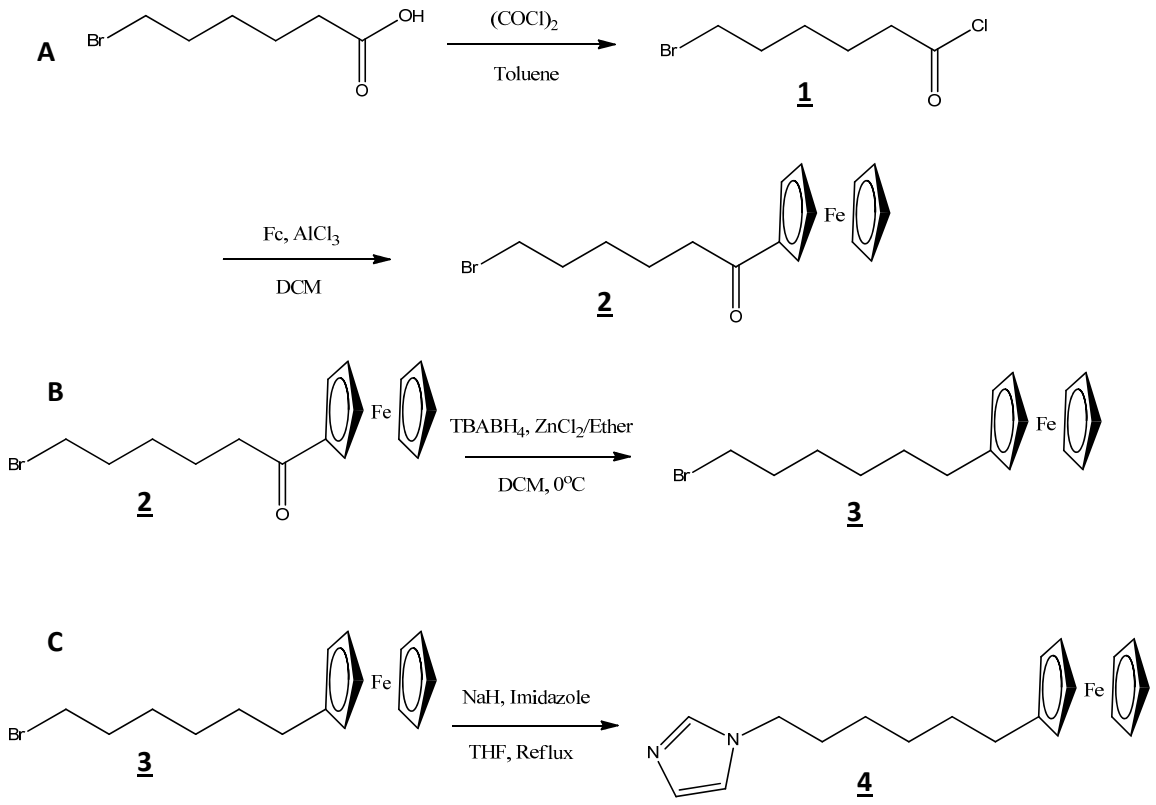
A
Br
OH
O
(COCl)2
Toluene
Br
Cl
O
1
Fc, AlCl3
DCM
Br
Fe
O
2
B
Br
Fe
O
2
TBABH4, ZnCl2/Ether
DCM, 0°C
Br
Fe
3
C
Br
Fe
3
NaH, Imidazole
THF, Reflux
N
N
Fe
4

additional 2 hours. The reaction was quenched with ice chilled nano-pure water, and subsequently washed 2 times with saturated bicarbonate solution. The crude product was then purified via column chromatography (silica gel, 230-400 mesh grade 60) using hexane, and eluting with 20% ethyl acetate (53% yield). ^{1}H NMR ($CDCl_3$, δ/ppm): 1.51 (m, 2H), 1.71 (q, 2H), 1.90 (q, 2H), 2.70 (t, 2H), 3.42 (t, 2H), 4.17 (s, 5H), 4.47 (t, 2H), 4.75 (t, 2H).

3.2.5 6-Bromohexylcyclopentadienyl iron (3)

6-Bromohexanoylcyclopentadienyl **2** iron was taken and reacted with tetrabutylammonium borohydride and zinc chloride (in ether) in methylene chloride (Scheme 3.1). **2** and tetrabutylammonium borohydride were dissolved in methylene chloride in an argon atmosphere and cooled to 0°C using an ice bath. The zinc chloride solution was then added very slowly drop wise. The reaction was then allowed to stir for 30 minutes while coming to room temperature. The solution was then quenched by dumping into 25 mL of nano-pure water and the crude product was extracted using methylene chloride and the organic phase was further washed with a brine (NaCl) solution, dried using Na_2SO_4, and filtered to remove solid impurities. The crude product was then purified using a silica gel column loaded with 10% triethyamine in hexanes, and the product was eluted with 10% methylene chloride in hexanes (54% yield). ^{1}H NMR ($CDCl_3$, δ/ppm): 1.35 (m, 2H), 1.46 (m, 2H), 1.52 (m, 2H), 1.86 (q, 2H), 2.33 (t, 2H), 3.41 (t, 2H), 4.05 (s, 4H), 4.10 (t, 5H).

3.2.6 6-Imidazolehexylcyclopentadienyl iron (4)

A single equivalent of **2** or was reacted with 1.4 equivalents of imidazole and 1.4 equivalents of sodium hydride in THF under argon atmosphere (Scheme 3.1). The sodium hydride was added to the imidazole in THF after they had been cooled in an ice bath, and

after the addition the reaction was brought to reflux for 2 hours before **2** was added and then refluxed over night (~18 hours). The reaction was quenched with a small amount of water, extracted with ethyl acetate, and washed 3 times with water. The crude material was purified on a silica gel column using 10% ethanol in hexanes to elude the purified product (21.8%). ^{1}H NMR ($CDCl_3$, δ/ppm): 1.33 (m, 4H), 1.50 (m, 2H), 1.78 (p, 2H), 2.32 (t, 2H), 2.81 (t, 2H), 4.01 (t, 2H), 4.05 (d, 2H), 4.09 (s, 5H), 6.89 (s, 1H), 7.07 (s, 1H), 7.49 (s, 1H).

3.2.7 Propylamine Based Molecule (Monomer, 5)

6-bromohexanoic acid (1 equivalent) is reacted with oxalyl chloride (1.6 equivalents) in a small amount of sieve-dry toluene under argon atmosphere (Figure 3.2). The reaction is initiated through the use of a heat gun (until violent bubbling begins), and the reaction is then stirred for an additional 30 minutes. The resulting 6-bromohexanoylchloride (**1**) was then reacted with propylamine under argon in an ice bath with triethylamine added slowly and the reaction was allowed to warm to room temperature over night while continuing to react (~12 hours). The reaction was quenched with a few milliliters of nano-pure water and then extracted with ethylacetate, washed twice with water, twice with brine, dried with Na_2SO_4 and then filtered. The material was then purified using a silica gel column eluted with 50% ethylacetate in hexanes (71% yield). ^{1}H NMR ($CDCl_3$, δ/ppm): 0.92 (t, 3H), 1.49 (m, 4H), 1.65 (p, 2H), 1.85 (p, 2H), 2.17 (t, 2H), 3.18 (q, 2H), 3.39 (t, 2H), 5.52 (br s, 1H).

The above material is then reacted with **4** in THF by refluxing overnight to result in the final ionic liquid product with a bromide counter anion. ^{1}H NMR (Acetone-D6, δ/ppm): 0.85 (t, 3H), 1.42 (br m, 14H), 1.63 (p, 2H), 1.97 (q, 2H), 2.16 (t, 2H), 2.33 (t, 2H), 3.12 (q,

Figure 3.2 First, the preparative synthesis of propylamine with 6-bromohexanoylchloride **1**, and then reacted with 6-Imidazolehexylcyclopentadienyl iron **4** to produce the final "monomer" ionic liquid product **5** with a bromide counterion (not shown). The bromide counterion is later exchanged out for hexafluorophosphate (PF_6^-) or bis(trifluoromethylsulfonyl)imide (NTf_2^-) using the ion metathesis procedure.

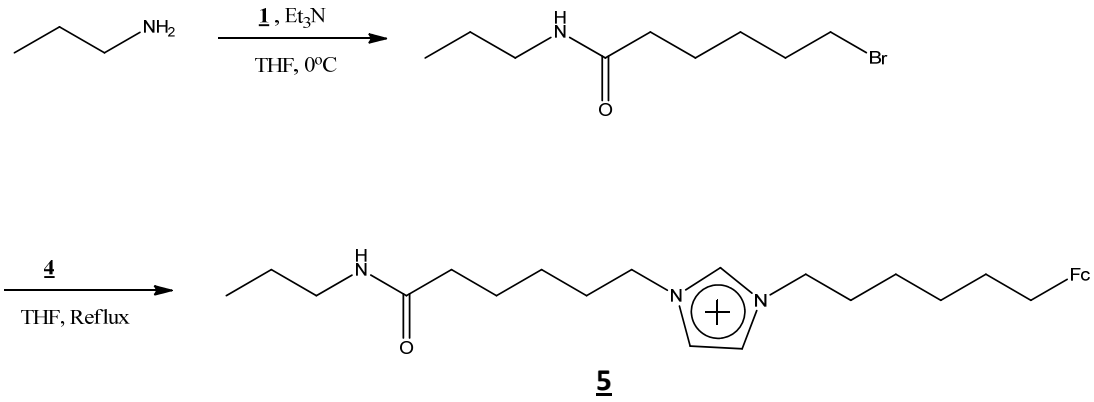

5

2H), 4.01 (t, 2H), 4.05 (d, 2H), 4.06 (s, 5H), 4.39 (t, 4H), 7.81 (s, 1H), 7.83 (s, 1H), 9.42 (s, 1H).

3.2.8 Tris(2-aminoethyl)amine Based Molecule (Trimer, 6)

The "trimer" material was prepared in nearly the same way as the "monomer" above. 6-bromohexanoic acid (1 equivalent) is reacted with oxalyl chloride (1.6 equivalents) in a small amount of sieve-dry toluene under argon atmosphere (Figure 3.3). The reaction is initiated through the use of a heat gun (until violent bubbling begins), and the reaction is then stirred for an additional 30 minutes. The resulting 6-bromohexanoylchloride (**1**) was then reacted as 3.6 equivlaents to 1 equivalent of tris(2-aminoethyl)amine under argon in an ice bath with triethylamine added slowly and the reaction was allowed to warm to room temperature over night while continuing to react (~12 hours). The reaction was quenched with a few milliliters of nano-pure water as well as sodium hydroxide (until additional chemical produces no further reaction), then extracted with methylene chloride, washed twice with water, twice with brine, dried with Na_2SO_4 and then filtered. The crude material was then purified using a silica gel column and eluted with 20% ethanol in methylene chloride (51% yield). ^{1}H NMR ($CDCl_3$, δ/ppm): 1.49 (p, 6H), 1.67 (p, 6H), 1.89 (p, 6H), 2.23 (t, 6H), 2.54 (m, 6H), 3.28 (q, 6H), 3.42 (t, 6H), 6.54 (t, 3H).

The above material is then reacted with **4** in THF by refluxing overnight to result in the final ionic liquid product with bromide counter anions. ^{1}H NMR (Methanol-D4, δ/ppm): 1.24 (m, 21H), 1.42 (m, 10H), 1.56 (m, 10H), 1.81 (br m, 16H), 2.16 (m, 6H), 2.24 (m, 6H), 2.53 (br s, 6H), 3.9-4.0 (br m, 27H), 4.14 (m, 12H), 7.59 (s, 6H), 8.99 (s, 3H).

Figure 3.3 Tris(2-aminoethyl)amine is first reacted with 6-bromohexanoylchloride **1**, and that intermediate product is then reacted with 6-Imidazolehexylcyclopentadienyl iron **4** to produce the final "trimer" ionic liquid product **6** with bromide counterions (not shown). The bromide counterions are later exchanged out for hexafluorophosphate (PF_6^-) or bis(trifluoromethylsulfonyl)imide (NTf_2^-) using the ion metathesis procedure.

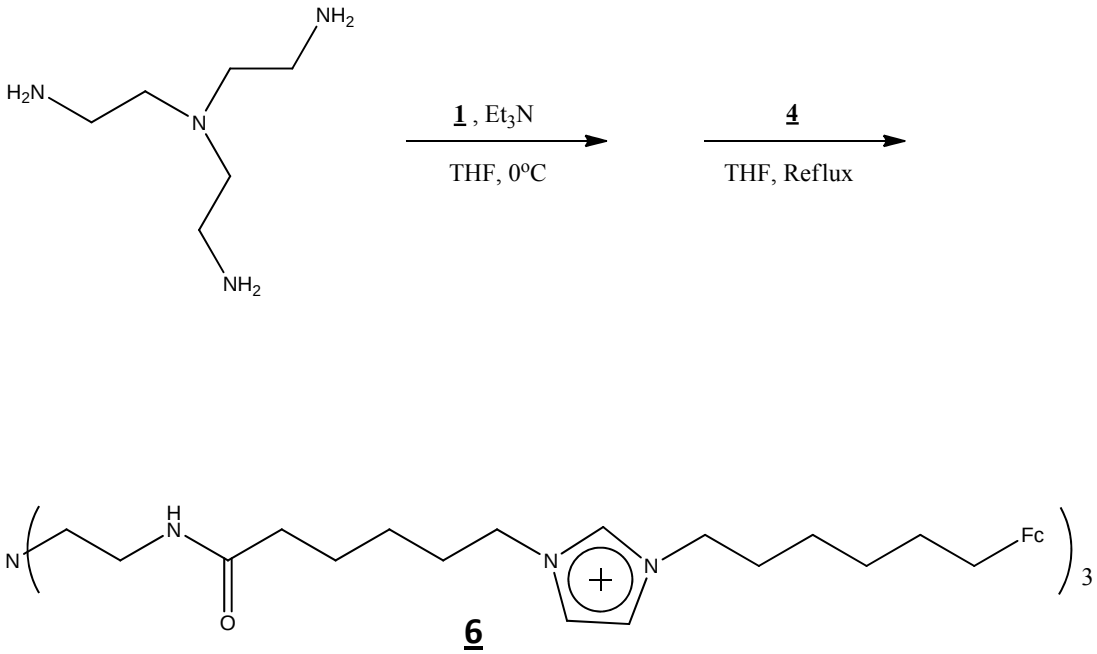

6

3.2.9 Poly(propylene imine) (PPI, 7)

The two dendrimer core materials were prepared nearly identical to the above "trimer" material (Figure 3.4). 6-bromohexanoic acid (1 equivalent) is reacted with oxalyl chloride (1.6 equivalents) in a small amount of sieve-dry toluene under argon atmosphere. The reaction is initiated through the use of a heat gun (until violent bubbling begins), and the reaction is then stirred for an additional 30 minutes. The resulting 6-bromohexanoylchloride (**1**) was then reacted as 4.8 equivlaents to 1 equivalent of either PAMAM or PPI under argon in an ice bath with triethylamine added slowly and the reaction was allowed to warm to room temperature over night while continuing to react (~12 hours). The reaction was quenched with a few milliliters of nano-pure water as well as sodium hydroxide (until additional chemical produces no further reaction), then extracted with methylene chloride, washed twice with water, twice with brine, dried with Na_2SO_4 and then filtered. The crude material was then purified using a silica gel column and eluted with 20% ethanol in methylene chloride (~50% yield).

The above material is then reacted with **4** in THF by refluxing overnight to result in the final ionic liquid product with bromide counter anions.

3.2.10 General Ion Exchange (Metathesis) Procedure

A single equivalent of the ionic liquid material to have its counter anion exchanged was reacted with 1.1 equivalents of the new counter anion containing salt, either sodium hexafluorophosphate ($NaPF_6$) or lithium bis(trifluromethylsulfonyl)imide ($LiN(SO_2CF_3)_2$, or $LiNTf_2$), in a solution of 50/50 acetone and ethanol. The reaction would proceed in an argon

Figure 3.4 Poly(propylene imine) (PPI) is reacted with 6-bromohexanoylchloride **1**, and the intermediate product is then reacted with 6-Imidazolehexylcyclopentadienyl iron **4** to produce the final PPI ionic liquid product **7** with bromide counterions (again not shown). The bromide counterions are later exchanged out for hexafluorophosphate (PF_6^-) or bis(trifluoromethylsulfonyl)imide (NTf_2^-) using the ion metathesis procedure.

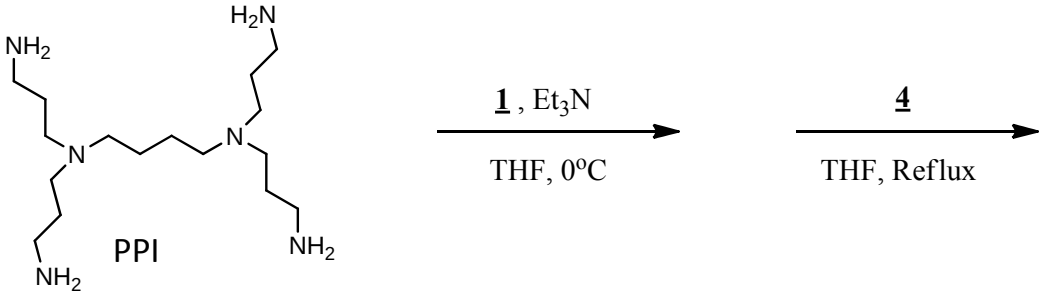

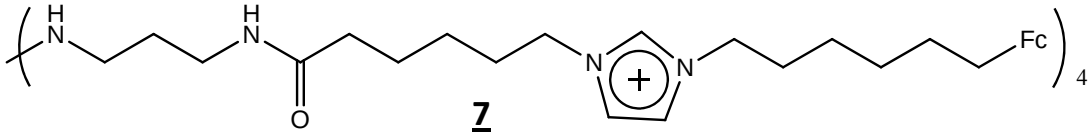

7

atmosphere over night (~12 hours), the reaction solvent would be removed, the product is then dissolved in methylene chloride and washed 3 times with brine. The resulting products would be analyzed by ESI-MS to determine the complete ion exchange.

3.2.11 Electrochemical Measurements

The electrochemistry of non-dilute ionic liquids is carried out using a setup that has been described previously for redox polyether hybrids and is outlined in greater detail in chapter 2.[42] Approximately 15-20 mg of an ionic liquid is drop-cast using dichloromethane as the solvent onto the surface of a homemade four electrode assembly consisting of a 25µm diameter Pt micro-disk working electrode, Ag quasi-reference, and two 0.4 mm diameter Pt disk electrodes. The two 0.4mm Pt disk electrodes are used together for 2-electrode AC impedance spectroscopy measurements, and one is used as a counter electrode for 3-electrode voltammetry.

In the case of melt electrochemisty, the sample is drop-cast on the electrode and placed in the temperature controlled chamber described[42] and held under vacuum at approximately 75 ºC for at least 12 hours to assure complete dryness. Both voltammetry and AC impedance measurements were performed in a Faraday cage using a CH Instruments Electrochemical Workstation. Samples were kept under vacuum for the duration of the experiments and measurements were taken at various temperatures with time given between temperature changes to assure equilibration. The high pressure CO2 experiments used the same electrode setup as above, but used a completely different homemade setup designed for high pressure electrochemistry that is thoroughly described by Lee et al.[43]

AC impedance spectroscopy measurements were taken over a range of frequencies from 1 Hz to 100 KHz, with a 0 V DC bias, 2 second quiet time, and a 5 mV to 400 mV amplitude. Ionic conductivity was calculated from the real x-axis intercept found in a Nyquist plot. Cyclic voltammetry was performed with a 30 second quiet time, 10 mV/s scan rate, with a varied potential range depending on the redox potentials of the specific material and the amount of Ohmic drop observed. The cyclic voltammogram of each material at each temperature was used to determine the potential step used in chronoamperometry. Chronoamperometry was performed with a 400 second pulse width and a 450 to 600 second quiet time.

3.2.12 Dilute Solution Voltammetry

Cyclic voltammetry to inspect for general electrochemical behavior was performed on ca. 1.0 mM solutions of the phosphonium ionic liquids in dichloromethane or acetonitrile with 0.1 M tetrabutylamonium perchlorate as supporting electrolyte. The 20 mL glass vial cells contained 1.6 mm diameter Pt disk working, Pt mesh counter, and aqueous Ag/AgCl/0.1M NaCl reference electrodes, which were controlled using a CHI Instruments Electrochemical Workstation. Scan rates of 50, 100, and 200 mV/s were commonly employed for these voltammetry measurements.

3.3 Results and Discussion

Redox functionalized, ionic liquid dendrimers were created in moderate yields with relatively high purity based on NMR analysis. Although the original intent of this project was to examine these materials in the same manner as several previous redox functionalized materials have been,[26-34] some of these materials did not display the fluidity hoped for and

were consequentially unusable for the intended solid state electron hopping project. However, there was still some interesting data to be had from solution and melt electrochemistry as wells as CO_2 plasticization of the neat material.

3.3.1 Solution Electrochemistry

Solution electrochemical of these materials verifies the electrochemical purity of each compound, which essentially means that there is only one type of ferrocene in the final product and there are no ferrocene or other electroactive compounds present in the final products. The E^o for the monomer product **5** is 516mV (vs. Ag/AgCl), the final trimer product **6** was found to be 435mV (vs. Ag/AgCl), and the product PPI material **7** was found to be 382mV (vs. Ag/AgCl). All three potentials vary slightly from a ferrocene reference of 443mV (vs. Ag/AgCl), but they do follow an interesting trend of decreasing E^o for more branching and consequently more ferrocene redox species per molecule.

Figure 3.5 shows the cyclic voltammogram of the final product monomer and trimer material, and it can be seen that there is a slight difference in shape and magnitude of the reduction wave as compared to the oxidation wave with the trimer. This is likely due to ferrocenium's lack of solubility in dichlormethane and upon oxidizing this material forms a film on the electrode surface, but fully resolubilizes upon reduction. It is commonly known that Ferrocenium has little solubility in dichloromethane; unfortunately the trimer product itself had negligible solubility in acetonitrile, which is commonly used for ferrocene/ferrocenium redox couples. The result is that the reduction wave is more narrow and larger in peak current (i_p) due to its inability to freely diffuse from the electrode surface and into the bulk solution.

Figure 3.5 Dilute solution voltammetry was conducted using a 1.6mm diameter platinum disk working electrode, with a large surface area platinum mesh counter electrode, and a Ag/AgCl reference electrode. A) Solution voltammetry of the monomer ionic liquid product **5** with PF_6^- counter ion; in acetonitrile with tetrabutylamonium perchlorate as the added electrolyte. 100mV/s scan rate and E^o is 516mV. B) Solution voltammetry of the trimer ionic liquid product **6** with PF_6^- counter ion; in dichloromethane with tetrabutylamonium perchlorate as the added electrolyte. 100mV/s scan rate and E^o is 435mV.

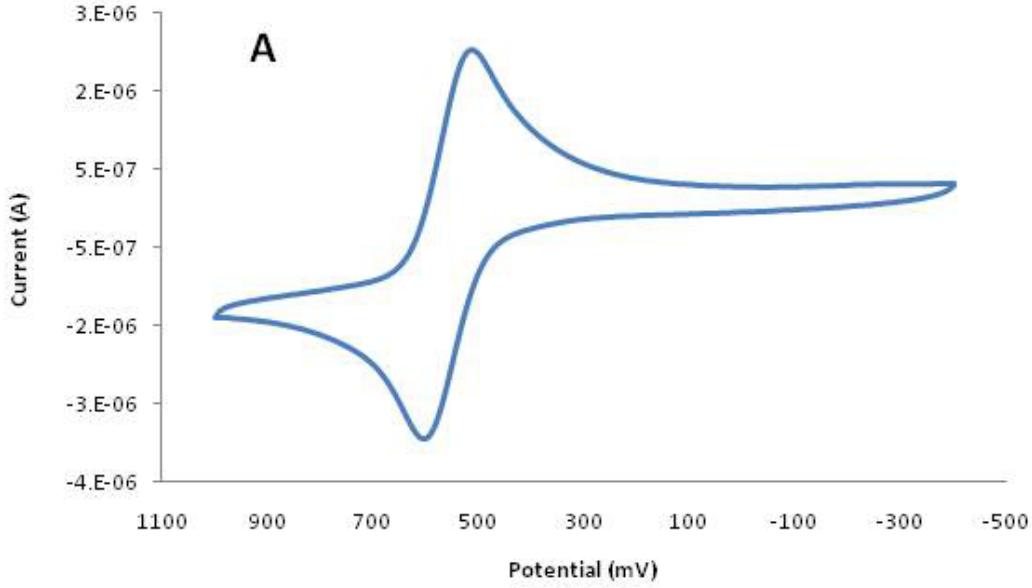
A
3.E-06
2.E-06
5.E-07
-5.E-07
-2.E-06
-3.E-06
-4.E-06
Current (A)
1100
900
700
500
300
100
-100
-300
-500
Potential (mV)

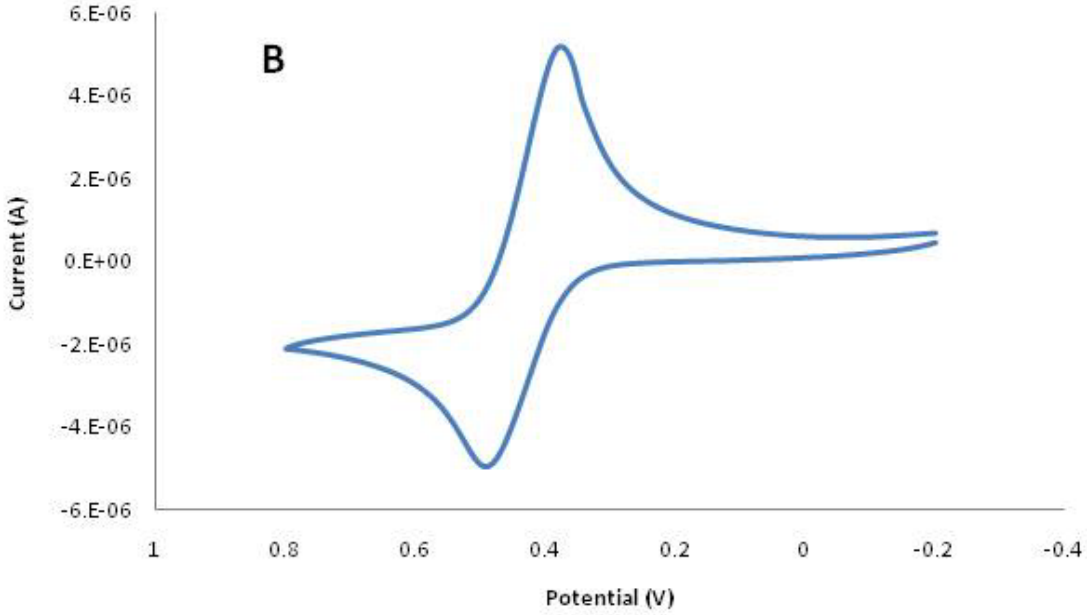
B
6.E-06
4.E-06
2.E-06
0.E+00
-2.E-06
-4.E-06
-6.E-06
Current (A)
1
0.8
0.6
0.4
0.2
0
-0.2
-0.4
Potential (V)

In contrast to the trimer, the PPI product had no apparent solubility problems when oxidized in dichloromethane (Figure 3.6). It may be that the added organic content from the additional branch and backbone allows for increased solubility despite ferrocenium's natural lack thereof. Figure 3.6-A shows a prominent and irreversible bromide oxidation wave from a sample prior to the anion metathesis reaction and the obvious disappearance of the bromide wave can be seen in the sample after anion metathesis with bis(trifluoromethylsulfonyl)imide (NTf_2^-) (Figure 3.6-B). This shows that the anion metathesis was successful, and the final product (as seen in Figure 3.6-B) is electrochemically pure.

3.3.2 Monomer and Trimer Neat Melt Electrochemistry

The undiluted (neat) electrochemistry of monomer and trimer melts is presented here along with a summary of their respective thermodynamic and kinetic exchange properties. The neat cyclic voltammograms were similar to those seen for other materials[26-34] with only a few notable exceptions (Figure 3.7). One notable exception is that neither the monomer nor the trimer display voltammetry that is as perfectly diffusion diffusion limited as has been seen in previously studied materials. This is likely due to the also observed larger ohmic drops (lower overall material conductivity) and higher viscosities of the material in their neat compositions. In terms of appearance of the AC impedance measurements, there is nothing more remarkable about them than to say that they do exhibit the higher resistances predicted by the cyclic voltammograms and otherwise conform to the standard Nyquist plot shapes (Figure 3.8). In a similar way, chronoamperometry data is also fairly plain; it does however

Figure 3.6 Dilute solution voltammetry was conducted using a 1.6mm diameter platinum disk working electrode, with a large surface area platinum mesh counter electrode, and a Ag/AgCl reference electrode. A) Solution voltammetry of the PPI ionic liquid product **7** with Br^- counter ion; in acetonitrile with tetrabutylamonium perchlorate as the added electrolyte. 100mV/s scan rate. Bromide oxidation is obvious at ~815mV. B) Solution voltammetry of the PPI ionic liquid product with NTf_2^- counter ion; in dichloromethane with tetrabutylamonium perchlorate as the added electrolyte. After ion metathesis, the disappearance of the bromide oxidation wave is obvious, indicating a full ion exchange. 100mV/s scan rate and E^o is 382mV.

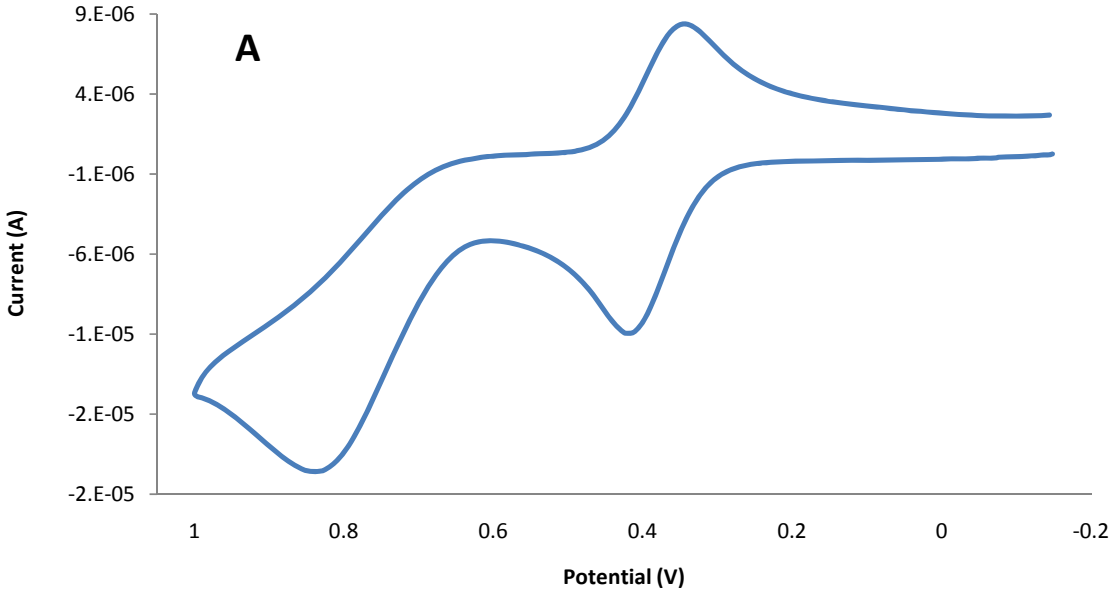
A
9.E-06
4.E-06
-1.E-06
-6.E-06
-1.E-05
-2.E-05
-2.E-05
Current (A)
1
0.8
0.6
0.4
0.2
0
-0.2
Potential (V)

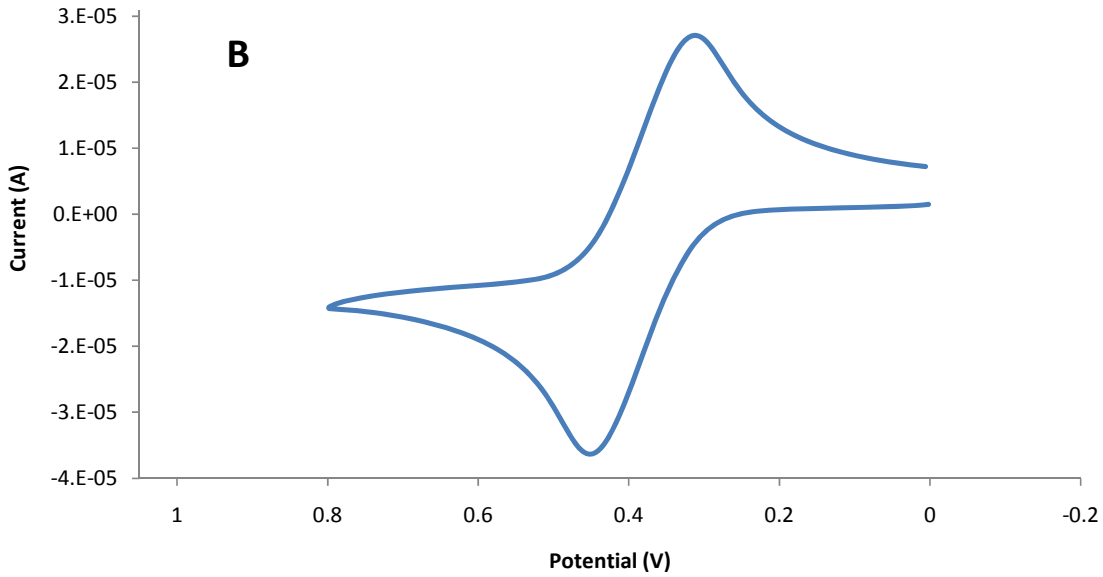
B
3.E-05
2.E-05
1.E-05
0.E+00
-1.E-05
-2.E-05
-3.E-05
-4.E-05
Current (A)
1
0.8
0.6
0.4
0.2
0
-0.2
Potential (V)

Figure 3.7 Neat melt voltammetry was conducted using a 25μm diameter Pt micro-disk working electrode, a .5mm diameter Ag quasi-reference, and a 0.4 mm diameter Pt disk counter electrode. There is no solvent and no added electrolyte for these data. A) Neat voltammetry of the monomer ionic liquid product **5** under vacuum at ~75°C; the scan rate used is 5mV/s. B) Neat voltammetry of the trimer ionic liquid product **6** under vacuum at ~75°C; the scan rate used is 5mV/s.

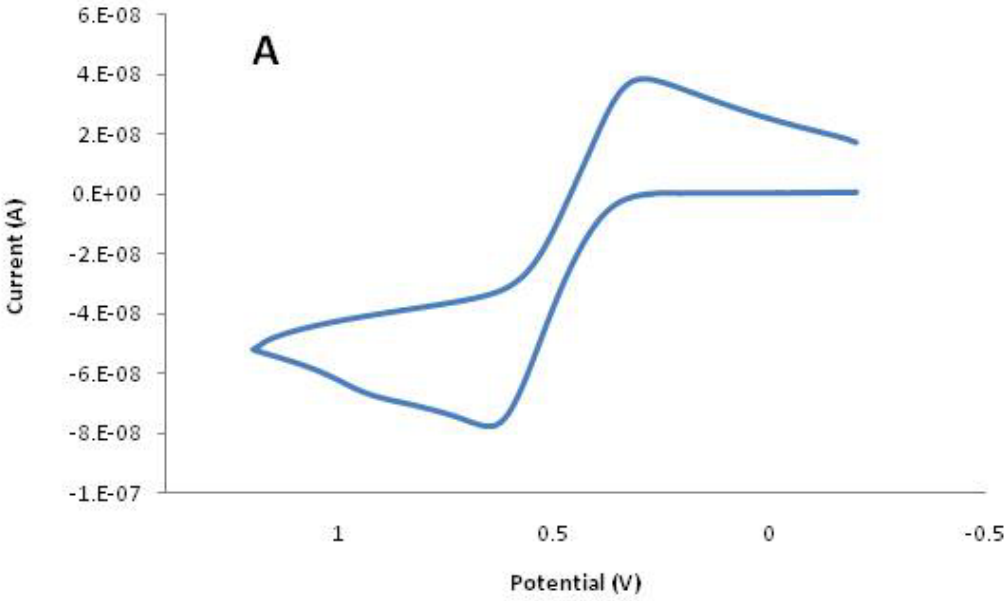
A
6.E-08
4.E-08
2.E-08
0.E+00
-2.E-08
-4.E-08
-6.E-08
-8.E-08
-1.E-07
Current (A)
1
0.5
0
-0.5
Potential (V)

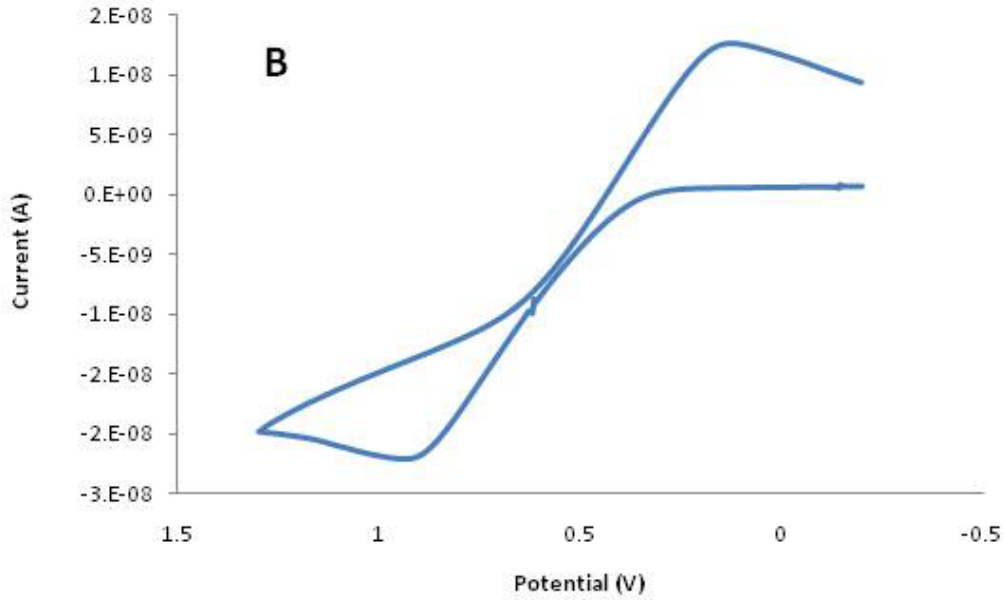
B
2.E-08
1.E-08
5.E-09
0.E+00
-5.E-09
-1.E-08
-2.E-08
-2.E-08
-3.E-08
Current (A)
1.5
1
0.5
0
-0.5
Potential (V)

Figure 3.8 Neat melt AC impedance was conducted using two 0.4 mm diameter Pt disk electrodes. There is no solvent and no added electrolyte for these data. A) Neat impedance of the monomer ionic liquid product **5** under vacuum at ~75°C. B) Neat impedance of the trimer ionic liquid product **6** under vacuum at ~75°C.

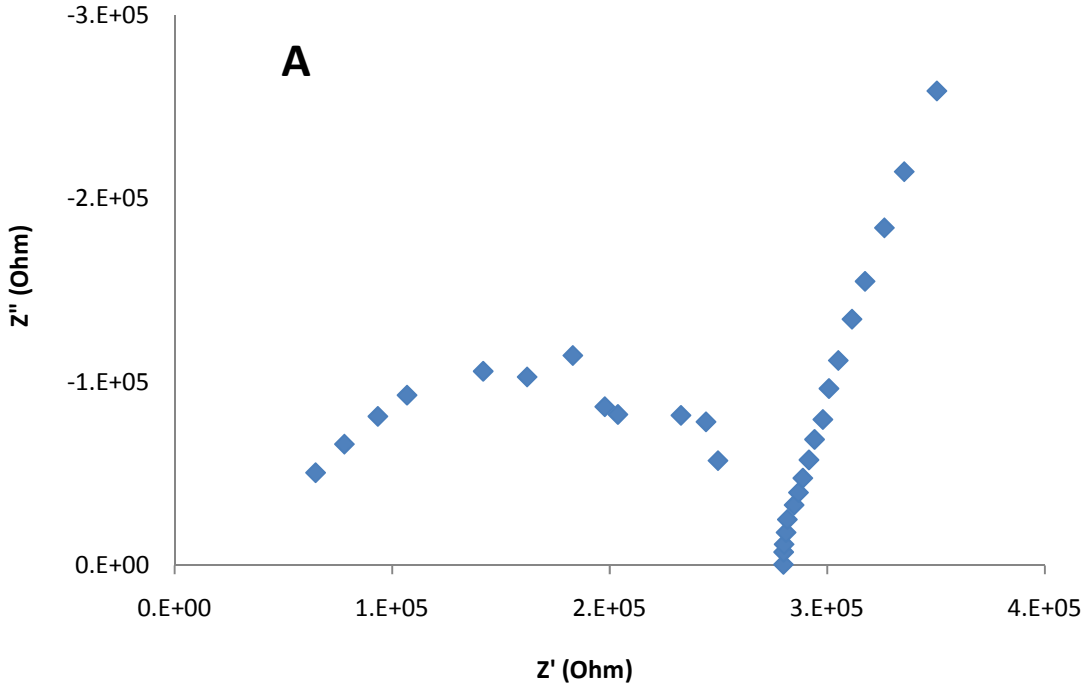
A
-3.E+05
-2.E+05
-1.E+05
0.E+00
Z'' (Ohm)
0.E+00
1.E+05
2.E+05
3.E+05
4.E+05
Z' (Ohm)

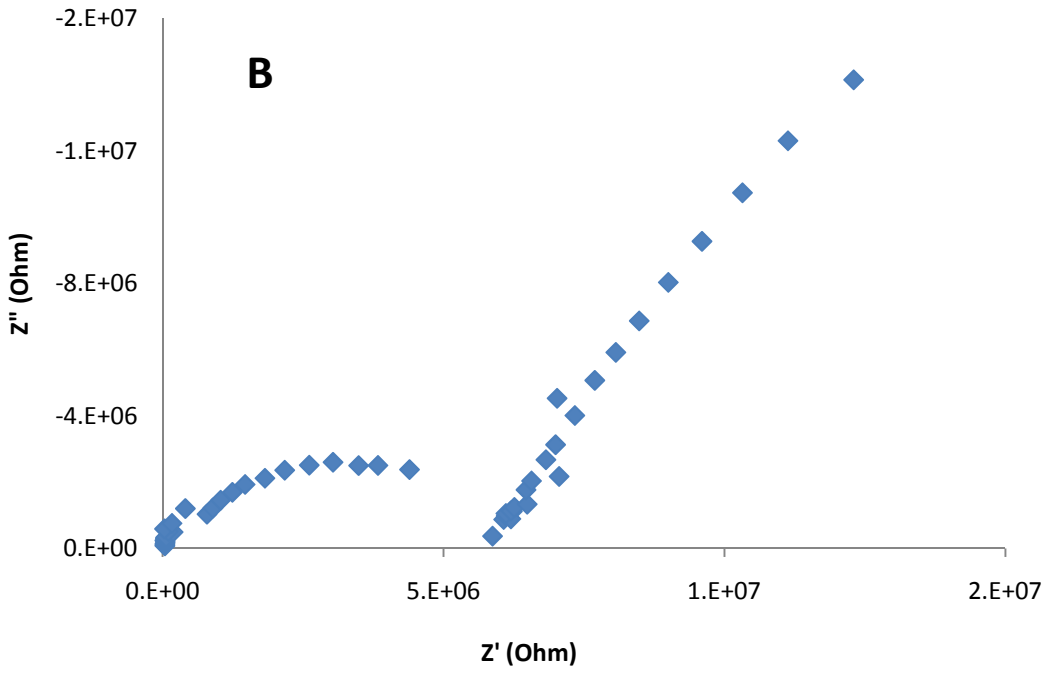
B
-2.E+07
-1.E+07
-8.E+06
-4.E+06
0.E+00
Z'' (Ohm)
0.E+00
5.E+06
1.E+07
2.E+07
Z' (Ohm)

show a very obvious difference in the amount of current that is immediately passed through the trimer material as compared to the monomer counterpart (Figure 3.9).

Chronoamperometric potential steps (to values calculated to overwhelm ΔE_{PEAK} effects) were employed to measure the apparent diffusion coefficient (D_{app}) in the dendrimer melts. Values of D_{APP} (Table 3.1) are obtained from current vs. $t^{-1/2}$ plots[44] of the current-time responses. By analogy to previous experience,[26-34] we assume that physical diffusion (D_{phys}) is very slow given both the steric bulk of the dendrimer ionic liquid cation and the melt viscosity, so that electron hopping (D_E) is the primary source of charge diffusion. This assumption has been amply justified by experimental measurements of D_{phys} for other similar redox ionic liquid species.[26]

A cubic lattice model is assumed for the system so that it is possible to derive a value for the apparent rates of electron self-exchange (k_{EX}) from the calculated D_e value through the extension of the Dahms-Ruff equation.[45-47]

$$D_{app} = D_{phys} + D_e = D_{phys} + \frac{k_{ex}\delta^2 C}{6} \qquad \text{(eqn. 1)}$$

These values, given in Table 3.1, can be plotted as $\ln(k_{ex})$ against reciprocal temperature (Arrhenius plot) to derive the heat of activation for the electron transport parameter ($E_{a,et}$) from the slope of the derived Arrhenius equation (Table 3.1)

$$\ln(k_{EX}) = \frac{-E_{a,et}}{R}\frac{1}{T} + \ln(A) \qquad \text{(eqn. 2)}$$

Figure 3.9 Neat melt chronoamperometry was conducted using a 25μm diameter Pt micro-disk working electrode, a .5mm diameter Ag quasi-reference, and a 0.4 mm diameter Pt disk counter electrode. There is no solvent and no added electrolyte for these data. A) Neat chronoamperometry of the monomer ionic liquid product **5** under vacuum at ~75°C; a 450s quiet time, a 400s pulse width, and a step from 0V to 0.85V (to exceed the large IR drop of the melt). B) Neat chronoamperometry of the trimer ionic liquid product **6** under vacuum at ~75°C; same parameters as A, but a step to 1.4V instead (to compensate for the even larger IR drop).

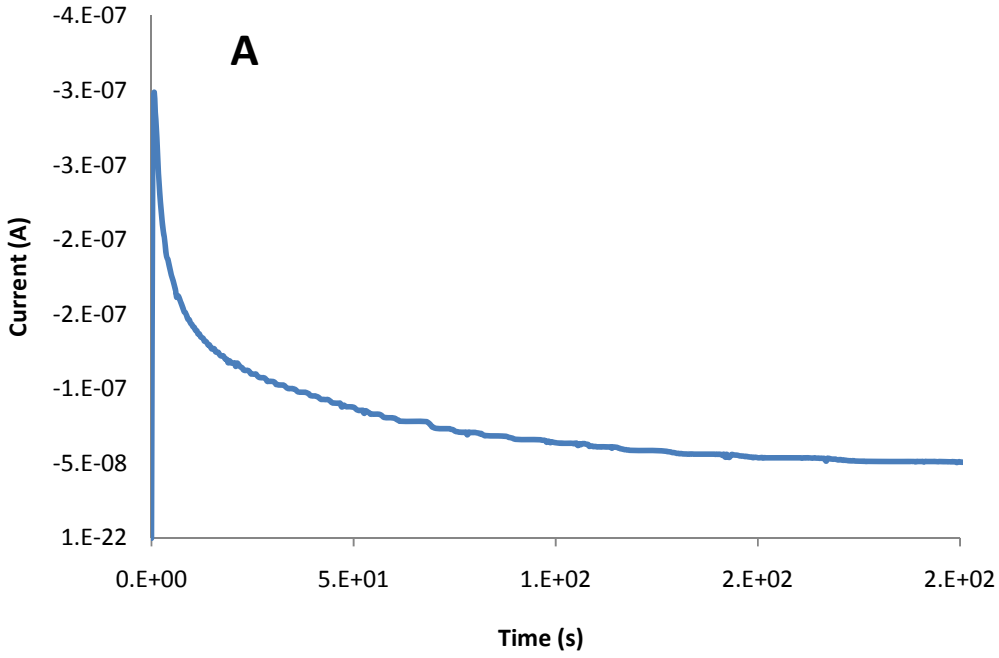
A
-4.E-07
-3.E-07
-3.E-07
-2.E-07
-2.E-07
-1.E-07
-5.E-08
1.E-22
Current (A)
0.E+00
5.E+01
1.E+02
2.E+02
2.E+02
Time (s)

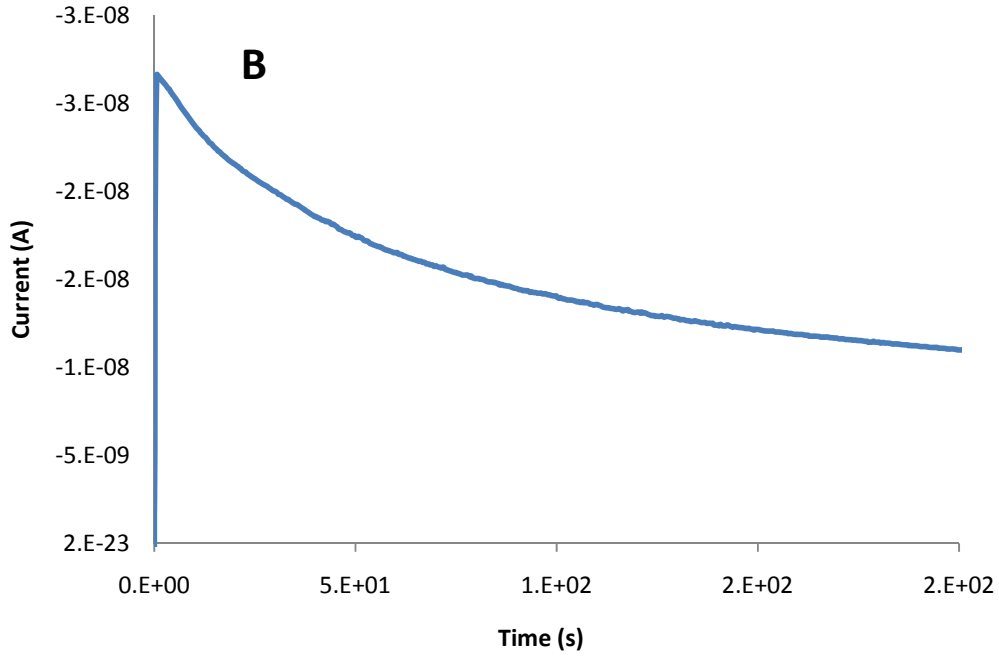
B
-3.E-08
-3.E-08
-2.E-08
-2.E-08
-1.E-08
-5.E-09
2.E-23
Current (A)
0.E+00
5.E+01
1.E+02
2.E+02
2.E+02
Time (s)

Table 3.1 The data collected and calculated from both the amperometry and impedance measurements is presented. It is clear from the data that the apparent diffusion coefficients (D_{app}) for the trimer are much smaller than those for the monomer, and consequently the k_{ex} values are much lower as well. This is backed up by the much smaller conductivity (σ) values observed for the trimer and lower counterion diffusion (D_{cion}) values as well. There is a small difference between energy of activation of electron transfer ($E_{A,et}$) and energy of activation of ion rearrangement ($E_{A,ion}$). Normally, under the ion-atmosphere relaxation model, these numbers should be the same, but (as explained in Chapter 2.3.2) there is often an electronic migration effect that yields exagerated D_{app}, k_{ex}, and $E_{A,et}$ values.

Sample	Temp (K)	C^* (mol/cm^3)	D_{APP} (cm^2/s)	k_{EX} ($M^{-1}\ s^{-1}$)	$E_{A,ET}$ (KJ/mol)	σ ($S*cm^{-1}$)	D_{CION} (cm^2/s)	$E_{A,ION}$ (KJ/mol)
Monomer with NTf2-	348	2.0E-3	9.3E-07	3.2E+08	**52**	3.5E-05	5.6E-09	**45**
	338		5.5E-07	1.9E+08		2.4E-05	3.8E-09	
	328		2.5E-07	8.5E+07		1.1E-05	1.7E-09	
	318		2.1E-07	7.3E+07		1.0E-05	1.5E-09	
	308		8.0E-08	2.7E+07		5.0E-06	7.1E-10	
Trimer with NTf2-	348	2.0E-3	5.4E-08	1.8E+07	**70**	1.7E-06	2.6E-10	**64**
	339		2.8E-08	9.7E+06		9.5E-07	1.4E-10	

where R is the ideal gas constant and A is the pre-exponential factor of the Arrhenius equation. Because the electron self-exchange is symmetrical, the entropy of activation is zero and the activation barrier energies are also free energies of activation.

Testing the ion atmosphere relaxation model that has been successfully applied to other ionic liquid systems[27,30,34] requires measurement of the physical diffusivity of the melts' counterions. The counterion diffusion coefficient (D_{cion}) can be calculated using the Nernst-Einstein equation where z, D, and C are charge, diffusion coefficient, and concentration of the noted species respectively, F is Faraday's constant and σ_{ion} is the measured ionic conductivity for the undiluted ionic liquid.[43]

$$\sigma_{ion} = \frac{F^2}{RT}[z_{Fc}^2 D_{Fc} C_{Fc} + z_{counterion}^2 D_{counterion} C_{counterion}] \qquad \text{(eqn. 3)}$$

We assume that the diffusivity of the bulky dendrimer cation (D_{Fc}) is negligible in comparison to that of the smaller nimble anions. Thus, measurement of σ_{ion} provides a path to calculation of the counterion D_{cion}. The ionic conductivities (σ_{ion}) were calculated from impedance data gathered using AC impedance by way of an electrode specific cell constant, and are given in Table 3.1. The collective D_{cion} values can then be applied to an Arrhenius type plot similar to that for k_{EX}, and the activation energy of anion atmosphere rearrangement ($E_{a,ion}$) then be calculated.

These data indicate, as expected, that while the monomer **5** is directly on par with other redox functionalized IL materials,[26-32] the trimer **6** material does have significantly lower conductivity and k_{ex} values and a much higher E_A as well. One note of particular interest is that it is apparent from AC impedance data, and the resulting calculations, that the

counterion diffusivity (D_{cion}) is considerable lower as well despite the counterion being unchanged. This strongly, and not unexpectedly, implicates viscosity and lack of overall ion mobility for the deteriorated conductivity of this material.

3.3.3 CO_2 Plasticized PPI-Based Ionic Liquid Electrochemistry

The concept behind the electrochemistry conducted in the CO_2 plasticized material differs very little from that of the neat systems. The idea is that the high CO_2 pressures cause the gas to permeate the liquid and loosen the high levels of viscosity that are present in the dendrimer based molecules. The result of this is a level of conductivity that can actually be used, however, it is important to remember that the data is somewhat artificial in terms of magnitude, but it does still give an idea of how electrons are exchanged in these materials.

Figure 3.10 is an example cyclic voltammogram of the PPI ionic liquid when under high CO_2 pressures (1000 PSI in this case). It is easy to see that the PPI material has at this point a similar degree of IR drop and level of current as compared to the monomer and trimer ionic liquids when they were in their neat states. This can also be seen in Figure 3.11, which also gives a good indication of how resistance decreases (conductivity increases) with increasing CO_2 pressures.

3.4 Conclusions

Despite not being able to conduct neat melt electrochemical studies of the PPI dendrimer ionic liquids as desired from the outset, there was still a considerable amount of interesting data obtained from this study. The trimer (three armed) material was able to be studied and compared to a monomer material. It was found that the trimer had

Figure 3.10 CO_2 plasticized melt voltammetry was conducted using a 25μm diameter Pt micro-disk working electrode, a .5mm diameter Ag quasi-reference, and a 0.4 mm diameter Pt disk counter electrode. There is no solvent in the traditional sense and no added electrolyte for these data. Voltammetry is of the PPI ionic liquid product **7** at 1000 PSI CO_2 pressure and ~30°C; the scan rate used is 5mV/s.

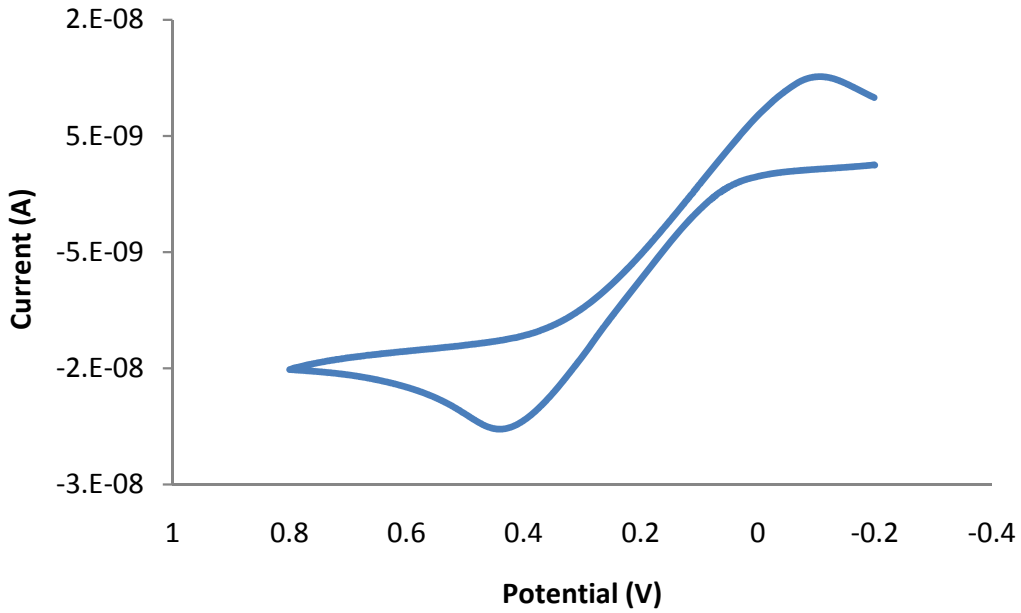
2.E-08
5.E-09
-5.E-09
-2.E-08
-3.E-08
Current (A)
1
0.8
0.6
0.4
0.2
0
-0.2
-0.4
Potential (V)

Figure 3.11 CO_2 plasticized melt AC impedance was conducted using two 0.4 mm diameter Pt disk counter electrodes. There is no solvent in the traditional sense and no added electrolyte for these data. The sample is the PPI ionic liquid product **7**. Impedance data was collected at CO_2 pressures of 0(vacuum), 200, 300, 400, 500, 600, 700, 800, and 900 PSI as seen in the legend of B, which gives the actual data of each pressure except 0 and 200 PSI (which have impedance values so large that it is difficult to see the higher pressure data). A) A simple plot of impedance as a result of increasing CO_2 pressure shows a fast decay of impedance with increasing pressures.

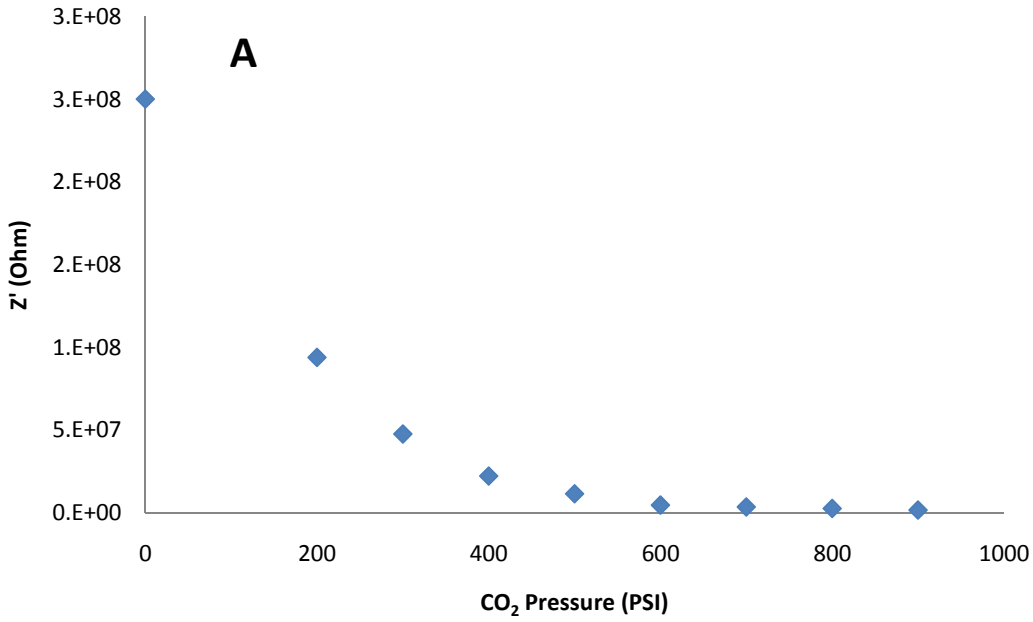
A
3.E+08
3.E+08
2.E+08
2.E+08
1.E+08
5.E+07
0.E+00
Z' (Ohm)
0
200
400
600
800
1000
CO2 Pressure (PSI)

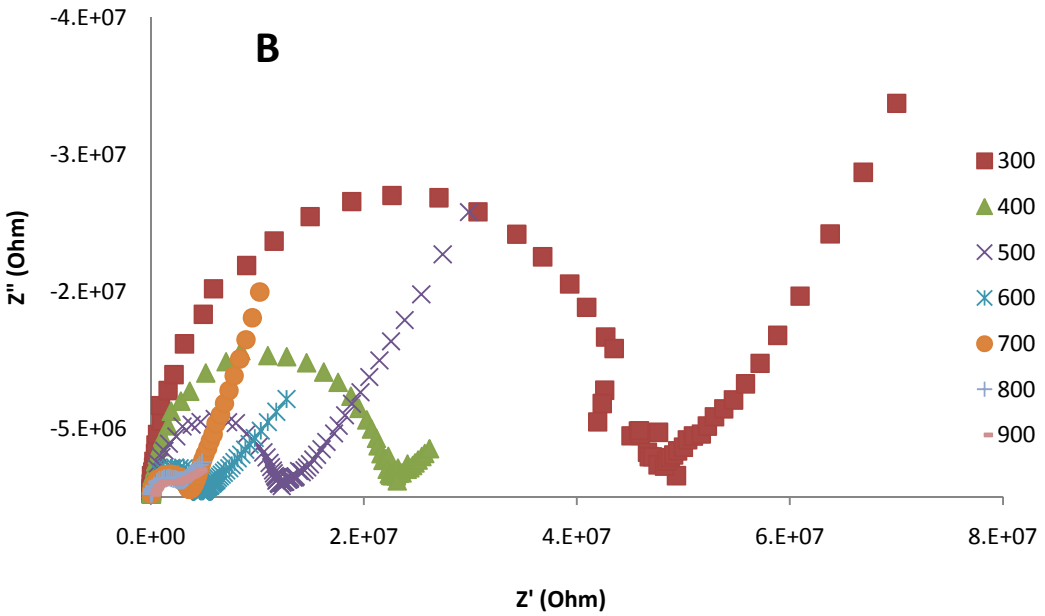
B
-4.E+07
-3.E+07
-2.E+07
-5.E+06
Z'' (Ohm)
0.E+00
2.E+07
4.E+07
6.E+07
8.E+07
Z' (Ohm)
300
400
500
600
700
800
900

electrochemical behavior that was representative of its greatly reduced fluidity, but was still able to conduct at elevated temperatures. Despite not being conductive as a neat material in the temperature range available for this study, the PPI ionic liquid material did produce some interesting conductivity data when plasticized with high pressures of CO2. Overall, these materials lack the low temperature fluidity to be of practical use as a neat melt; however, it is entirely possible that they may still find uses in their solvated state.

3.5 References

(1) Buhleier, E.W.; Wehner, W.; Vögtle, F. *Synthesis* **1978**, 155-158.

(2) Denkwalter, R.G.; Kolc, J.; Lukasavage, W.J. U.S. Pat. 4,289,872, Sept. 15, 1981.

(3) Tomalia, D.A.; Baker, H.; Dewald, J.R.; Hall, M.; Kallos, G.; Martin, Sl; Roeck, J.; Ryder, J.; Smith, P. *Polym. J. (Tokyo)* **1985**, 17, 117-132.

(4) Tomalia, D.A.; Baker, H.; Dewald, J.R.; Hall, M.; Kallos, G.; Martin, Sl; Roeck, J.; Ryder, J.; Smith, P. *Macromolecules* **1986**, 19, 2466-2468.

(5) Wörner, C.; Mülhaupt, R. *Angew. Chem., Int. Ed. Engl.* **1993**, 32, 1306-1308.

(6) De Brabander-van den Berg, E.M.M.; Meijer, E.W. *Angew. Chem., Int. Ed. Engl.* **1993**, 32, 1308-1311.

(7) Hawker, C.J.; Fréchet, J.M.J. *J. Am. Chem. Soc.* **1990**, 112, 7638-7647.

(8) Hawker, C.J.; Fréchet, J.M.J. *J. Chem. Soc. Comm.* **1990**, 1010-1013.

(9) Moore, J.S.; Xu, Z. *Macromolecules* **1991**, 24, 5893-5894.

(10) Xu, Z.; Moore, J.S. *Angew. Chem, Int. Ed. Engl.* **1993**, 32-246-248.

(11) Kawaguchi, T.; Walker, K.L; Wilkins, C.L.; Moore, J.S., *J. Am. Chem. Soc.* **1995**, 117, 2159-2165.

(12) Moore, J.S. *Acc. Chem. Res.* **1997**, 30, 402-413.

(13) Bosman, A.W., Janssen, H.M., and Meijer, E.W. *Chem. Rev.* **1999**, 99, 1665-1688.

(14) Hummelen, J.C.; van Dongen, J.L.J.; Meijer, E.W. *Chem. Eur. J.* **1997**, 3, 1489-1493.
(15) Kallos, G.J.; Tomalia, D.A.; Hedstrand, D.M.; Lewis, S.; Zhou, J. *Rapid Commun. Mass Spectrom.* **1995**, 9, 1552-1555.

(16) Barron, J.A.; Bernhard, S.; Houston, P.L.; Abruna, H.D.; Ruglovsky, J.L.; Maliaras, G.G. *J. Phys. Chem. A* **2003**, 107(40), 8130-8133.

(17) Takada, K.; Diaz, D.J.; Abruna, H.D.; Cuadrado, I.; Casado, C.; Alonso, B.; Moran, M.; Losada, J. *J. Am. Chem. Soc.* **1997**, 119, 10763-10773.

(18) Gonzalez, B.; Alonso, B.; Losada, J.; Garcia-Armada, M.P.; Casado, C.M. *Organomettalics* **2006**, 25, 3558-3561.

(19) Tsuda, T.; Hussey, C.L. *Interface* **2007**, Spring, 42-49.

(20) Lopes, J. N. C.; Gomes, M. F. C.; Padua, A. A. H. *J. Phys. Chem. B* **2006**, *110*, 16816-16818.

(21) Canongia Lopes, J. N.; Padua, A. A. H. *J. Phys. Chem. B* **2006**, *110*, 19586-19592.

(22) Silvester, D. S.; Aldous, L.; Hardacre, C.; Compton, R. G. *J. Phys. Chem. B* **2007**, *111*, 5000-5007.

(23) Ye, C.; Shreeve, J. n. M. *J. Phys. Chem. A* **2007**, *111*, 1456-1461.

(24) Lynden-Bell, R. M. *J. Phys. Chem. B* **2007**, *111*, 10800-10806.

(25) Rickert, P. G.; Antonio, M. R.; Firestone, M. A.; Kubatko, K.-A.; Szreder, T.; Wishart, J. F.; Dietz, M. L. *J. Phys. Chem. B* **2007**, *111*, 4685-4692.

(26) Balasubramanian, R.; Wang, W.; Murray, R. W. *Journal of the American Chemical Society* **2006**, *128*, 9994-9995.

(27) Harper, A. S.; Lee, D.; Crooker, J. C.; Wang, W.; Williams, M. E.; Murray, R. W. *J. Phys. Chem. B* **2004**, *108*, 1866-1873.

(28) Harper, A. S.; Leone, A. M.; Lee, D.; Wang, W.; Ranganathan, S.; Williams, M. E.; Murray, R. W. *J. Phys. Chem. B* **2005**, *109*, 18852-18859.

(29) Leone, A. M.; Brennaman, M. K.; Tibodeau, J. D.; Papanikolas, J. M.; Murray, R. W.; Thorp, H. H. *J. Phys. Chem. B* **2003**, *107*, 6469-6473.

(30) Leone, A. M.; Hull, D. O.; Wang, W.; Thorp, H. H.; Murray, R. W. *J. Phys. Chem. A* **2004**, *108*, 9787-9793.

(31) Leone, A. M.; Tibodeau, J. D.; Bull, S. H.; Feldberg, S. W.; Thorp, H. H.; Murray, R. W. *Journal of the American Chemical Society* **2003**, *125*, 6784-6790.
(32) Leone, A. M.; Weatherly, S. C.; Williams, M. E.; Thorp, H. H.; Murray, R. W. *Journal of the American Chemical Society* **2001**, *123*, 218-222.

(33) Ranganathan, S.; Murray, R. W. *J. Phys. Chem. B* **2004**, *108*, 19982-19989.

(34) Wang, W.; Lee, D.; Leone, A. M.; Murray, R. W. *Chem. Phys.* **2005**, *319*, 126-135.

(35) Forsyth, S. A.; Pringle, J. M.; MacFarlane, D. R. *Australian Journal of Chemistry* **2004**, *57*, 113-119.

(36) Han, X.; Armstrong, D.W. *Org. Lett.* **2005**, 7(19), 4205.

(37) Payagala, T.; Huang, J.; Breitbach, Z.S.; Sharma, P.S.; Armstrong, D.W. *Chem. Mater.* **2007**, 19, 5848.

(38) Wanigasekara, E.; Zhang, X.; Nanayakkara, Y.; Payagala, T.; Moon, H.; Armstrong, D.W. *Appl. Mater. Interfaces* **2009**, 1(10), 2126-2133.

(39) Breitbach, Z.S.; Warnke, M.M.; Wanigasekara, E.; Zhang, X.; Armstrong, D.W. *Anal. Chem.* **2008**, 80, 8828.

(40) Soukup, H.; Remsburg, J.W.; Breitbach, Z.S.; Sharma, P.S.; Payagala, T.; Wanigasekara, E.; Huang, J.; Armstrong, D.W. *Anal. Chem.* **2008**, 80, 2612-2616.

(41) Payagala, T.; Zhang, Y.; Wanigasekara, E.; Huang, K.; Breitbach, Z.S.; Sharma, P.S.; Sidisky, L.M.; Armstrong, D.W. *Anal. Chem.* **2009**, 81, 160-173.

(42) Lee, D.; Hutchison, J. C.; Leone, A. M.; DeSimone, J. M.; Murray, R. W. *Journal of the American Chemical Society* **2002**, *124*, 9310-9317.

(43) Lee, D.; Harper, A.S.; DeSimone, J. M.; Murray, R.W. *J. Am. Chem. Soc.* **2003**, 125, 1096-1103.

(44) Bard, A.J.; Faulkner, L.R. *Electrochemical Methods: Fundamentals and Applications*, 2nd ed.; Wiley and Sons: New York, 2001.

(45) Dahms, H. *J. Phys. Chem.* **1968**, 72, 362.

(46) Ruff, I.; Friedrich, V.J. *J. Phys. Chem.* **1971**, 75, 3297.

(47) Majda, M. In *Molecular Design of Electrode Surfaces*; Murray, R.W., Ed.; John Wiley & Sons: New York, **1992**.

CHAPTER 4

THE EFFECT OF THIOPHENOL LIGAND ρ-SUBSTITUENTS ON THE ELECTRON EXCHANGE KINETICS OF $Au_{25}(L)_{18}$ NANOPARTICLES

4.1 Introduction

Understanding the way that electrons are exchanged in any system is the fundamental basis of understanding most electronic behavior. Electron self-exchange is one of the easiest types of systems that can be studied, and there has already been massive amounts of research put into this field. Gold nanoparticles have been studied extensively for many years now, and likely one of the best characterized particles is $Au_{25}(L)_{18}$, which even has an entire review dedicated to summarizing this work.[1] Some characterization techniques that have been studied extensively include mass spectrometry,[2,3] electrochemistry, luminescence, optical absorbance,[4] NMR,[5] density functional theory calculations[6] and crystal structure.[7] Recently, there has been a growing interest in these particles' abilities to store and release charge for capacitive applications.[8,9] For this reason, understanding the nature of electron exchange in these materials becomes very important. Electron self-exchange has previously been studied for several mixed-valent solid state gold nanoparticles including $Au_{25}(SCH_2CH_2Ph)_{18}$ [10] and $Au_{144}(SC_6H_{13})_{60}$.[11] The original Au_{144} study was focused on measuring electron exchange rate constants in this class of nanomaterials with very specific size dependant electronic and spectroscopic properties. The later study of the Au_{25} material was focused on comparison to, and identifying the differences between, the larger Au_{144}

material. Au_{25} has been repeatedly defined as having very molecule-like behavior with a well defined homo-lumo band gap, where as Au_{144} is considered to have a more metallic electronic structure and charging character.[12] This difference was evidenced by the significantly faster electron exchange rate for the larger Au_{144} particles when compared to Au_{25}. The study reported here is a comparison of the effect of electron withdrawing and donating ligands on the Au_{25} electron self-exchange rate constant and other thermodynamic parameters. It has previously been reported that electron donating and withdrawing ligands can have a large impact on the formal potential (E^0) of both the first and second oxidation/reduction wave in voltammetry.[13]

Nanoparticles are a particularly good choice for this study because their molecular structure has been clearly characterized by X-ray crystalography of both the reduced $(-1)^7$ and oxidized $(0)^{14}$ states. The crystal structures indicate that there is a 13 atom icosahedron core (12 icosahedron vertices, with a single atom located at the very center) that is surrounded by a total of 6 semi-rings with 5 atom structures that include a thiolate-Au-thiolate-Au-thiolate pattern. Each thiolate on either end of the semi-ring is then attached to a gold atom on the core. It is already clear from the two different oxidation state structures that there is a structural difference between the two states. This structural difference has been attributed to the association of a large bulky cation in the reduced state vs. no counterion in the oxidized state. In the reduced state, the semi-ring structures that surround the core take on a puckering behavior in order to accommodate the cation. What this means in terms of electron exchange mechanics is that we expect to see a large reorganization energy associated with the $Au_{25}^{-1/0}$ electron transfer event.

$Au_{25}(SCH_2CH_2)_{18}$ can be easily prepared from a new,[15-17] but well established method that is still roughly based on the original Brust synthesis. The particle products are very monodisperse and easily further purified by a solvent extraction procedure. Once isolated, the particles can safely be stored as a dry material for extended periods of time with no decomposition or other alteration to the product. The particles are then subjected to a simple ligand exchange reaction to modify the particle with nearly any ligand of choice. In this research, 2-Phenylethanethiol (HSC2Ph, $HSCH_2CH_2Ph$) is replaced with either an electron withdrawing ligand 4-bromothiophenol (SPhBr) or an electron donating ligand 4-methoxythiophenol (SPhOCH3) (Figure 4.1). The ligand exchange can be driven to near completion by successive exchanges, but that extensiveness is not pursued in this study due to stability issues encountered in the oxidized versions of highly exchanged particles. The extent of exchange is, however, well established using matrix assisted laser desorption ionization (MALDI) mass spectrometry, which shows a nice binomial distribution of exchanged ligands for each exchange product.

In particular, the measurement of electron transport properties through solid films is of interest for potential applications in sensing and other nanoscale devices. Previous studies of nanoparticle materials have shown that there is a strong dependency of conductivity on the charge state composition of the mixed valency film, which can be explained by a bimolecular rate law for the self exchange reaction.

4.2 Experimental

4.2.1 Chemicals and Reagents

Figure 4.1 (From Left to Right) 4-Bromothiophenol (HSPhBr), 4-Methoxythiophenol (HSPhOMe), and 2-Phenylethanethiol (HSC2Ph, $HSCH_2CH_2Ph$).

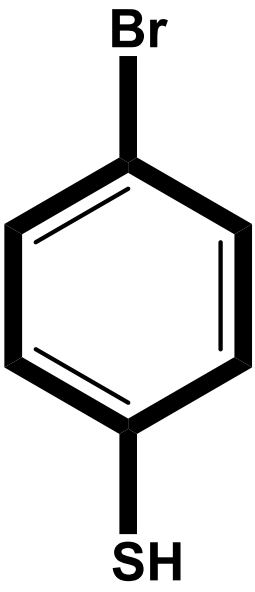
Br
SH

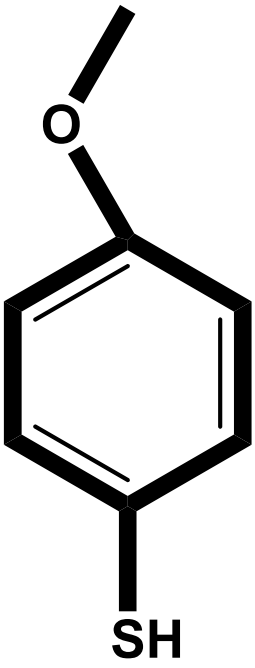
O
SH

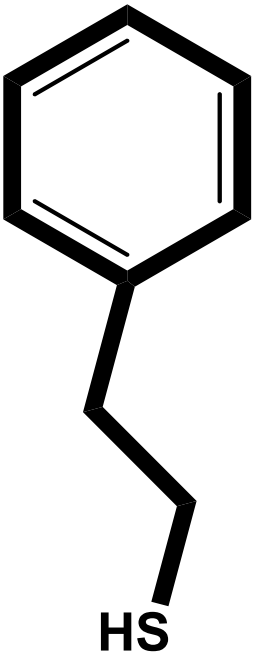
HS

Hydrogen tetrachloroaurate(III) trihydrate ($HAuCl_4 \bullet 3H_2O$) was synthesized using a well established literature method.[18,19] Cerium(IV) sulfate ($Ce(SO_4)_2$), phenylethanethiol ($PhCH_2CH_2SH$ or PhC_2SH, 98%), 4-bromothiophenol (BrPhSH, 95%), 4-methoxythiophenol (MeOPhSH, 98%), sodium borohydride (NaBH4, 99%), tetraoctylammonium bromide (Oct_4NBr, 98%), sodium perchlorate ($NaClO_4$, 99%), and tetrabutylammonium perchlorate (Bu_4NClO_4, ≥ 99.0%) were purchased from Sigma-Aldrich (St. Louis, MO). Methanol (Optima grade), acetonitrile (CH_3CN, Optima grade), tetrahydrofuran (THF, Optima grade), ethanol (Decon Labs, King of Prussia, PA, 200 Proof), and dichloromethane (CH_2Cl_2, Optima grade) were purchased from Thermo Fisher Scientific (Waltham, MA). All chemicals were used with no further purification. Deionized water (DI or NP, > 18MΩ) was prepared using a Millipore Nanopure water purification system.

4.2.2 Synthesis of $Au_{25}(SCH_2CH_2Ph)_{18}$

In this synthesis, $HAuCl_4 \cdot 3H_2O$ (1.00 g, 2.54 mmol) and Oct_4NBr (1.56 g, 2.85 mmol) were combined and dissolved in tetrahydrofuran (THF, 70 mL) and stirred for 15 minutes. Phenylethanethiol (1.80 mL, 12.6 mmol) was added at room temperature and stirred for at least 12 hours, until the solution was completely colorless. Meanwhile, sodium borohydride ($NaBH_4$, 0.967 g, 25.6 mmol) was dissolved in 24 mL Nanopure water and stirred at 0^oC for 1 hour prior to rapid addition to the THF solution. The reaction mixture was allowed to stir for no less than 48 hours. Over the course of the reaction, the product color slowly evolves from blackish to a murky brown color which is indicative of a high proportion of $Au_{25}(S(CH_2)_2Ph)_{18}^-$. The product solution was then gravity filtered to remove any insoluble materials, rotovapped to dryness, and then dissolved in toluene (30 mL). The toluene solution was extracted five times using 150 mL Nanopure water. The toluene layer

was subsequently rotovapped to dryness and the resulting product washed thoroughly with methanol to remove any traces of excess thiol and Oct_4NBr, leaving pure $[Oct_4N^+][Au_{25}(S(CH_2)_2Ph)_{18}^-]$ (243 mg, 30% yield by Au).

4.2.3 Ligand Exchange with *para*-substituted thiophenolates

In these large scale (often greater than 100 mg) ligand exchange reactions, $[Oct_4N^+][Au_{25}(S(CH_2)_2Ph)_{18}^-]$ was dissolved in dichloromethane at concentrations of 0.63 mM and incoming *para*-substituted thiophenol (HSPhX, X = Br, OCH_3) concentrations of 23 mM to 57 mM. After reactions times ranging from 12-24 hours, the nanoparticle product solution was dried to completion using a rotary evaporator and washed thoroughly with methanol to achieve pure ligand exchanged materials. MALDI-TOF Mass Spectrometry was then used to quantify the extent of ligand exchange and solid-state electrochemistry was used to measure the conductivity and subsequently the electron-exchange rate information as described previously.[23]

4.2.4 Chemical Oxidation of $Au_{25}(L)_{18}$ Nanoparticles

The oxidant Ce(IV) was used to oxidize the nanoparticles and achieve various percentages of charge state composition for many samples[11] (but was later discarded in favor of electrochemical oxidation techniques that were easier on the fragile high percentage oxidation states of the substituted thiophenols). An aqueous solution (10 ml) was prepared with 5mM $Ce(SO_4)_2$ and .1M NaClO4 and then stirred with a CH_2Cl_2 solution of ~0.1 mM Au_{25} with 0.05 M Bu_4NClO_4. The stirring time is roughly proportional to the percentages of oxidized and reduced nanoparticles present in the end mixture. The organic phase is then extracted from the aqueous phase and then washed 3x50ml NP H_2O. Following this, the

CH_2Cl_2 is removed using rotary evaporation, and the particles are then washed 5x50ml methanol to remove excess electrolyte (Bu_4NClO_4). The countercation at this point is assumed to be Bu_4N^+ due to its very large excess present in the reaction as compared to the Oct_4N^+ present at the beginning of the oxidation.

4.2.5 Electrochemical Oxidation of $Au_{25}(L)_{18}$ Nanoparticles

As mentioned above, higher oxidation percentages required using an electrochemical oxidation technique to achieve in thiophenol substituted particles. An organic solution in CH_2Cl_2 (5ml) was prepared with ~20mg of $Au_{25}(L)_{18}$ and 1M Bu_4NClO_4. Bulk electrolysis was performed (using a standard 3 electrode setup described below) setting the potential to the desired rest potential for the final solution, and the solution stirred for the duration of the experiment.

4.2.6 Solution Electrochemical Measurements

Cyclic voltammetry (CV), differential pulse voltammetry (DPV), rest potential (E_R), bulk electrolysis, and alternating current (AC) impedance spectroscopy of Au_{25} NP solutions (DCM) were carried out with a CH Instruments (Austin, TX) model 660 or 760 electrochemical workstation. Generally the cell contained a 1.6mm diameter Pt working electrode, a Pt mesh counter electrode, and a Ag/AgCl reference electrode.

4.2.7 Film Preparation on Interdigitated Array (IDA) Electrodes and Electronic Conductivity (σ_{EL}) Measurements

The IDA electrodes used were purchased from Abtech Scientific (Richmond, VA) and were composed of a total 50 fingers (25 from each electrode); each finger 20μm wide,

20μm apart, 3mm long, and 150nm high. Gold nanoparticle films were made by successively dropcasting a highly concentrated nanoparticle solution (~20mg/20μL DCM) on to the surface of the IDA until a film thickness greater than 1μm was achieved. This thickness is significantly higher than the electrode height and was previously shown to be a point at which the conductivity is no longer hindered by height. The films were then dried under vacuum for a minimum of 12 hours at room temperature. The total film concentrations are assumed to be 0.17M, the same as have been previously reported for Au_{25} nanoparticle films. The film-coated IDA was then placed in a temperature controlled vacuum chamber and allowed to temperature equilibrate for a minimum of 1 hour.

The electronic conductivities of the films were then measured from the slope of linear potential scans between ±1V (start and end potential is 0V) at 100mV/s. Measurements were taken at varying temperatures in 10°C increments from 30.0°C down to -10.0°C with 30 minute equilibration in between each. The electronic conductivity (σ_{EL}) was calculated from the $\Delta i/\Delta E$ slopes,

$$\sigma_{EL} = \frac{d\Delta i}{A_{TOTAL}\Delta E} \quad (1)$$

where d is the IDA gap and A_{TOTAL} is defined as the area of the walls of the facing parallel plate finger electrodes of height equal to the nanoparticle film thickness (1μm) and of length equal to the finger length times (N-1), where N is the number of IDA fingers. The ratio of d/A_{TOTAL} is called the geometric cell constant (C_{CELL}) and is equal to 1.36 cm^{-1} for all IDA experiments described.

4.3 Results and Discussion

4.3.1 Establishing Ligand Exchange and Final Ligand Composition

Matrix assisted laser desorption ionization mass spectrometry (MALDI-MS) was employed to document the extent of ligand exchange and the average number of exchanged ligands per particle. This method has been thoroughly documented.[25] The MALDI data for the SPhBr exchange shows an average total molecule composition of $Au_{25}(SCH_2CH_2Ph)_7(SPhBr)_{11}$ (Figure 4.2-A). Samples that were fully, or nearly fully, exchanged were synthesized, but proved too unstable when oxidized to be suitable for electrochemical study. However, these semi-fully exchanged particles exhibit significant changes in electrochemical behavior that is more than suitable for the purposes of this study. The MALDI data for the SPhOMe exchange shows an average total molecule composition of $Au_{25}(SCH_2CH_2Ph)_{11}(SPhOMe)_7$ (Figure 4.2-B). The SPhOMe ligand has much slower exchange kinetics than SPhBr and results in much lower extents of exchange over the same period of time and has been previously documented by Guo et al.[13] Like the SPhBr exchange, this quantity of exchange was more than adequate for the purpose of this study.

4.3.2 Establishing Charge State Composition

Room temperature voltammetry has been thoroughly explored at this point and is very well characterized to show that there are multiple reversible single electron oxidations and one reduction from the most common native Au_{25}^{-1} state.[4,20] This means that Au_{25}^{-2}, Au_{25}^{0}, Au_{25}^{+1}, and Au_{25}^{+2} are all accessible electrochemically, however, experience indicates that some species are significantly more stable than others at ambient conditions, where Au_{25}^{-1} and Au_{25}^{0} are the most stable oxidation states. The nanoparticles were prepared either by chemical oxidation with $Ce(SO_4)_2$ as the oxidizer, as used previously, or the particles were oxidized electrochemically. There is no difference in the optical spectra or electrochemistry of the two different preparation methods; however, the electrochemically produced species

Figure 4.2 MALDI data for A) $Au_{25}(SC2Ph)_{18}$ exchanged with SPhBr ligands shows an average exchange of 11 ligands. In the case of SPhBr exchanged particles, X = 11 giving the formula $Au_{25}(SCH_2CH_2Ph)_7(SPhBr)_{11}$; B) $Au_{25}(SC2Ph)_{18}$ exchanged with SPhOMe ligands shows an average exchange of 7 ligands. In the case of SPhOMe exchanged particles, X = 7 giving the formula $Au_{25}(SCH_2CH_2Ph)_{11}(SPhOMe)_7$.

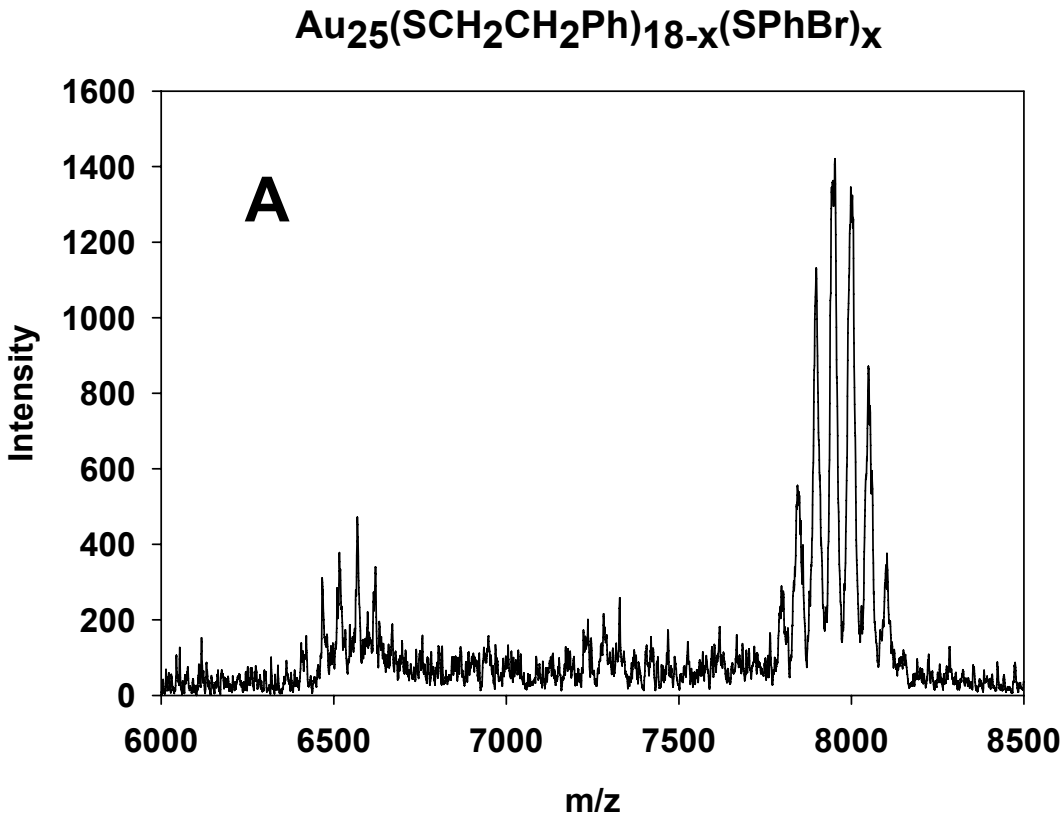
Au25(SCH2CH2Ph)18-x(SPhBr)x
A
Intensity
m/z
0
200
400
600
800
1000
1200
1400
1600
6000
6500
7000
7500
8000
8500

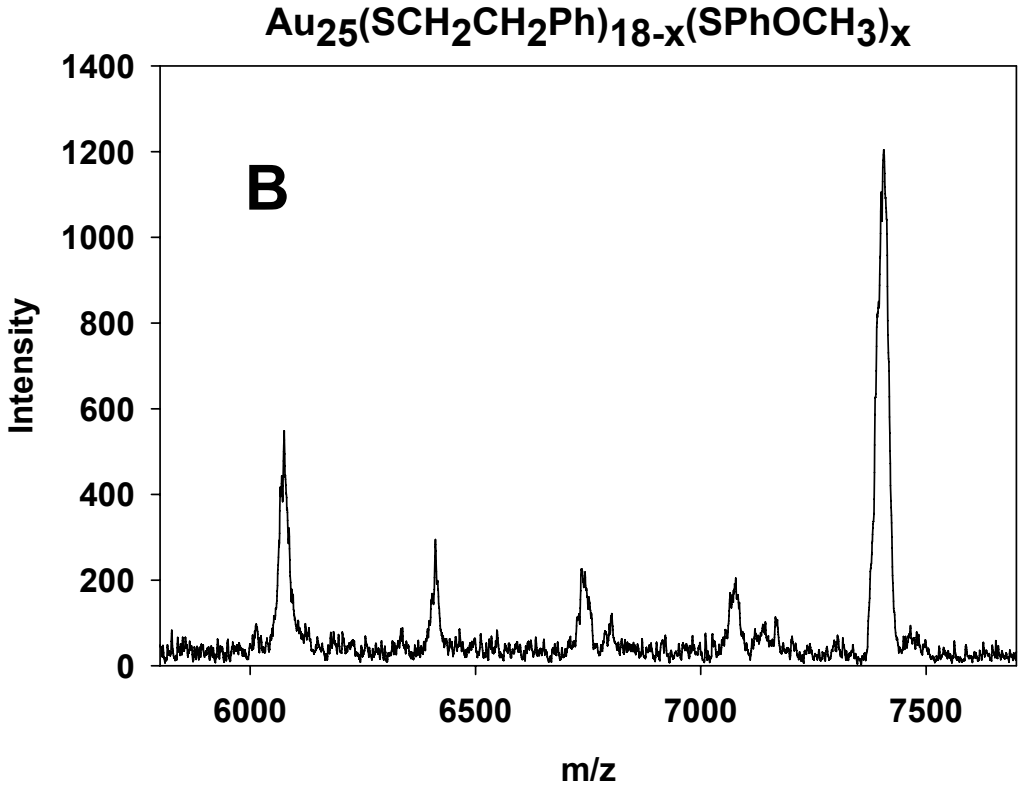
Au25(SCH2CH2Ph)18-x(SPhOCH3)x
B
Intensity
m/z
0
200
400
600
800
1000
1200
1400
6000
6500
7000
7500

are stable for longer periods of time. This is most likely due to residual $Ce(SO_4)_2$ in the sample after the reaction, but prior to washing, that continues to oxidize and then degrade the nanoparticle product. The rest potential was measured and then the electrolyte was washed from the particles and they were then prepared immediately by dropcasting as films on the IDA electrodes and placed under vacuum. The rest potentials that were measured are related to the relative concentration of each species in solution and can be used to solve for the concentration of each species (Au_{25}^{-1} and Au_{25}^{0}) present in the mixture using the Nernst equation[21] (which has previously been shown to be applicable to these particle solutions):

$$E_R - E^{\circ\prime} = 0.059 log \frac{[Au_{25}^0]}{[Au_{25}^{-1}]} \quad (2)$$

where $E^{\circ\prime}$ is the formal potential as measured from DPV and E_R is the measured rest potential. Table 4.1 shows the measured E_R values as well as the calculated corresponding charge state compositions of the mixtures before drop-casting on the IDA electrode surface.

4.3.3 Measurement of σ_{EL} and the Homogeneous Rate Constant k°_{homo} From Linear Sweep Voltammetry

To obtain an electric field-driven electron hopping conductivity measurement, electrolysis measurements must be avoided at the electrode film interface, which means that ion-mobility must be negligible on the experimental time scale.[11] A lack of hysteresis in the *i-E* linear sweep plot indicates that no electrolysis is taking place (Figure 4.3). Electron transport through films of these nanoparticle materials has been shown[10,11] to occur through a series of bimolecular electron exchange reactions with a rate constant that is proportional to the film's measured electronic conductivity:

Table 4.1 Percentages of each redox species present in the film casting solutions as calculated from Eq. 2.

		charge state composition in film (%)	
nanoparticle	**E_R (V vs Ag/AgCl)**	**-1**	**0**
$Au_{25}(SC_2Ph)_{11}(SPhOMe)_7$	-0.03	98.6%	1.4%
	0.03	84.7%	15.3%
	0.05	71.3%	28.7%
	0.08	49.6%	50.4%
	0.07	55.7%	44.3%
	0.11	20.7%	79.3%
	0.13	9.7%	90.3%
$Au_{25}(SC_2Ph)_7(SPhBr)_{11}$	0.07	98.7%	1.3%
	0.13	90.2%	9.8%
	0.15	77.4%	22.6%
	0.17	63.5%	36.5%
	0.24	12.0%	88.0%

Figure 4.3 *i-E* plots for $Au_{25}(SC2Ph)_{11}(SPhOMe)_7$ at 1% oxidized (A) and 55% oxidized (B) that illustrate the difference in current between the less and more mixed valence samples, and also showing the complete lack of hysteresis in the linear sweep measurements.

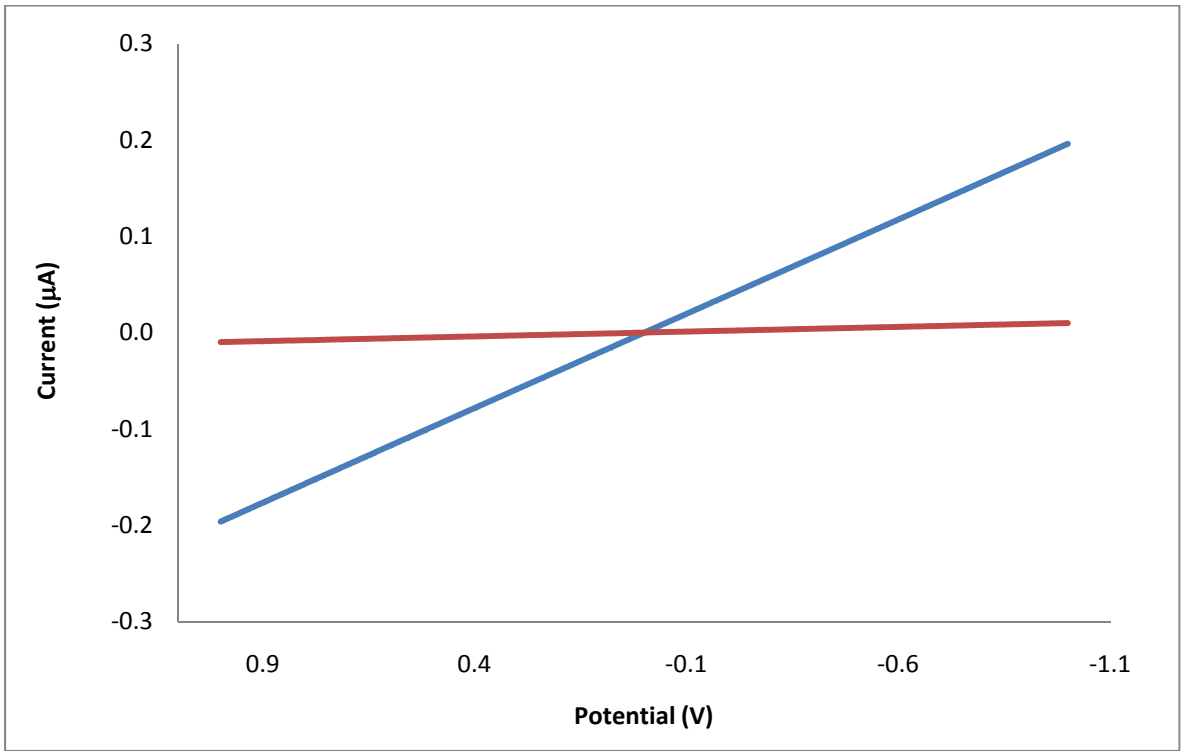
0.3
0.2
0.1
0.0
-0.1
-0.2
-0.3
Current (µA)
0.9
0.4
-0.1
-0.6
-1.1
Potential (V)

$$Au_{25}^{-1} + Au_{25}^{0} \xrightarrow{k_{EX}} Au_{25}^{0} + Au_{25}^{-1} \quad (3)$$

This bimolecular reaction indicates that the rate and conductivity are dependent on the proportions of the concentrations of Au_{25}^{-1} and Au_{25}^{0} that are present in the film. This means that σ_{EL} should decrease as the proportion of oxidized species reaches low percentages and high percentages as well, and the highest conductivity should be found when the ratio of the two oxidation states are close to equal. This behavior is clearly observed in both Table 4.2 and Figure 4.4 and shown compared to previous studies of $Au_{25}(SC2Ph)_{18}^{-/0}$ and $Au_{144}(SC6)_{60}^{0/+}$. Shapes in Figure 4.4 indicate the experimental values observed for the various nanoparticles and the solid lines are 2nd-order rate simulations for the various types of particle.

The measured electronic conductivities are converted to electron self-exchange rate constants (k_{EX}) through the commonly used[10,11,22] cubic lattice model approximation for film structure:

$$k_{EX} = \frac{6RT\sigma_{EL}}{10^{-3}F^2\delta^2[Au_{25}^{-1}][Au_{25}^{0}]} \quad (4)$$

where the center to center distance for electron hopping is

$$\delta = 2\left(r_{core} + l_{app}\right) = 2\sqrt[3]{\frac{0.7}{10^{-3}(4/3)}\pi C_{FILM} N_A} \quad (5)$$

and 0.7 is a hexagonal packing fill factor, r_{core} is the core radius (0.6nm), l_{app} is the apparent ligand length (0.6nm), C_{FILM} is the film concentration (0.17M),[23] and N_A is Avogadro's number (δ = 2.4 nm based on C_{FILM}).

Table 4.2 Presented is data from both samples studied here, $Au_{25}(SC_2Ph)_4(SPhOMe)_{14}$ and $Au_{25}(SC_2Ph)_4(SPhBr)_{14}$, along with a comparison to two previously studied molecules, $Au_{25}(SC_2Ph)_{18}$ [10] and $Au_{140}(SC6)_{53}$.[11] The "film % oxidized" is calculated from the solution rest potential using the E^0 (from DPV) and the Nernst equation[21] (eq 2). Percentages as similar as possible were used in order to accurately compare σ_{EL} and k_{EX} values.

nanoparticle	film % oxidized	σ_{EL} ($\Omega^{-1}cm^{-1}$)	k_{EX} ($M^{-1}s^{-1}$)	log(σEL) (Ω-1cm-1)
$Au_{25}(SC_2Ph)_4(SPhOMe)_{14}$	1.4%	1.35E-08	9.48E+05	-7.87
	15.3%	4.01E-08	3.00E+05	-7.40
	28.7%	1.08E-07	5.12E+05	-6.97
	44.3%	1.80E-07	6.98E+05	-6.74
	50.4%	2.67E-07	1.05E+06	-6.57
	79.3%	4.36E-08	2.57E+05	-7.36
	90.3%	5.20E-09	5.76E+04	-8.28
$Au_{25}(SC_2Ph)_4(SPhBr)_{14}$	1.3%	1.21E-08	9.14E+05	-7.92
	9.8%	1.74E-07	1.91E+06	-6.76
	22.6%	3.02E-07	1.67E+06	-6.52
	36.5%	5.88E-07	2.46E+06	-6.23
	88.0%	9.41E-07	8.64E+06	-6.03
$Au_{25}(SC_2Ph)_{18}$ [10]	1.0%	6.10E-09	5.97E+05	-8.21
	24.0%	1.90E-07	1.01E+06	-6.72
	34.0%	2.70E-07	1.17E+06	-6.57
	45.0%	4.80E-07	1.88E+06	-6.32
	58.0%	7.00E-07	2.79E+06	-6.15
	79.0%	3.20E-07	1.87E+06	-6.49
	98.0%	1.20E-07	5.94E+06	-6.92
$Au_{140}(SC6)_{53}$ [11]	1.0%	2.90E-05	2.84E+09	-4.54
	2.0%	4.00E-05	1.98E+09	-4.40
	3.0%	4.80E-05	1.60E+09	-4.32
	7.0%	7.20E-05	1.07E+09	-4.14
	19.0%	2.20E-04	1.39E+09	-3.66
	97.0%	6.40E-05	2.13E+09	-4.19

Figure 4.4 Second order rate plots of the experimental (shapes) and theoretical (lines) values for each nanoparticle-ligand set. × and – are $Au_{144}(SC6)_{60}$, ■ and – are $Au_{25}(SPhBr)_{11}(SC2Ph)_7$, ▲ and – are $Au_{25}(SC2Ph)_{18}$, and ◆ and – are $Au_{25}(SPhOMe)_7(SC2Ph)_{11}$. The k_{EX} values used for the theoretical data are $4.3x10^9$ $M^{-1}s^{-1}$, $2.5\ x10^6$ $M^{-1}s^{-1}$, $1.5\ x10^6$ $M^{-1}s^{-1}$, and $7.0\ x10^5$ $M^{-1}s^{-1}$ respectively.

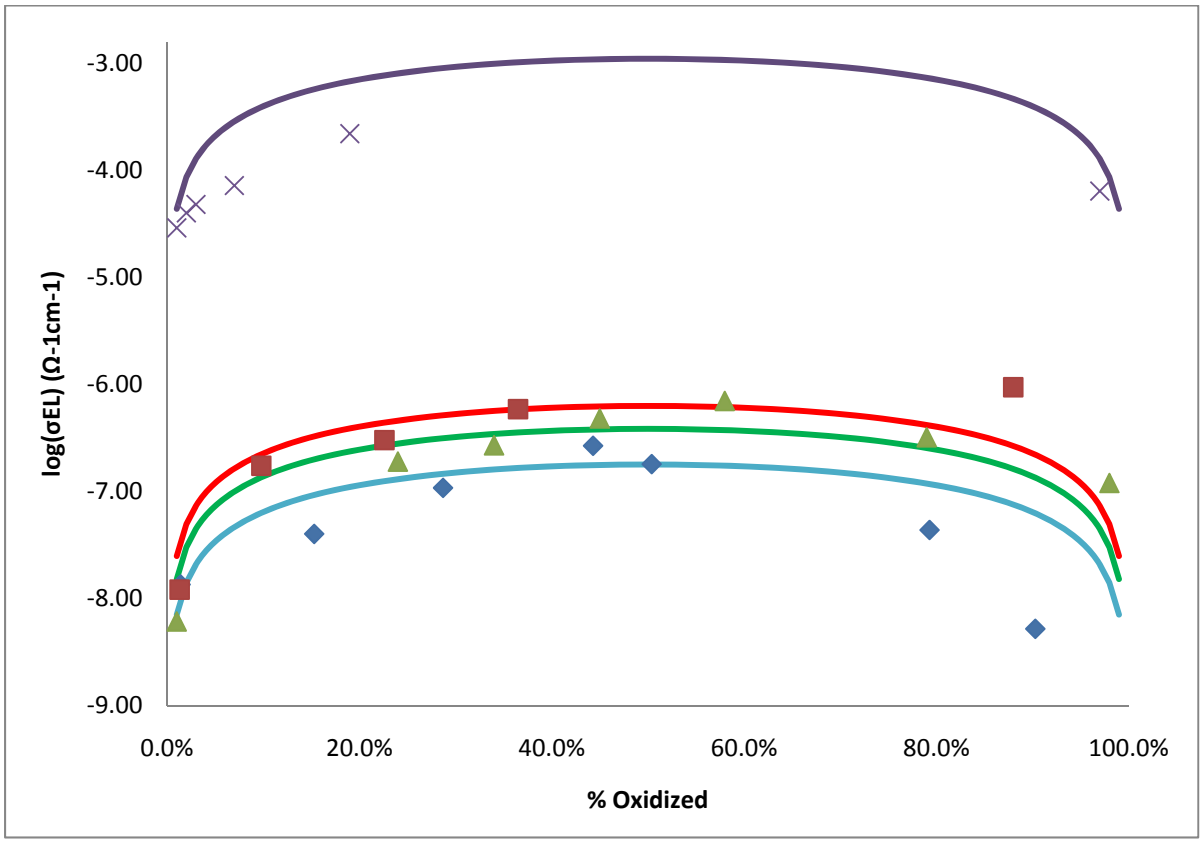
-3.00
-4.00
-5.00
-6.00
-7.00
-8.00
-9.00
log(σEL) (Ω-1cm-1)
0.0%
20.0%
40.0%
60.0%
80.0%
100.0%
% Oxidized

4.3.4 The Effect of ρ-Substituted Thiophenol Ligands on e^- Exchange Dynamics

It has previously been discovered and discussed that the σ_{EL} and k_{EX} values obtained for Au_{25} particles are much smaller than those of Au_{144}, which is likely due in part to the native negative charge on the Au_{25} particle and the associated semi-ring distortion due to counter-cation association in dry films. This may also be associated with the change in bandgap from larger and more molecule like HOMO-LUMO spacing in the smaller (Au_{25}) particles to much smaller quantized double layer charging behavior in the larger particles (Au_{144} and Au_{225}). It has also previously been shown that the electronic nature of a thiophenol ligand can have a strong effect on the rest-potential and consequently the energy associated with redox reactions in voltammetry measurements.[13] Here, it has been shown that the electronic nature of the ligand also has an impact on the ability of the particles themselves to exchange electrons under these circumstances. Electron withdrawing ligands are found to increase the rate at which electrons can be exchanged, and conversely, electron donating groups are found to slow the rate at which electrons can be exchanged (Table 4.2 and Figure 4.4).

By changing the ligand on the Au_{25} particles and conducting the linear sweep experiments described above, it is possible to compare σ_{EL} and k_{EX} between the different ligand protected particles (Figure 4.5). A summary of the data can be found in both Figure 4.4 and Table 4.2. Figure 4.4 is a plot of both the measured conductivity and the conductivity simulated from second order rate equations for the exchange, where σ_{EL} for every oxidation percentage is calculated from a single k_{EX} value using Equation 4 from

Figure 4.5 Using IDA electrodes composed of a total 50 fingers (25 from each electrode); each finger 20μm wide, 20μm apart, 3mm long, and 150nm high. There is no solvent; these particular measurements are conducted under vacuum at 30°C. A) Linear sweep data for $Au_{25}(SC_2Ph)_4(SPhOMe)_{14}$ and B) linear sweep data for $Au_{25}(SC_2Ph)_4(SPhBr)_{14}$, which has noticeably larger currents over the same potential sweep.

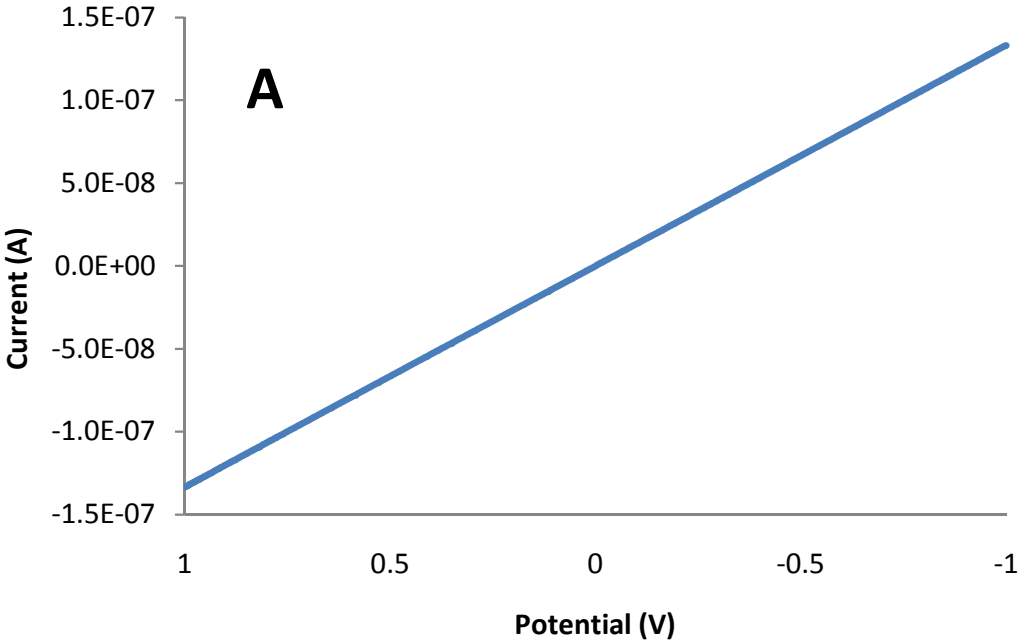
A
1.5E-07
1.0E-07
5.0E-08
0.0E+00
-5.0E-08
-1.0E-07
-1.5E-07
Current (A)
1
0.5
0
-0.5
-1
Potential (V)

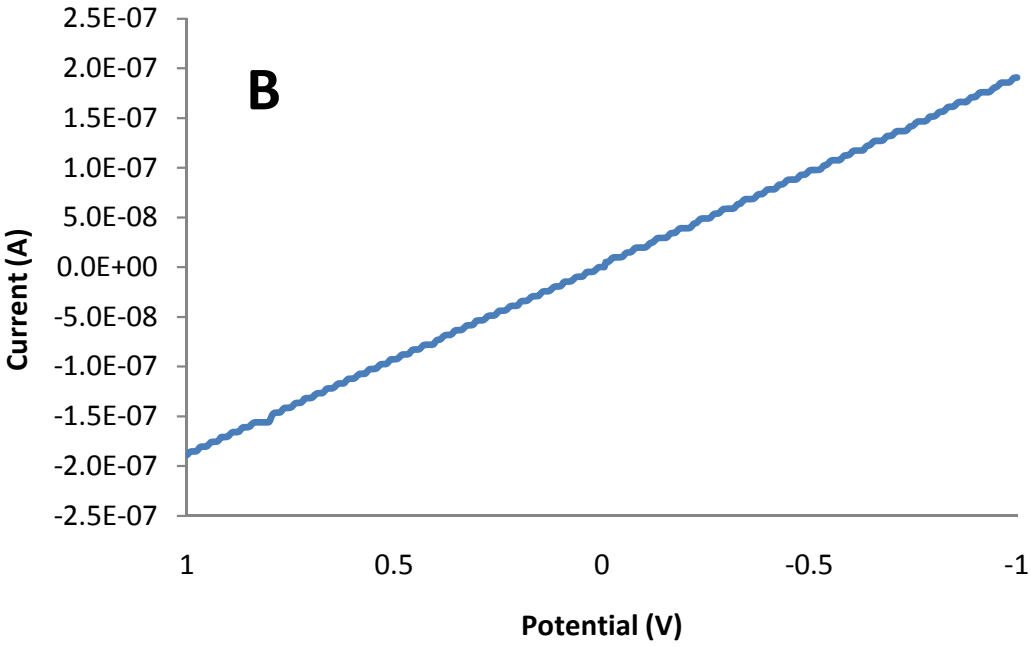
B
2.5E-07
2.0E-07
1.5E-07
1.0E-07
5.0E-08
0.0E+00
-5.0E-08
-1.0E-07
-1.5E-07
-2.0E-07
-2.5E-07
Current (A)
1
0.5
0
-0.5
-1
Potential (V)

above. The simulated plots are based on the k_{EX} value measured closest to 50% oxidized for each sample because those values should contain the smallest deviation due to the large mix of valency.

The results indicate that there is an effect of the ligand's electron character on the particle exchange rate in films. It is clear from Figure 4.4 and Table 4.2 that the electron withdrawing ligand SPhBr somewhat increases the rate of electron exchange in films, while the electron donating ligand SPhOMe slightly decreases the rate of electron exchange in films. The overall effect of this is approximately 4-fold. Any explanation for this effect is somewhat speculative at this point, however, an experimental and theoretical paper published recently by Parker et al. presents density functional theory (DFT) calculations showing that a ligand with an electron withdrawing group, chloride in the case of their study, does in fact pull electron density away from gold atoms that are located in the aforementioned semi-ring structure.[24] Although in the calculations the core appears to be unaffected by this withdrawing nature, the difference in electron character of the semi-ring may allow for energetically easier (or harder in the case of an electron donating group) oxidation of the particle. A change in the degree of semi-ring puckering is one explicit possibility.

4.3.5 Measuring the Heterogeneous Rate Constant k°_{het} From AC Impedance Spectroscopy

As a point of reference and to compare the values found from solid film linear sweep voltammetry for these nanoparticle materials, AC Impedance measurements were used to determine whether the ligand differences in electron exchange kinetics found in films are also present in solutions (Figure 4.6). These values are obviously not directly comparable as they are the result of different overall exchange processes, but the faster kinetics found in

Figure 4.6 Sample AC Impedance data collected using a 1.6mm platinum disk electrode and a large surface area platinum mesh electrode. All measurements were taken in dichloromethane with 1M tetrabutylammonium perchlorate as supporting electrolyte and the DC potential set to the formal potential (E^0) of the nanoparticle 0/-1 redox couple as measured by DPV. All experimental data is in blue, and the red lines are complex nonlinear least squares fits.[26] A) Sample of $Au_{25}(SC_2Ph)_{18}$ at a concentration of 6.4mM. B) Sample of $Au_{25}(SC_2Ph)_7(SPhBr)_{11}$ at a concentration of 0.06mM. C) Sample of $Au_{25}(SC_2Ph)_{11}(SPhOMe)_7$ at a concentration of 0.09mM.

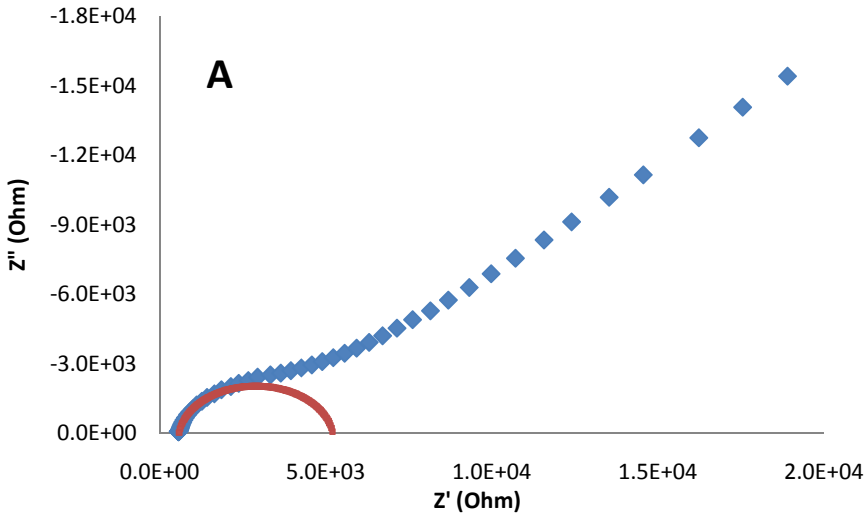
A
-1.8E+04
-1.5E+04
-1.2E+04
-9.0E+03
-6.0E+03
-3.0E+03
0.0E+00
Z'' (Ohm)
0.0E+00
5.0E+03
1.0E+04
1.5E+04
2.0E+04
Z' (Ohm)

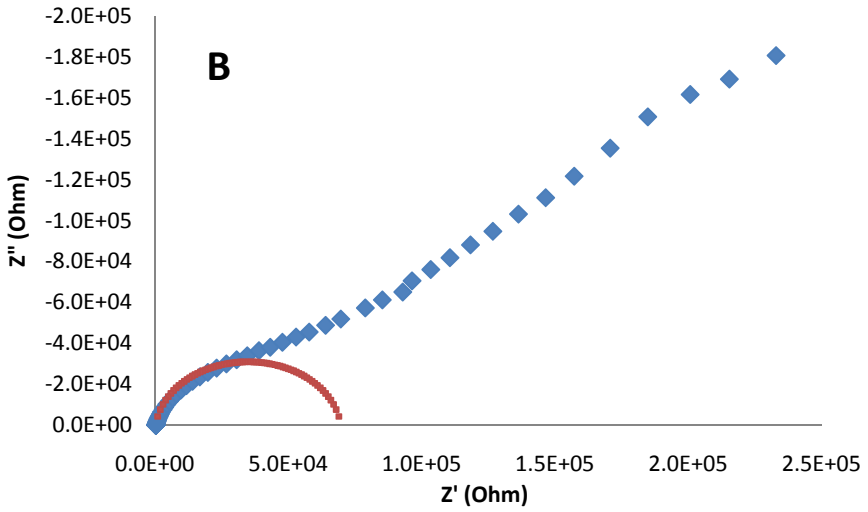
B
-2.0E+05
-1.8E+05
-1.6E+05
-1.4E+05
-1.2E+05
-1.0E+05
-8.0E+04
-6.0E+04
-4.0E+04
-2.0E+04
0.0E+00
Z'' (Ohm)
0.0E+00
5.0E+04
1.0E+05
1.5E+05
2.0E+05
2.5E+05
Z' (Ohm)

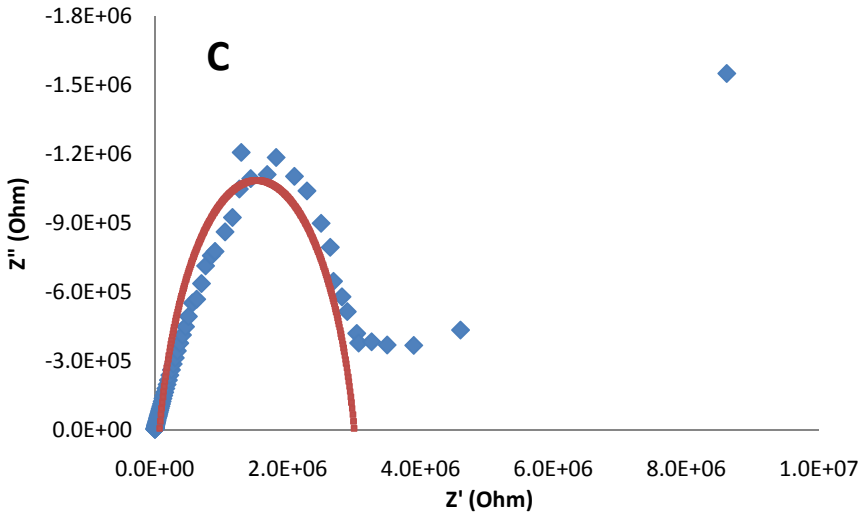
C
-1.8E+06
-1.5E+06
-1.2E+06
-9.0E+05
-6.0E+05
-3.0E+05
0.0E+00
Z'' (Ohm)
0.0E+00
2.0E+06
4.0E+06
6.0E+06
8.0E+06
1.0E+07
Z' (Ohm)

Figure 4.7 Exchange current (i_0) calculated from AC impedance R_{CT} data (eq. 6) and plotted as a function of nanoparticle concentration gives a slope that can be used to calculate k^0_{het} (eq. 7) for $Au_{25}(SCH_2CH_2Ph)_{18}$ (Top) and $Au_{25}(SCH_2CH_2Ph)_7(SPhBr)_{11}$ (Bottom).

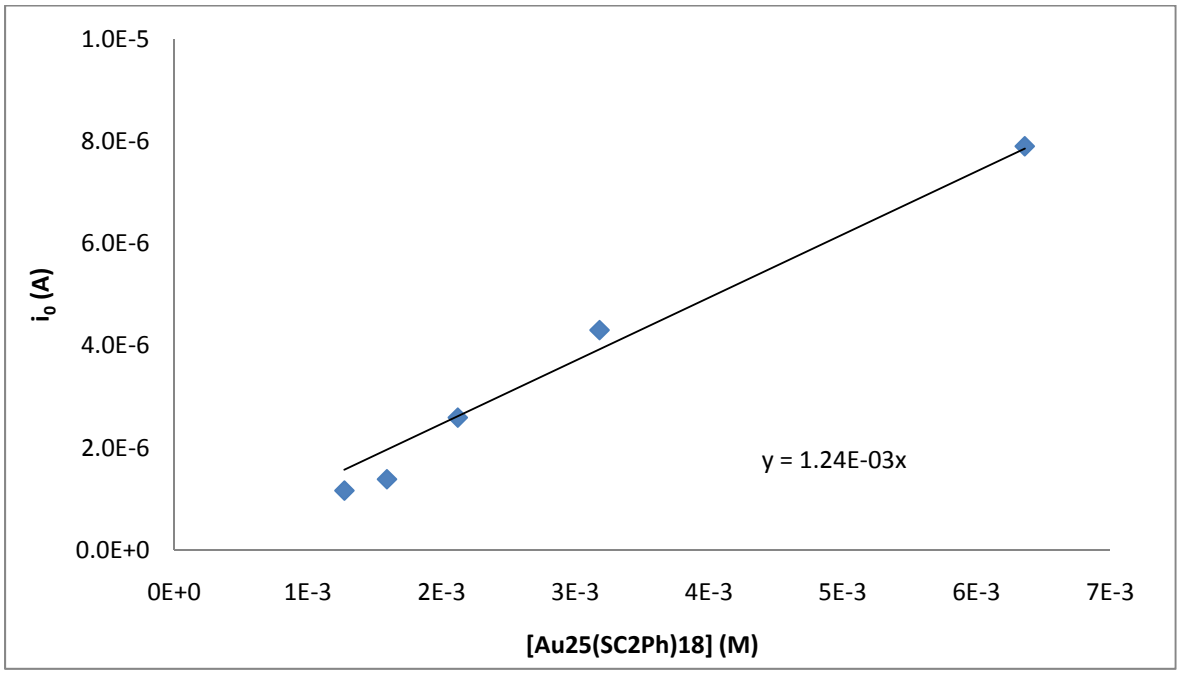
1.0E-5
8.0E-6
6.0E-6
4.0E-6
2.0E-6
0.0E+0
i0 (A)
y = 1.24E-03x
0E+0
1E-3
2E-3
3E-3
4E-3
5E-3
6E-3
7E-3
[Au25(SC2Ph)18] (M)

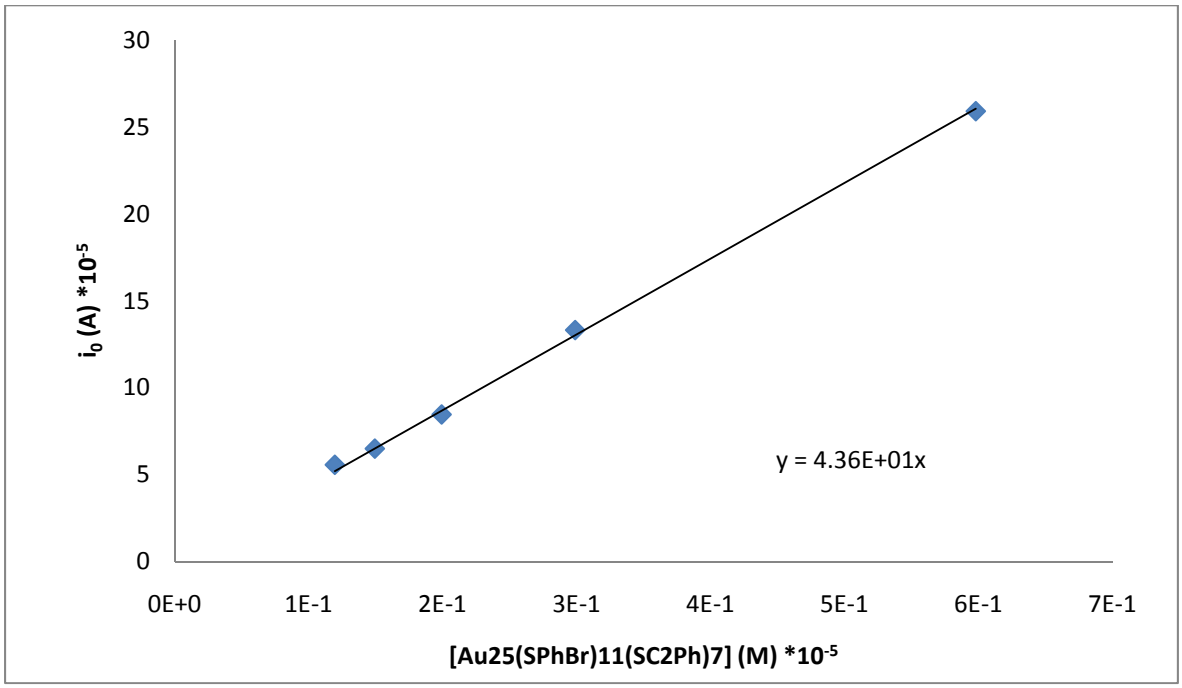
30
25
20
15
10
5
0
i0 (A) *10-5
y = 4.36E+01x
0E+0
1E-1
2E-1
3E-1
4E-1
5E-1
6E-1
7E-1
[Au25(SPhBr)11(SC2Ph)7] (M) *10-5

$Au_{25}(SPhBr)_{18}$ films should qualitatively relate to faster solution exchange kinetics of the same particles in comparison to $Au_{25}(SC2Ph)_{18}$.

The charge transfer resistance (R_{CT}) measured by AC impedance can be converted into exchange current (i_o)[21]:

$$i_o = \frac{RT}{FR_{CT}} \tag{6}$$

where R is the ideal gas constant, T is the ambient Temperature, and F is Faraday's constant. This value can then be plotted (Figure 4.7) as a function of concentration (C), and used to calculate k^o_{het} from the slope of the line:

$$\frac{i_o}{C} = FAk^0_{het} \tag{7}$$

where F is again Faraday's constant and A is the electrode surface area. For each experimental sample, the nanoparticle solution (initially 2ml) is held at the E^0 for several minutes to assure an even distribution of oxidized and reduced species, which simplifies the use of the concentration value in the equation. For each subsequent sample, the solution is then diluted by 2ml for a total of 4 dilutions. Table 4.3 presents the final compilation of data for these experiments for both the $Au_{25}(SC2Ph)_7(SPhBr)_{11}$ and $Au_{25}(SC2Ph)_{18}$ nanoparticles. These data show k_{het} values that are a few orders of magnitude slower than those previously reported by Maran et al. by a different method.[27] Most importantly, it is obvious that there is an enhancement in the rate of electron transfer in solution, as was also seen in films, for the electron withdrawing ligand protected particle $Au_{25}(SPhBr)x$ over that of the $Au_{25}(SC2Ph)_{18}$ particle.

4.4 Conclusion

As evidenced by this study, there does seem to be a strong effect of the electronic nature of a ligand on a small gold nanoparticles ability to exchange electrons in both film and

Table 4.3 This compilation of data shows that the difference in electron exchange rate constants present in linear sweep voltammetry IDA film work is also present in solution samples measured using AC impedance. All impedance data was collected from methylene chloride solutions with 1.0M tetrabutylammonium perchlorate electrolyte at 27˚C.

Sample	Sample Vol	R_{ct} (Ohm)*10^4	C (mol/L)*10^{-4}	i_0 (A)*10^{-4}	k^0_{het} (cm/s)	k^0_{het}/k_{homo}
$Au_{25}(SPhBr)_{14}(SC2Ph)_4$	Initial (2ml)	9.9	0.60	26	$1.8 \times 10^{-3} \pm 2 \times 10^{-6}$	1.97E-09
	+2ml	19	0.30	13		
	+4ml	30	0.20	8.5		
	+6ml	39	0.15	6.5		
	+8ml	46	0.12	5.6		
$Au_{25}(SC2Ph)_{18}$	Initial (2ml)	0.32	64	0.079	$5.0 \times 10^{-4} \pm 1 \times 10^{-5}$	8.38E-10
	+2ml	0.59	32	0.043		
	+4ml	0.99	21	0.026		
	+6ml	1.8	16	0.014		
	+8ml	2.2	13	0.012		

in solution. The electron withdrawing ligand SPhBr slightly increases the rate at which $Au_{25}(L)_{18}$ nanoparticles are able to exchange electrons while the electron donating ligand SPhOMe slightly decreases the rate at which the particles exchange electrons. This may be due to an effect previously reported showing from theoretical DFT calculations that the electron character of gold atoms in the semi-rings of the nanoparticle structure are affected by the electronic nature of the ligand.

REFERENCES

(1) Parker, J.F.; Fields-Zinna, C.A.; Murray, R.W. *Accounts Paper Details*

(2) Negishi, Y.; Nobusada, K.; Tsukuda, T. *J. Am. Chem. Soc.* **2005**, 127, 5261-5270.

(3) Tracy, J.B.; Kalyuzhny, G.; Crowe, M.C.; Balasubramanian, R.; Choi, J.-P.; Murray, R.W. *J. Am. Chem. Soc.* **2007**, 129, 6706-6707.

(4) Lee, D.; Donkers, R.L.; Wang, G.; Harper, A.S.; Murray, R.W. *J. Am. Chem. Soc.* **2004**, 126, 6193-6199.

(5) Parker, J.F; Choi, J-P; Wang, W.; Murray, R.W. *J. Phys. Chem. C* **2008**, 112, 13976-13981.

(6) Akola, J.; Walter, M.; Whetten, R.L.; Häkkinen, H.; Grönbeck, H. *J. Am. Chem. Soc.* **2008**, 130, 3756-3757.

(7) Heaven, M.W.; Dass, A.; White, P.S.; Holt, K.M.; Murray, R.W. *J. Am. Chem. Soc.* **2008**, 130, 3754-3755.

(8) Wolfe, R.L.; Balasubramanian, R.; Tracy, J.B.; Murray, R.W. *Langmuir* **2007,** 23 (4), 2247-2254.

(9) Beasley, C.A. and Murray, R.W. *Langmuir* **2009**, 25(17), 10370-10375.

(10) Choi, J-P. and Murray, R.W. *J. Am. Chem. Soc.* **2006**, 128, 10496.

(11) Wuelfing, W.P.; Green, S.; Pietron, J.J.; Cliffel, D.E.; Murray, R.W. *J. Am. Chem. Soc.* **2000**, 122, 11465

(12) Murray, R.W. *Chem. Rev.* **2008**, 108, 2688-2720.

(13) Guo, R.; Murray, R.W. *J. Am. Chem. Soc.* **2005**, 127, 12140-12143.

(14) Zhu, M.; Aikens, C.M.; Hollander, F.J.; Schatz, G.C.; Jin, R. *J. Am. Chem. Soc.* **2008**, 130, 5883-5885.

(15) Wu, Z.; Suhan, J.; Jin, R. *J. Mater. Chem.* **2009**, 19, 622-626.

(16) Price, R. C.; Whetten, R.L. *J. Am. Chem. Soc.* **2005**, 127, 13750-13751.

(17) Parker, J.F.; Weaver, J.E.F.; McCallum, F.; Murray, R.W. **2010**, Submitted.

(18) *Handbook of Preparative Inorganic Chemistry*; Brauer, G., Ed.; Academic Press: New York, 1965; p 1054.

(19) Block, B.P. *Inor. Synth.* **1953**, 4, 14.

(20) Lee, D.; Donkers. R.L.; DeSimone, J.M.; Murray, R.W. *J. Am. Chem. Soc.* **2003**, 125, 1182.

(21) Bard, A.J.; Faulkner, L.R. *Electrochemical Methods: Fundamentals and Applications*, 2nd ed.; Wiley and Sons: New York, 2001.

(22) Wuelfing, W.P.; Murray, R.W. *J. Phys. Chem. B* **2002**, 106, 32139.

(23) Assumed to be approximately the same as previous estimates for these materials (see ref 10, Choi et al. for details).

(24) Parker, J.F.; Kacprzak, K.A.; Lopez-Acebedo, O.; Häkkinen, H.; Murray, R.W. *J. Phys. Chem. C* **2010**, 114 (18), 8276.

(25) A. Dass, K. Holt, J. Parker, S. Feldberg, R. W. Murray, *J. Phys. Chem. C.* **2008**, 112, 20276-20283.

(26) Complex nonlinear least squares fits were made using James Ross Macdonald's LEVM program, which is available free of charge from his website.

(27) Antonello, S.; Holm, A.H.; Instuli, E.; Maran, F. *J. Am. Chem. Soc.* **2007**, 129, 9836.